CATALYTIC CONVERSION OF METHANE TO PARTIALLY OXIDIZED PRODUCTS OVER COPPER-EXCHANGED ZEOLITES

by

Kimberly T. Dinh

M. S. Chemical Engineering Practice, Massachusetts Institute of Technology, 2017
Bachelor of Chemical Engineering, University of Wisconsin-Madison, 2015

Submitted to the Department of Chemical Engineering
in partial fulfillment of the requirements for the degree of

Doctor of Philosophy in Chemical Engineering

at the

MASSACHUSETTS INSTITUTE OF TECHNOLOGY

September 2020

Author.....
Department of Chemical Engineering
May 26, 2020

Certified by.....
Yuriy Román-Leshkov
Professor of Chemical Engineering
Thesis Supervisor

Accepted by .....
Patrick S. Doyle
Robert T. Haslam Professor of Chemical Engineering
Singapore Research Professor
Chairman, Committee for Graduate Students

Catalytic Conversion of Methane to Partially Oxidized Products over Copper-Exchanged Zeolites

by

Kimberly T. Dinh

Submitted to the Department of Chemical Engineering on May 26, 2020
in partial fulfillment of the requirements for the degree of
Doctor of Philosophy in Chemical Engineering

Abstract

The selective conversion of methane to liquid oxygenated compounds is a grand challenge in catalysis. Although natural gas can be processed industrially in large-scale facilities, new catalytic processes are required that economically directly convert methane to liquid products in small-scale units to exploit highly abundant but difficult-to-access gas reserves. Our group recently reported the first instance of a continuous, gas phase catalytic process for the direct conversion of methane to methanol using copper-exchanged zeolites by feeding only methane, water, and oxygen at 473 K. While this continuous system is an attractive route for the mild conversion of methane to value-added products, fundamental understanding of the reaction pathway and active site is necessary to engineer improved catalysts and an improved process. Thus, my thesis has investigated the fundamental kinetics and active site requirements for continuous partial methane oxidation and using this knowledge to design an improved process.

First, a reaction pathway and a $[Cu\text{-}O\text{-}Cu]^{2+}$ motif as the active site were identified for the selective catalytic conversion of methane to methanol. Kinetic analysis on copper-exchanged SSZ-13 zeolites across a range of Cu loadings and Al spatial distributions revealed the reaction pathway is initiated by rate-limiting C-H bond scission of methane. Water is kinetically inconsequential, but required for methanol desorption. Carbon dioxide is generated from the sequential over oxidation of partially oxidized intermediates and downstream methanol oxidation. Selective partial oxidation was achieved with catalyst samples of high Al content and moderate Cu content (Cu/cage<0.3) with high methane partial pressure in the presence of water. These learnings were used to design a tandem partial oxidation and alkylation process that effectively scavenges methanol to produce toluene by introducing an H-ZSM-5 catalyst and benzene co-feed. Benzene reacts with methanol over Brønsted acid sites, arresting methanol over oxidation and enabling 59% selectivity for partial oxidation products at 0.66% methane conversion. In total, these findings resulted in a process that can circumvent the thermodynamic selectivity-conversion limit for the direct partial oxidation of methane to methanol and provide a new avenue of research in product protection to increase methane conversion while maintaining high product selectivity over heterogeneous catalysts.

Thesis Supervisor: Yuriy Román-Leshkov
Title: Professor of Chemical Engineering

Acknowledgements

This thesis was the culmination of 4.5 years of a lot of work and it would not have happened without the support and help of a lot of people. First, I need to thank my advisor, Yuriy, who has been instrumental in helping me become the scientist I am today. It's been said many times by all of us, but your passion for science always left me feeling energized and more motivated to solve the most current problem, even when I had results that were not great. More importantly, thank you for giving me the freedom to explore interesting leads, to fail again and again, and all the resources to do good science.

Along with Yuriy's guidance, I am also immensely grateful for the input from my thesis committee: Mircea, Allan, and Bill. Reflecting back on my very first meeting at my thesis proposal, I realize how I had threads of ideas but nothing fully fleshed out. Thank you for always probing my ideas and conclusions to get me to think about my data and conclusions in a deeper manner. I also need to thank my collaborators, Randall and Pedro, who were thinking about methane activation just as deeply as me but always brought a fresh perspective to my results and had new ideas for experiments.

Along with my faculty mentors and collaborators, reaching this point was not possible without the support of my group. In the group I found a great group of friends and colleagues who were and just as passionate about catalysis as I am. All of you were so supportive, friendly, and willing to help whenever I had a question and always willing to get a beer after a long day. I especially need to thank Dr. Karthik "Angry" Narsimhan who set the groundwork for my thesis work and being my first mentor. I also have to thank Dr. Jen Lewis and Dr. Kenta Iyoki for teaching me about zeolite and to always be safe in lab. I have to express a lot of thanks also to Dr. Mark Sullivan who joined this project and truly helped me develop my ideas while we worked closely together while Yuriy was on sabbatical. Finally, I also have to thank Stan. I am so glad we got to know each other during practice school and our friendship has continued. Thank you for being a great safety officer and also someone who worked just as hard (and more) than me and kept late hours so that whenever we were working late we could always discuss science, talk about life, or just vent. A big shout out also goes to Mark, Stan, and Amanda and the rest

of my group who has gone on so many XAS trips and were there through some of the most frustrating and grueling times.

Undoubtedly, there were so many ups and downs throughout this journey and my friends helped get me out of the lab, do fun things, and talk about life and not science. To my friends from my first year cohort, Colin, Ki-Joo, Sam, Will, Max, Christina, Alan, you guys are some of my closest friends and I am so glad I got to know you. My practice school cohort also deserves a shout out – admittedly, I didn't know half of you very well prior to it – and I'm glad we bonded and had so much fun amidst a bunch of flux. Colin, Ki-Joo, Sam, Terry, Stan, SK, Minkyung, thank you. The Club Golf team was always an outlet to get outside of the world of Chemical Engineering and meet other people so I thank everyone for that, especially Alex and Ally who together we restarted the golf team. Finally, I also have to say thank you so much to my friends from my undergrad and high school days who continued to cheer me on even as we've scattered across the US. Each one of you has inspired me to do great things. Amanda, I'm so glad also you also were in Boston and we could keep doing fun things! Thank you, Kelly, Amanda, Brenda, Maggie, Leah, Susie.

Finally, I need to thank my family and Tony. Thank you for all the love and support every step of the way. And, thank you, for getting me to take vacations and try new things. Paul and Chris, thank you for being some of the smartest people I know, even though both of you don't admit it, and no matter what, we can always have fun together. Mom and Dad, thank you for being wonderful role models of striving for excellence and to work hard. And Tony, thank you for being you, and so incredibly supportive and positive. The last 5 years have been hard doing long-distance, but you were always there for me to cheer me on through my successes and always pick me up when I was frustrated and things weren't working and wanted to quit. I couldn't have done it without you by my side. I can't wait to start this new chapter together and all the adventures that await us.

Table of Contents

List of Figures:

List of Tables:

I. Introduction

Section I.2 was adapted with permission from Dinh, K. T.; Sullivan, M. M.; Serna, P.; Meyer, R. J.; Dincă, M.; Román-Leshkov, Y. Viewpoint on the Partial Oxidation of Methane to Methanol Using Cu- and Fe-Exchanged Zeolites. *ACS Catal.* 2018, 8, 8, 8306-8313.[1] Copyright 2018 American Chemical Society.

Natural gas production has risen steadily since the mid-2000s due to the development of hydraulic fracturing, commonly known as "fracking." Hydraulic fracturing has enabled access to previously hard to extract petroleum in shale and tight oil plays in remote areas.[2] With shale and tight oil extraction also came an abundance of natural gas. Since 2009, global natural gas production has increased 2.8% on an annually compounded growth rate.[3] In the United States, tight and shale gas is projected to eventually account for 91% of domestic natural gas production by 2050 (Figure I-1A).[2]

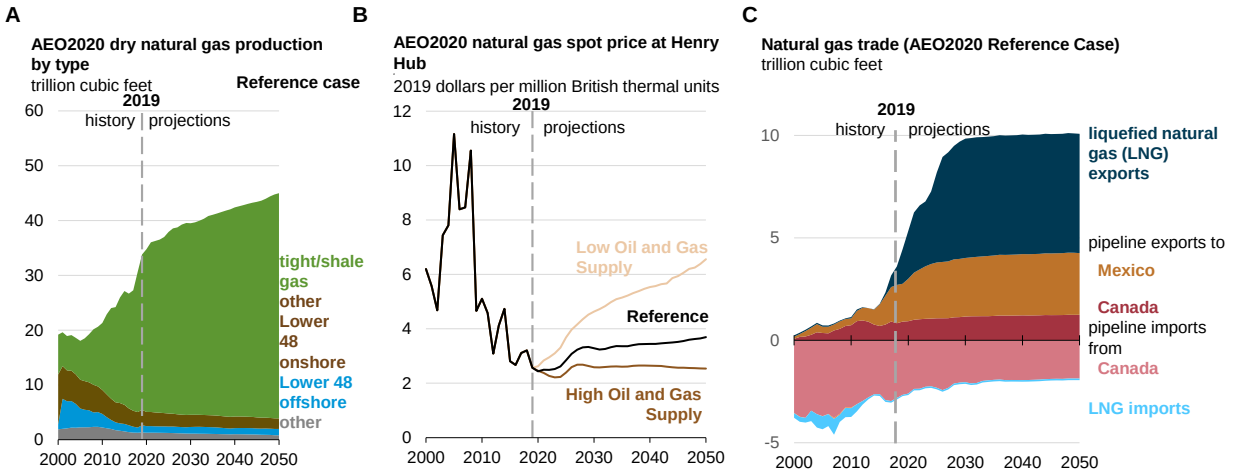

Figure I-1. A. Historical and projected dry natural gas production in the US **B.** Historical and projected natural gas spot price at Henry Hub and **C.** Historical and projected US natural gas imports and exports. All data from US Energy Information Administration's Annual Energy Outlook 2020.[2]

As a result of the abundance of natural gas, natural gas prices have fallen sharply since the 2000s (Figure I-1B) and, in 2017, for the first time, the U.S. was a net exporter of natural gas (Figure I-1C).[4] In the 2000s, natural gas prices were regularly above $8/million BTU but has since dropped to approximately $3/million BTU and is only expected to rise to $4/million BTU by 2050.[2]

The low price of natural gas combined with a lack of infrastructure near shale and tight gas plays to easily transport natural gas[5-6] has resulted in extensive flaring of natural gas as carbon dioxide (CO_2). In the first quarter of 2019, 661 million cubic feet of methane (CH_4, the primary component of natural gas) was flared per day in the Permian Basin (located in southwestern United States, primarily Texas), marking an all-time high and representing double the largest gas production facility on the US Gulf Coast.[7] Given the well-known concerns regarding climate change, the flaring of natural gas also exacerbates this problem. (CH_4 is a potent greenhouse gas, trapping roughly 28-36x more heat in the atmosphere than the same mass of CO_2 on a 100 year time scale.[8])

The abundance of cheap natural gas and, to some extent, environmental concerns, have stimulated renewed interest in the conversion of CH_4 to useful products, especially liquids, which would enable facile transportation of a CH_4 carrier. Liquefying CH_4 itself is not as attractive because a combination of cryogenic temperatures and high pressures is required. Industrially, CH_4 is converted to liquid products in a two-step process (Figure I-2) that first converts CH_4 to syngas (a mixture of CO and H_2) at high temperatures (> 1100 K).[9] Syngas is then converted to liquids such as long chain hydrocarbons by Fischer-Tropsch or CH_3OH.[10] Both Fischer-Tropsch and CH_3OH production operate at milder temperatures but higher pressures (473 – 573 K, 10 – 40 bar[11] and ~500 K, 50-100 bar[12], respectively) than what is used for the initial production of syngas. Due to the required process conditions, the two-step conversion of CH_4 to liquid products is currently only economical at large scales (e.g., production capacity of ~1 million metric tons per year[13]). The production of syngas often accounts for 60% of capital costs.[10]

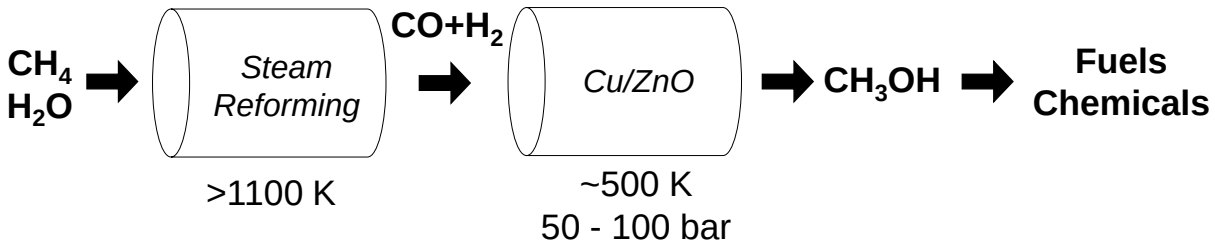

Figure I-2. Block flow diagram depicting industrial production of CH_3OH and other products from CH_4.

Despite similar process conditions, the discussion here will be limited to producing CH_3OH from CH_4. For one, CH_3OH is useful both as a fuel and as a feedstock for chemicals such as olefins, acetic acid, formaldehyde, and methyl methacrylate.[14] CH_3OH's usefulness is highlighted by global methanol demand being projected to grow between 3 and 4% on a compound annual growth rate[15-16] over the next five years, mainly driven by China as they develop methanol to hydrocarbon plants[17] to leverage their large coal reserves.[18] And secondly, CH_3OH synthesis is a simpler process with >99% product selectivity than Fischer-Tropsch synthesis. Specifically, the long chain hydrocarbons from Fischer-Tropsch may require subsequent hydrocracking to achieve the necessary product distribution appropriate for the typical end use of gasoline or diesel.[19]

Inhibiting the construction of a large CH_4-to-CH_3OH processing plant near shale gas plays is the size of shale gas plays are often not well known and production drops rapidly upon the start of production. In some of the largest US plays, natural gas production dropped between 80 and 95% after three years, which requires continual exploration and drilling for new plays.[20] Thus, processes that can transform CH_4 to liquid products, especially, CH_3OH, on small scales commensurate with the production capabilities of shale gas plays are desirable. Simulations have indicated mobile modular plants can be profitable to utilize the stranded gas from these plays.[21] This is most simply achieved if processes can convert CH_4 to liquid products directly at mild conditions with readily available and cheap reactants.

Despite the desirability of a process that converts CH_4 directly to liquid products at small scales, no process can yet achieve this at industrially relevant targets. This is mainly a result of the thermodynamics for CH_4 conversion where the over oxidation of CH_3OH to CO_2 (ΔH_{rxn} = -676.2 kJ mol^{-1}) is more thermodynamically favorable than the selective oxidation of CH_4 to CH_3OH (ΔH_{rxn} = -126.6 kJ mol^{-1}). Furthermore, CH_4 has a higher C-H bond dissociation energy at 435 kJ mol^{-1} than CH_3OH (402 kJ mol^{-1}), which is a result of the lack of functionality on CH_4.[22] The more favorable over oxidation of products to CO_2 combined with a higher C-H bond scission energy renders selective conversion of CH_4 at appreciable yield and mild conditions difficult (Figure I-3). Working within these thermodynamic constraints, selective and direct CH_4 activation to CH_3OH has been and continues to be an active area of research.[23-28] The following sections will summarize research in this field.

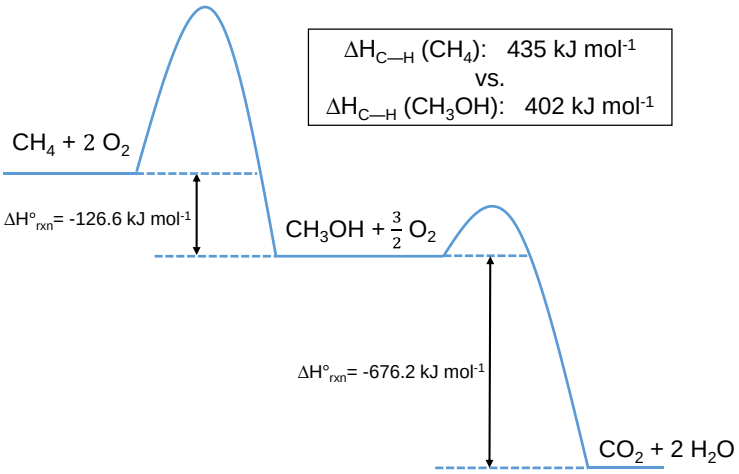

Figure I-3. Schematic depicting heats of reactions and C-H bond dissociation energies for CH_4 activation.[22]

1. Notable Work to Directly Activate Methane to Methanol

Directly activating CH_4 to liquid products has captured the attention of researchers since as early as 1905. Lance and Elworthy filed one of the first patents for CH_4 oxidation to methanol over iron sulfates using hydrogen peroxide as the oxidant.[29] In the 1920s, high pressure CH_4 conversion systems gained interest with the most promising results coming from Boomer and Thomas who explored electrolytic copper.[30] The authors reported 94% selectivity for CH_3OH at almost 2% CH_4 conversion. At higher CH_4 conversion, selectivity for CH_3OH rapidly decreased. While initial results were promising, this process required conditions of upwards of P = 184 bar and T = 748 K.[30] Between these initial results and the 1960s, the focus of partial CH_4 oxidation research centered on understanding the reaction mechanism and kinetics of this process.[27] Given the extremely high pressures required, this process is not attractive for industrial implementation for small scale CH_4 conversion. This research does underscore that selectively activating methane can be obtained but catalysts are necessary to access both milder conditions and improved selectivities as CH_4 conversion increases.

1.1. Heterogeneous Catalysts for Selective Methane Oxidation to Methanol

High pressure systems continued to be studied but with metals other than Cu, including supported oxides of Ag, Zn, Ni, Mo, Pd, Co, Cu, Mn, Ce, V, Fe, and Ti.[27, 31-32] Molybdenum oxide based catalysts demonstrated some of the most promise with 19% selectivity for CH_3OH at 2.3% CH_4 conversion. However, CH_3OH selectivity was increased to 51% with the introduction of zinc oxide.[33] These results were one of the first indicators of the need for multicomponent catalysts to balance the kinetic and thermodynamic challenges of selectively activating CH_4. To further maintain CH_3OH selectivity with increasing CH_4 conversion, Liu et al. used N_2O as an oxidant, instead of molecular oxygen. The authors reported at 8.1% CH_4 conversion, 84.6% selectivity was obtained for CH_3OH and formaldehyde.[34]

These results spurred research in the direction of MoO_3 and V_2O_5 based catalysts with N_2O and O_2[35] as oxidants during the 1980s and 1990s with particular emphasis given to identification of the reaction mechanism and optimizing yields. Notably, it was shown that undesirable CO_2 forms over MoO_3 from a parallel pathway while CO_2 forms over V_2O_5 by a sequential pathway, offering an opportunity for improved CH_3OH yield.[36] Increasing conversion resulted in a rapid decrease in methanol selectivity with 57% selectivity observed at 0.07% CH_4 conversion and 10% selectivity at 1.7% CH_4 conversion over a V_2O_5 catalyst[37], in line with expected thermodynamic limitations.[38] Until the discovery that Cu- and Fe-exchanged zeolites were active for the partial oxidation of methane, these catalysts were some of the most active catalysts at milder conditions than previously reported (P = 1 bar, 723 – 863 K[36, 39]). The best results were obtained with N_2O so the application of these catalysts are industrially limited due to N_2O's expense. Cu- and Fe-exchanged zeolites will be discussed in more detail in Section I.2.

1.2. Homogeneous Catalysts for Selective Methane Oxidation to Methanol

Selectivity for CH_3OH > 70% is typically limited to less than 2% CH_4 conversion over heterogeneous catalysts. In contrast, >70% CH_3OH selectivity was observed at ~10% CH_4 conversion with a homogeneous catalyst.[27] When producing methanol derivatives such as methyl ester and methyl bisulfates, selectivity as high as 81% was observed with 90% CH_4 conversion over the Pt-based Periana catalyst.[40] These values on their own are quite impressive, but these systems also exhibit multiple drawbacks. For one, homogeneous catalysts require additional expensive separation steps to recover the catalyst. Furthermore, many of these homogeneous methane activation operate in harsh solutions such as fuming sulfuric acid or trifluoroacetic acid, which present safety challenges. Additional shortcomings of the Periana system include the product methyl bisulfate requires an additional hydrolysis step to methanol, SO_2 must be reoxidized, and it is unknown if activity is inhibited as water accumulates within the system.[27] All of these issues combined have precluded commercialization of the Periana catalyst and other homogeneous catalysts for partial CH_4 oxidation.

Palkovits et al. reported the heterogenization of the Periana catalyst by anchoring Pt within a covalent traizine-based framework. However, fuming sulfuric acid was still required, again limiting commercial application.[41] Despite the lack of commercial application, these homogeneous systems highlight significant CH_4 conversion with high product selectivity can be obtained by stabilizing the product so that it is more resistant to over oxidation. This idea will be discussed in more detail in Section I.3.3.

1.3. Other Chemistries to Convert Methane Directly to Hydrocarbons

While this discussion has focused on the direct conversion of CH_4 to CH_3OH, it must be noted that other processes for the conversion of CH_4 to other hydrocarbons have also garnered interest and will be mentioned briefly here. These chemistries include pyrolysis, dehydroaromatization, oxidative and non-oxidative coupling to hydrocarbons, and halogenation and oxyhalogenation. Methane pyrolysis is the decomposition of methane and equilibrium calculations suggest ethylene, acetylene, benzene, and hydrogen may be obtained. High yields can be obtained but because the reaction is endothermic, high temperatures are required (> 1700 K).[42] The main challenge is preventing excessive carbon formation. Methane dehydroaromatization is methane pyrolysis over a catalyst. Temperatures can be lowered to ~1000 K and the main products are benzene, toluene, naphthalene, and hydrogen.[10] The main limitation is equilibrium conversion is limited to between 12 and 24%, depending on temperature.[43] Recent work has indicated equilibrium conversion can be surpassed by introduction of a H_2 scavenger.[43] Oxidative and non-oxidative coupling of CH_4 involves the coupling of CH_4 to form longer chained hydrocarbons, either in the presence or absence of O_2. Controlling product selectivity is the main challenge.[10] Finally, CH_4 can be converted to CH_3OH or ethylene in the presence of HCl (or other (oxy)halogens), but this chemistry involves toxic and corrosive reagents.[10]

2. Iron and Copper-Exchanged Zeolites for Selective Methane Oxidation to Methanol

Since the late 1990s, Fe[44-45] and Cu-exchanged zeolites[46-47] have garnered much attention for partial CH_4 oxidation to CH_3OH due to their heterogeneous nature, remarkably high selectivity, and function at mild operating conditions (P = 1 bar, T < 573 K). Zeolites are microporous materials containing a crystalline network of Si and Al atoms. While Si is charge neutral, the substitution of an Al into the zeolite structure creates a negative charge, necessitating a cation for charge balance, such as H^+, Fe^{2+}, Cu^{2+} (Figure I-4). Originally bioinspired catalysts, Fe and Cu-exchanged zeolites display > 70% selectivity for CH_3OH, albeit at low CH_4 conversions (< 1%). Especially attractive are Cu-exchanged zeolites as they only require H_2O and O_2 as additional reactants. In contrast, Fe-exchanged zeolites require an oxidant such as N_2O or H_2O_2, both of which are more expensive than CH_3OH. I also note that the potential use of other catalytic metals within zeolites has not been fully explored. For example, Flytzani-Stephanopoulos and coworkers[48] have demonstrated the use of isolated Rh-sites for methane C-H activation, opening up new catalytic avenues for study aside from Cu and Fe.

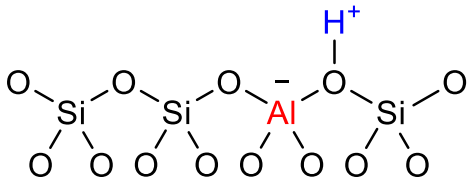

Figure I-4. Chemical structure of a zeolite depicting need for charge balancing cations

Stemming from these initial reports, a significant amount of work on CH_4-to-CH_3OH chemistry has focused on the use of Cu- and Fe-based catalysts, especially on active site identification, designing improved catalysts and optimizing process conditions. This section will provide an overview of the work completed on Cu- and Fe-based catalysts for the direct conversion of CH_4-to-CH_3OH, beginning with providing context of enzymatic systems, before moving to zeolites and wrapping up with a brief discussion of metal organic frameworks.

2.1. Methane Monooxygenases for Methane Conversion to Methanol

Biologically-derived methane monooxygenase proteins (MMOs) transform CH_4 and O_2 into CH_3OH with remarkable selectivity[49-50] under ambient conditions through the use of NADH as a reducing agent for the activation of O_2 prior to partial oxidation of CH_4 on iron (soluble MMO) or copper active centers (particulate MMO).[49] However, despite their attractiveness, these enzymes are hard to purify and have limited temperature stability, driving research towards bioinspired synthetic catalysts that mimic these enzymes. But, knowledge of how these enzymes function is necessary to design selective catalysts for CH_4 oxidation.

MMOs use a combination of effects that are difficult to replicate in artificial systems. Specifically, MMOs possess two key features that result in selective methanol production: 1) ligand fields that induce high-spin electronic configurations at the transition metal sites to induce highly reactive oxidative and reductive environments and 2) a complex gating mechanism that influences the lability and dynamic binding of reagents to the active site which transports CH_3OH out of the active site pocket while also forbidding back diffusion.[51]2) a complex gating mechanism that influences the lability and dynamic binding of reagents to the active site which transports CH_3OH out of the active site pocket while also forbidding back diffusion.[51]

In nature, the ability to generate reactive oxygen species at metal active sites is critical to selective CH_4 oxidation. Proshlyakov and coworkers confirmed the previously hypothesized structure of Q, a key intermediate in the soluble MMO (sMMO) catalytic cycle, as a bis-μ-oxo diiron diamond core structure (Figure I-5).[52-56] In sMMO, Q forms from intermediate P, a *cis*-μ-1,2 peroxo-bridged diiron complex, via proton transfer and homolytic cleavage of the O-O bond.[57-58] Formation of P occurs by a two electron transfer to the two iron atoms to obtain Fe(II),[59] association of O_2 to an open binding site,[60] and then conversion to a peroxo-species.[61]

The mechanism for the activation of CH_4 is unknown in sMMO. Multiple C-H activation mechanisms for sMMO have been proposed, including radical, cationic, and concerted mechanisms. In sMMO, using chiral ethane as a substrate, hydrogen abstraction from CH_4 was suggested to occur via a radical intermediate where the methyl radical rotation is constrained by interaction with the diiron center.[62-63]

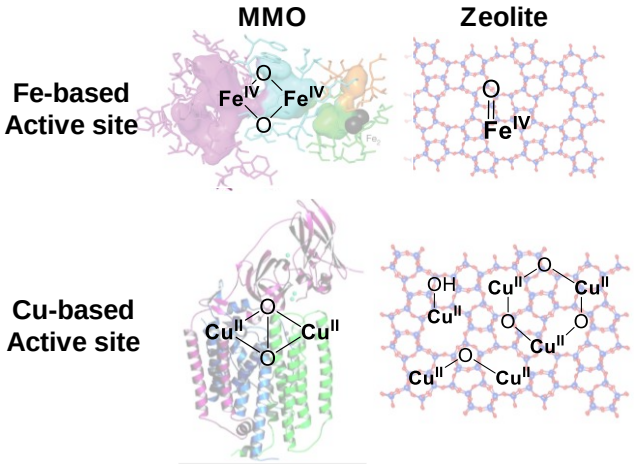

Figure I-5. Active site motifs for Fe- and Cu-based enzymes and zeolites

While the structures of key Fe intermediates in sMMO have been identified and extensively studied, there is no consensus on the structure of the Cu active site nor its mechanism for CH_4 activation in particulate MMO (pMMO). Some of this lack of knowledge can be attributed to challenges with enzyme purification. Mononuclear, binuclear, and trinuclear copper complexes have all been proposed. Most recently, Rosenzweig and coworkers displayed evidence for a binuclear copper core through the use of kinetic and EXAFS experiments.[64] Based on density functional theory and quantum mechanical/molecular mechanics calculations, both mononuclear and dinuclear Cu centers are capable of oxidizing CH_4. However, both active site motifs exhibit shortcomings: mononuclear Cu was modeled as a nonconserved site[65] and the proposed mechanism involving a dinuclear Cu site proceeds via Cu(III)[65-66], which has not been observed experimentally.[67] The proposed dinuclear oxygen activation mechanism necessitates O_2 insertion to form a μ-η^2: η^2-peroxo-Cu_2(II) site that is then converted to a C-H activating catalyst site (either a di(μ-oxo)Cu(II)Cu(III) or di(μ-oxo)(μ-hydroxo)Cu(II)Cu(III) species). Limited reports evince a μ-η^2: η^2-peroxo-Cu_2(II) species and this formulation was not observed upon incubation of pMMO with a saturated oxygen buffer.[65-66] Limited mechanistic studies have been performed with pMMO. Activation of chiral ethane in pMMO was suggested to occur via a concerted pentacoordinate C-Cu or C-O intermediate before insertion of oxygen and cleavage of the C-H bond.[68] However, a radical or cationic mechanism cannot be ruled out if pMMO slows the rate of C-C bond rotation similar to sMMO.[69]

2.2. Fe-Exchanged Zeolites for Partial Methane Oxidation

In an attempt to replicate the Fe sites present in sMMO, Fe-exchanged zeolites have been heavily investigated. Partial CH_4 oxidation in Fe-exchanged zeolites was first observed by Panov and coworkers, who demonstrated CH_3OH can be obtained in a cyclic process.[44-45, 70] Specifically, the Fe active site was first activated by N_2O at high temperatures (approximately 523 K) to form the α-site, followed by the introduction of CH_4 and the formation of CH_3O- and –OH species on these active sites at reduced temperatures, often as low as room temperature, and finally extraction of CH_3OH with water. While water was required to extract CH_3OH, surface-bound CH_3OH was shown to migrate from the α-site and localize on other Brønsted acid sites, allowing for regeneration of the active site in a quasicatalytic process.[71-72] Above 473 K, CH_3OH desorbed spontaneously, resulting in a continuous process.[71] Recently, Snyder, et. al. identified the active site as a mononuclear, high-spin Fe(IV)=O species using magnetic circular dichroism.[73] These authors highlighted the importance of the zeolite topology, which provides the appropriate geometric constraints around Fe to maintain vacant the *trans* axial position of α-O and produce an entatic state.[73] Activation of Fe with molecular O_2 at mild temperatures has not been demonstrated to date.

In an alternative aqueous synthetic pathway, CH_3OH was produced over Fe-zeolite catalysts using H_2O_2 as an oxidant at low temperature (~323 K). In a batch system, a maximum conversion of 10.1% and a CH_3OH selectivity of 93% was reported[74] while, in a continuous system, a maximum conversion of 0.5% and a CH_3OH selectivity of 92.2% was reported.[74-76] The catalytic cycle proceeded by the formation of methylhydroperoxide that sequentially decomposed to CH_3OH and then to formic acid.[77] Selectivity was further improved by introducing Cu alongside Fe within the zeolite that prevented the oxidation of CH_3OH to formic acid.[74] CO_2 accounted for the balance of products. Characterization studies demonstrated that the active site is an extra-framework diiron site that upon activation with H_2O_2 forms an Fe-OOH intermediate.[78]

Although understanding of the genesis of active sites and the reaction mechanism involved in CH_4 oxidation is critical for future catalyst design, the Fe-based zeolite approach is industrially unfeasible because expensive oxidants (in many cases more valuable than CH_3OH itself) are needed to activate the Fe site. Additionally, a gas phase approach would require a looping process with temperature and feed changes that are challenging to implement industrially. The aqueous route is also limited primarily due to the challenge of recovering dilute methanol from an aqueous solution.[79] Further study of these systems should focus on using abundant and cheap oxidants in a continuous system.

2.3. Cu-Exchanged Zeolites for Partial Methane Oxidation

Cu-exchanged zeolites have also been heavily studied in an attempt to replicate the copper activity of pMMO. The catalytic conversion of CH_4 to CH_3OH over Cu-exchanged zeolites is enabled by the oxidizing capability of Cu-based catalysts. Cu has been used to catalyze a plethora of oxidation chemistries[80] and copper oxides are known to promote CH_4 combustion.[81] Process conditions, zeolite composition and structure, and Cu speciation need to be optimized in order to singly oxidize CH_4 and avoid complete combustion to CO_2. Catalytic conversion of CH_4 to CH_3OH can be accomplished by using H_2O_2 [75] and N_2O[47] as oxidants. Methane oxidation via aqueous H_2O_2 has been reported to result in high CH_3OH selectivity; Kalamaras et al.[82] reported ~75% selectivity to CH_3OH in the presence of 0.5 M H_2O_2 over a Cu/ZSM-5 catalyst. Samples catalyzed multiple turnovers as evidenced by a MeOH/Cu molar ratio >4 for a 2.6 wt% Cu/ZSM-5 catalyst, demonstrating that active sites are completing multiple catalytic cycles and selectively synthesizing CH_3OH beyond a stoichiometric amount while in the presence of excess oxidant.

For Cu-zeolites, proposed active sites involve mono-, di- and tri-copper species (Kulkarni et al.,[83] Groothaert et al.,[47] and Grundner et al.,[84] respectively). Results from density functional theory-based investigation of CH_4 activation support the homolytic cleavage of C-H bonds by radical-like oxygen atoms to form a radical methyl intermediate that is subsequently rebound to the hydroxyl species.[85-86] CH_3OH desorption often presents the largest energetic barrier to complete catalytic turnover and the presence of H_2O is purported to stabilize and facilitate CH_3OH desorption.[86] The complexities introduced by varying zeolite topologies, locally confined reactant concentrations, Cu-speciation, and the nature of the oxidant all inhibit overgeneralization of C-H activation mechanisms.[87-88]

When considering the use of O_2 as the oxidant, experimental precautions must be taken in order to minimize extensive oxidation. Cyclic chemical looping procedures have been shown to yield high selectivity to CH_3OH by completely separating the oxidant from CH_4 by using inert gas purges in between the O_2 activation step and the introduction of CH_4 over the Cu-zeolite.[27] These looping procedures circumvent over oxidation problems that arise due to the simultaneous presence of large concentrations of O_2 and CH_4. Cyclic chemical looping processes involve the activation of the Cu-exchanged zeolite under O_2 (often at elevated temperatures), deposition of CH_4 on the catalyst at lower temperature, extraction of CH_3OH either offline or with steam, and then reactivation of the catalyst.[47, 89-90] This process operates in a stepwise manner and is not catalytic because the number of CH_4 activated per Cu atom is never greater than one prior to catalyst reactivation.[39] More details of this process and a comparison to a catalytic process will be discussed in Section I.3.1.

Over oxidation of CH_3OH can also be minimized by limiting the amount of O_2 within the reactor. Román-Leshkov and coworkers have reported the steady state conversion of CH_4 to CH_3OH in the presence of very low concentrations of gaseous O_2 (~100 ppm)[91] under flow of CH_4, H_2O, and O_2. CH_3OH production rates were invariant with O_2 concentration over the ranges studied, demonstrating the thermodynamic favorability of Cu oxidation in the presence of extremely dilute O_2 concentrations. While this method of steady state production of methanol is appealing, careful consideration needs to be taken in order to optimize the concentration of O_2 to oxidize and maintain catalytically active sites while minimizing the presence of excess O_2 that results in deleterious complete combustion reactions. More recently, the use of H_2O as the sole oxidant to produce CH_3OH was published by Van Bokhoven and coworkers.[92] The relatively weak oxidative potential of H_2O relative to O_2 in conjunction with the natural abundance of water highlights the appeal of conversion processes based on these reactants. It should be noted that the thermodynamics of this system are challenging ($\Delta G_{reaction} \approx 117$ kJ mol^{-1} at 200°C[93]). Further study in this direction is definitely warranted.

2.4. Metal Organic Frameworks for Partial Methane Oxidation

Similar in essence to zeolites in terms of pore topology and local structure variability, metal organic frameworks (MOFs) are microporous materials made from inorganic building blocks bridged by organic ligands, defining a plethora of pores of 1-4 nm in diameter that offer virtually unparalleled tunability in the solid state. One of the most striking features of MOFs that remains remarkably unexplored is the unique coordination chemistry of the inorganic building units, which are nodes made from multi-metallic clusters. These nodes can be thought of as independent molecules that are pinned to a solid porous matrix and are therefore primed for interaction with small substrates such as O_2 and CH_4 (Figure I-6). MOFs are most commonly composed of common enzyme ligands including carboxylic acids, imidazoles, phenols, or thiols, and the MOF nodes define metal coordination environments with ligand field strengths that also mimic those of metalloenzymes. Reasons for the importance of the relatively weak fields conferred by MOF ligands in relation to reactivity are two-fold: 1) they establish labile bonds with the metal ions, thus offering dynamic, flexible coordination environments that could imitate enzymes and 2) they lead to high-spin electronic configurations, promoting more facile oxidative and reductive chemistries.

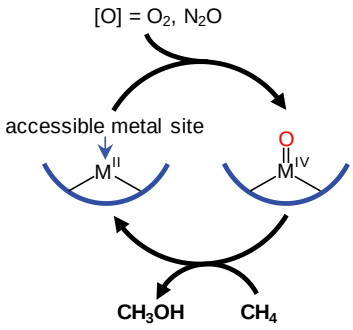

Figure I-6. Conceptual activation of CH_4 at a high-spin high-valent metal oxo species

As discussed above, a key feature contributing to the exquisite selectivity of enzymatic systems is site isolation. In MMOs, active sites are protected from deleterious reactions by protein scaffolds. This is typically impossible with homogeneous systems as attempts to control access to the active site necessarily result in changes to the chemical nature of the active site, adding further complexity to the tuning of homogeneous systems. Indeed, whereas structural models of virtually any metalloenzyme can be synthesized by judicious ligand design, functional mimicry of the natural systems remain elusive because bimolecular deactivation, aggregation, and ligand denaturation often compete with productive catalysis. Zeolites address the challenges faced by homogeneous systems by protecting the catalytic sites inside rigid pores that can be viewed as mimics of the protein scaffold, albeit using primarily inorganic framework elements, which limits the tenability of their transport properties (*vide infra*). However, the metal-loading in zeolites is often limited and the structure of the active site is often difficult to characterize. MOFs typically exhibit higher active site loadings and coordination environments that are structurally well-defined and more tunable insofar as electronic structure and reactivity are concerned. Recent work by Dincă and co-workers has shown that active metals can be substituted post-synthetically into MOFs.[94-97] Accordingly, Ikuno et al. recently demonstrated that the oxidation of CH_4 to CH_3OH occurs on copper-oxo clusters in NU-1000[98] while work by Osadchii et al. demonstrated this same chemistry with Fe on MIL-53.[99] We expect that these substituted high-valent metal cations will exhibit high spin states rendering them active for both electron acceptance and donation and are a promising avenue of research.

3. Open Areas of Study of Cu-Exchanged Zeolites for Partial Methane Oxidation

Based on the presented discussion, Cu-exchanged zeolites are a promising area of research for the direct and selective conversion of CH_4 to CH_3OH at mild conditions. Numerous studies have indicated >70% selectivity for CH_4 can be obtained in a chemical looping cycle or in continuous processes but large scale improvements have not yet been observed. This section will highlight open questions in the field.

3.1. Engineering Improved Catalysts and Processes

The ideal implementation of a catalytic CH_4-to-CH_3OH process on an industrial scale necessitates the investigation of multiple primary factors. When considering feasible industrial processes, rates of CH_3OH production should be examined in terms of catalyst quantity and total processing time. Within the chemical looping literature, CH_3OH production is often reported as normalized by catalyst loading, i.e. CH_3OH produced per mole of Cu or CH_3OH l per gram of catalyst, yet this reporting ignores relevant down time during implementation of cyclic processes. Narsimhan et al. provide the most direct comparison for the rates of CH_3OH production during stoichiometric and catalytic production over a single Cu-H-ZSM-5 at 483 K, reporting a yield of 82 μmol CH_3OH g_{cat}^{-1} during the stoichiometric regime immediately followed by a steady state production rate of 1.81 μmol CH_3OH g_{cat}^{-1} h^{-1} during the catalytic regime. The looping process involved heating from 483 K to 823 K, a 5 h hold at 623 K, cooling to 823 K, reactor purging with He for 0.5 h, CH_4 flow for 0.5 h, and finally H_2O-aided desorption of CH_3OH that lasted ~15 h.[91]

A looping process offers the inherent benefits of the separation of the oxidant from CH_4, aiding in extraction of desirable partially oxidized products and preventing the continued oxidation of desirable products. However, ignoring heating and cooling times, this entire process consumes >20 h per cycle. Using this timescale to normalize CH_4 production rates and assuming no deactivation between looping cycles yields a rate of production on the order of ~4 μmol CH_3OH g_{cat}^{-1} h^{-1}. At first glance, this is twice the rate of production of the catalytic regime. Methodological improvements for increasing the quantity of active sites for C-H activation is dependent upon catalyst formulation, requires further fundamental study, and cannot be simply manually adjusted. Both steady state and catalytic processes can be further optimized via catalyst synthesis, but there is no evidence to imply the selective benefit of catalyst makeup upon a looping process as opposed to a catalytic process.

Upon deeper consideration, one can recognize the inherent limitations of a stoichiometric, cyclic process: the rate of CH_3OH production is fundamentally controlled by the timescale to complete a single looping cycle, and the amount of CH_3OH produced per cycle is limited by the amount of active sites within a catalyst. The looping timescale can be modestly adjusted and optimized, but the nature of alternating flows and temperatures remains integral to the cyclic process. If a sufficiently high rate of CH_3OH production can be achieved per cycle, a cyclic process can have industrial application. Conversely, a steady state system can be manipulated and optimized simply by altering reaction temperature and space velocity to modify rates and selectivity. Using a feasible C-H activation energy of ~100 kJ mol^{-1} reported by Zhao et al.,[100] steady state CH_3OH production rates can be doubled simply by a 14 K increase in operating temperature, and this process can run without interruption barring catalyst deactivation. Unfortunately, a continuous process will always subject CH_3OH to contact with oxygen and subsequent oxidation events, whereas a looping system will innately limit overoxidation due to the separation of these species, resulting in inherently high selectivity in comparison to a continuous process. While both stepwise and continuous processes have pros and cons, it is unclear which process will be most industrially relevant. In this thesis, I focus on the development of a steady state process as it holds significant advantages over stepwise processes if product yield can be improved.

Two prominent factors in the development of a steady state methane to methanol process are 1) the oxidant used and 2) the selectivity achieved. As shown in previous work, the use of N_2O and H_2O_2 can provide large conversions and selectivities towards CH_3OH production. Unfortunately, these oxidants are themselves produced in costly industrial processes, minimizing the economic boon from CH_3OH production due to the stoichiometric necessity of costly oxidants. While the use of a reducing agent to facilitate O_2 activation prior to active site generation, much like NADH in MMOs, is attractive, a simple co-feed would not be straightforward as challenges such as the presence of both an oxidant (O_2) and a reductant (e.g., H_2) at elevated temperatures would promote undesirable, unselective reductant combustion. Therefore, the pursuit of an industrial catalytic process should focus on the use of abundant oxidants such as O_2[91] or H_2O[92]. Work towards an industrial catalytic process must first start with understanding necessary fundamentals of steady-state processes including understanding the role of each reactant and the pathway(s) for product formation.

3.2. Identification of the Active Site(s) for Methane-to-Methanol Conversion

Also necessary to engineering improved catalysts for steady-state CH_4-to-CH_3OH conversion are identifying the active site(s) responsible for selective C-H activation and understanding how these active site(s) are formed. Such understanding will provide important catalyst requirements for selective CH_3OH production and enable improved synthetic catalyst design.

As described previously, the nature of the active site in chemical looping processes is a subject of intense debate[47, 83-84] and the active site for the catalytic conversion of CH_4-to-CH_3OH is unknown. Thus, the combination of advanced characterization and synthesis techniques with rigorous kinetic studies is vital to identify and isolate the active site(s) responsible for the observed catalytic behavior. The most promising routes for resolving the true nature of the active site(s) necessitate *in situ* experimentation, and operando techniques such as atom-specific copper x-ray absorption spectroscopy (XAS) offer enormous potential for isolating active site precursors and observing changes that occur throughout the oxidation and reduction of Cu during the catalytic cycle. Operando XAS experimentation allows for the observation of both the oxidation state and local environment of the active site as they change throughout catalytic induction periods and reaction condition alterations. Although the technique does constitute a sample averaging that may include inactive moieties, changes observable under transient conditions will provide valuable information about the active site as the catalyst is transitioned between different phases of the catalytic cycle due to reactor and feed conditions. Thus, while there is a wealth of research that implements XAS analysis of active site oxidation state and local environment via ex situ measurements of transient, stoichiometric systems, the use of operando XAS in steady state systems should be pursued as a method for monitoring the evolution and maintenance of active centers in metal exchanged zeolites or MOFs for methane activation catalysis. Understanding the catalytically active site would allow for selective control and synthesis of the proper micro-environment necessary for C-H activation to form CH_3OH, which will also facilitate selective scavenging of reactive intermediates to preserve the high selectivity towards non-CO_2 products (*vide infra*).

While understanding of a catalyst's active site structure is vital to design improved catalysts, understanding of the active site's local environment is also vital. In this respect, the role of the zeolite framework must also be considered in partial CH_4 oxidation chemistry. Different local confinement effects and the pore sizes present in varying zeolite topologies can offer diverse environments that stabilize species along every step of the reaction pathway. The synthesis of Cu-zeolites also offers the opportunity to incorporate cooperative active sites within the catalyst, more specifically Cu-species and Brønsted acidic protons. Mahyuddin and coworkers[101] correlated the Cu-O-Cu angle to the alteration of the electron acceptor orbital of the $[Cu_2(\mu\text{-}O)]^{2+}$-zeolite species and subsequent decrease in activation energy of rate-determining C-H bond cleavage and this angle is specifically set by the zeolite topology and the crystallographic location of the active site. Sushkevich and others[92] have correlated the appearance of H^+ and $\text{-}OCH_3$ moieties via FTIR upon C-H activation, and Kalamaras and others[82] have demonstrated systematically increasing yields of CH_3OH as a function of increasing catalyst Brønsted acidity, implicating mechanistic relevance of protons in partial CH_4 oxidation chemistry. Synthetic control over the catalytic porous microstructure is a necessary tool to optimize reactant environment and active site densities to allow for tunable control over the reaction energetics; the knowledge to optimize catalyst synthesis procedures is predicated upon a fine understanding of the mechanistic details of C-H activation.

3.3. Inhibiting Methanol Over Oxidation to Carbon Dioxide

While identification of the active site and optimal reaction conditions in both Cu-exchanged zeolites and MMO's are necessary for a biomimetic approach to synthetic methane oxidation catalysts, understanding the role of the reactive environment to enhance transport of reactants and products within the micropores is an equally (if not a more) important task. A critical, yet commonly neglected topic in the community working on synthetic catalysts for partial CH_4 oxidation is the gating mechanism found in sMMOs that enables their near-perfect selectivity to CH_3OH. Specifically, elegant studies by Lippard and Cho, et al. showed that the di-iron active site is situated in a hydrophobic cavity in sMMO hydroxylase (MMOH) and that access to the active site is controlled by the regulatory B component (MMOB) inducing conformation changes within MMOH upon MMOB docking (Figure I-7)[51].

The enzymatic active site can be accessed via two separate routes: a hydrophobic passage and a hydrophilic pore. When MMOB is not docked on MMOH, the hydrophobic passage is separated from the active site cavity by a phenylalanine gate and the active site can be accessed via the hydrophilic pore. Upon binding to MMOH, MMOB induces a conformation change in this phenylalanine residue, allowing the diffusion of CH_4 and oxygen within the hydrophobic passage to the active site. Simultaneously, the hydrophilic pore is closed, preventing access of unwanted substrates. Once MMOB dissociates from MMOH, the hydrophobic passage is again gated and the hydrophilic pore opens, allowing for CH_3OH and water egress and proton and electron ingress.[51, 102] This gating mechanism thus facilitates the removal of CH_3OH to prevent its complete oxidation.

One shortcoming noted by Ross et al. is this model does not explain the observed first order dependence on the substrates when zero order kinetics would be expected by this gating mechanism, although this discrepancy could be accounted for by mass transfer limitations.[103] Similar hydrophobic and hydrophilic cavities have been identified in pMMO, but the roles of these cavities have not been identified.[69] It is possible a similar gating mechanism for substrate access as in sMMO is at play. Without a gating mechanism, the continued oxidation of CH_3OH is possible; the interception and removal of CH_3OH from the active site results in the high CH_3OH selectivity observed from sMMO-catalyzed oxidation. To this end, Colby et al. demonstrated that methane monooxygenase of *Methylococcus capsulatus* (Bath) is non-substrate specific and can oxidize CH_4 derivatives, including CH_3OH. In fact, CH_3OH was oxidized three times as fast as CH_5, despite being a product and having a larger Michaelis-Menten constant.[50]

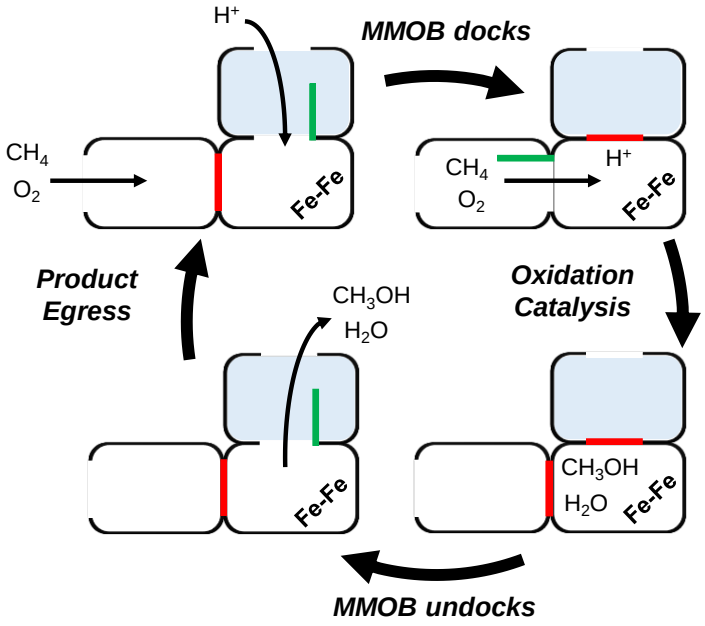

Figure I-7. Enzymatic gating process for CH_4 oxidation to CH_3OH

The direct mimicry of this bioenzymatic process, partially enabled by a flexible enzymatic topology, is difficult to accomplish with a zeolitic system due to the comparably rigid zeolite structures. Nonetheless, the shielding of singly activated C-H reaction intermediates can inspire the pursuit of other related capping mechanisms. Shilov et al. demonstrated one of the first instances of this idea using $Pt(II)Cl_2$ in aqueous solution to convert CH_4 to chloromethane, which can react further to obtain CH_3OH.[104] Using Hg and Pt-based catalysts in concentrated sulfuric acid, Periana and coworkers were able to activate CH_3OH to form methyl bisulfate, which could be subsequently hydrolyzed to CH_3OH.[40, 105] More recently, Surendranath and coworkers used $Pd^{II}SO_4$ in concentrated sulfuric acid to produce methyl bisulfate from CH_4 electrochemically.[106] Another route to be explored is the direct sulfonation of CH_4 with sulfur trioxide, which has been demonstrated in liquid methanesulfonic acid[107] and also in fuming sulfuric acid.[108] Methanesulfonic acid can be cracked to produce CH_3OH and sulfur dioxide, which can be reoxidized to sulfur trioxide and then recycled.

Selectivity is an inevitable function of the C-H activation mechanism. A clear distinction must be highlighted between radical-inducing C-H activation mechanisms initiated by homolytic C-H bond cleavage and Periana-type systems. The former inherently leads to unselective sequential oxidation events due to the weaker, more polarized C-H bonds of oxidized products, and the latter maintain selectivity to single oxidation events due to preferential C-H bond cleavage of the more reduced substrate as opposed to the more oxidized product by electrophilic, cationic catalysts.

These heterolytic methods to cleave C-H bonds mimic the enzymatic system by inhibiting CH_3OH oxidation via formation of reaction products less prone to oxidation after initial C-H activation. In a similar vein, the initial C-H activation of CH_4 over Cu-exchanged mordenite leads to the concurrent formation of zeolitic protons and methoxy groups as evinced by FTIR spectra of adsorbed pyridinium ions and $–OCH_3$ groups. These surface methoxy groups can be subsequently removed as gas phase methanol by H_2O co-feed.[92] The ideal implementation of a selective steady state process would involve the scavenging of the stable intermediate achieved after C-H activation (i.e. $-OCH_3$ groups) to yield products that are not as susceptible as CH_3OH to overoxidation. In this respect, Román-Leshkov and co-workers showed that Cu-exchanged mordenite zeolites are active for the production of acetic acid from CH_4 via tandem oxidation and carbonylation.[109] This transformation is possible by virtue of a cooperative catalytic effect between redox-active copper sites and carbonylation-active acid sites. Notably, since the acid sites in the 8-member ring side pockets of MOR are the only carbonylation-active sites in the zeolite, acetic acid production from CH_4 in Cu-MOR implies a previously unknown step in the mechanism involving CH_3OH migration from the copper center to the acid site in the side pocket in similar fashion to the methoxy mobility observed in Fe-based catalysts.[71-72] Industrial implementation of CH_4 activation chemistries could thus potentially lie in the removal of these initially activated C-H species into products that are less susceptible to subsequent oxidation events.

The concept of protecting CH_3OH from over oxidation is, therefore, vital for the success of CH_4 activation processes. To that end, successful CH_4 activation should be pursued by both designing catalysts with improved activity (e.g., higher active site loadings, tuning of electronic structure and local environment) and by scavenging intermediates resulting from initial C-H activation in order to form stable products that are more resistant to oxidation. For this reason, the “methane-to-methanol” process should be pursued more in terms of simple “methane C-H activation” as opposed to a primary pursuit of CH_3OH when considering the thermodynamic prevalence of complete oxidation of CH_3OH.

4. Aims and Scope of Thesis

The goal of this work then is to address the open questions described in Section I.3 specifically applied to the first-reported catalytic process for the conversion of CH_4 to CH_3OH over Cu-exchanged zeolites using oxygen as the sole oxidant with the goal of moving the process towards industrial application. As previously discussed, Cu-exchanged zeolites for partial CH_4 oxidation are industrially attractive due to the mild conditions and use of abundant reactants, but with reported conversion of 0.001%, there is much room for improvement. Of utmost interest is improving CH_4 conversion while maintaining selectivity for CH_3OH or other desirable partial oxidation products. Thus, this thesis will address the open questions by:

- Elucidating a reaction pathway for the catalytic conversion of CH_4 to CH_3OH
- Identifying the active site(s) for the catalytic conversion of CH_4 to CH_3OH

  and building upon these two aims

- Designing an improved process for catalytic CH_4 conversion by scavenging CH_3OH

Chapter II describes elucidation of a reaction pathway for the catalytic conversion of CH_4 to CH_3OH. By employing kinetic experiments (contact time, partial pressure, and temperature variations), I generate important kinetic insight regarding the role of each reactant. Specifically, I demonstrate the reaction pathway proceeds sequentially from CH_4 to CH_3OH to CO_2 where C-H scission of CH_4 is rate-limiting and re-oxidation of the active site is not rate-limiting. Furthermore, H_2O and protons are required for desorption of CH_3OH but H_2O is not kinetically relevant. In the absence of H_2O, CO_2 is the only product. High partial oxidation selectivity can be obtained with high methane and water partial pressures.

Chapter III then discusses the identification of a $[Cu\text{-}O\text{-}Cu]^{2+}$ motif as the active site responsible for the selective and catalytic conversion of CH_4 to CH_3OH. Chemical titration with ammonia (NH_3) and *in situ* x-ray absorption spectroscopy were combined to monitor Cu speciation under CH_3OH synthesis conditions. I hypothesize this motif forms *in situ* via the diffusion of hydrated Cu ions between Brønsted acid sites within the cages of SSZ-13 zeolites. Various Cu configurations may be present and active for methane oxidation, but a dimeric Cu motif is the primary active site. NH_3 titration demonstrates the Cu dimer motif is destroyed in the presence of NH_3 and can then form reversibly upon the complete desorption of NH_3. Thus, zeolites with moderate Cu loadings and an abundance of Al are required to promote the formation of Cu dimers selective for partial CH_4 oxidation.

Building on the work of Chapter III, Chapter IV investigates isolated Cu sites within zeolites for catalytic CH_4 to CH_3OH conversion. Zeolites with low Al content (Si/Al = 76 and 160) and similar Cu contents were studied with similar kinetic experiments as in Chapter II and combined with *in situ* x-ray absorption spectroscopy. Low Al content was chosen to prevent the diffusion of hydrated Cu ions to form Cu dimers. Product formation occurs by a parallel pathway where O_2 activation is partially rate-determining along with C-H scission of CH_4. *In situ* x-ray absorption spectroscopy suggests isolated Cu ions can be obtained but other species may be present. The species present within these low Al zeolites are distinct from the Cu dimers active for selective CH_4 oxidation. These results indicate zeolites with dilute Al promote formation of Cu sites that are active, but unselective, for partial CH_4 oxidation, and are not desirable for industrial application.

Chapter V then combines the learnings from Chapters II to IV to design an improved process for catalytic partial CH_4 oxidation. Inspired by methane monooxygenases that selectively transform CH_4 into CH_3OH via a chemical gating system, I demonstrate the implementation of a tandem reaction system for the catalytic conversion of CH_4 to CH_3OH to toluene using a copper-exchanged zeolite in combination with a proton-form zeolite. This tandem partial oxidation and alkylation system circumvents the thermodynamic CH_4 selectivity-conversion limit by chemically scavenging methanol by benzene alkylation to produce toluene. Introduction of a benzene co-feed and an H-ZSM-5 catalyst resulted in 84% toluene selectivity at 663 K and 1 bar and 89% selectivity at 543 K and 11 bar. Comparable conditions for partially oxidizing CH_4 to CH_3OH resulted in only 2% and 48% selectivity towards CH_3OH, respectively. We attained 72% desirable product selectivity (toluene and xylene) at 0.6% CH_4 conversion at 11 bar and 603 K, corresponding to 19,000 $\mu mol_{CH3OH}\ mol_{Cu}^{-1}\ min^{-1}$, which represents a 14x increase in yield for CH_4 activation over Cu-exchanged zeolites. These findings provide a pathway towards achieving industrially relevant CH_4 conversion and product selectivity at mild conditions.

Finally, Chapter VI summarizes the key findings of this work and an outlook for future directions. Specifically,

- The catalytic conversion of CH_4-to-CH_3OH over Cu-exchanged zeolites proceeds selectively via a sequential pathway over $[Cu\text{-}O\text{-}Cu]^{2+}$ with C-H bond scission of CH_4 as the rate-determining step,
- High CH_3OH selectivity can be obtained with high P_{CH4} and P_{H2O} with zeolites with high Al and low Cu content,
- $[Cu\text{-}O\text{-}Cu]^{2+}$ dimers are hypothesized to form by diffusion of hydrated Cu ions,
- Isolated Cu ions are active for CH_4 activation, but result in a majority of CO_2 instead of CH_3OH. O_2 activation over these sites is partially rate-determining.
- To break the selectivity-conversion limit of CH_4, stabilization or scavenging of CH_3OH is necessary,

- Aromatic alkylation over proton-form zeolites is an ideal chemistry for CH_3OH scavenging, enabling >70% selectivity for partial oxidation products as CH_4 conversion approaches 1%, representing an almost three order of magnitude increase from the beginning of this work,

  and

- Future work for CH_4 activation should focus on engineering catalysts and processes to enable improved CH_3OH scavenging.

II. Elucidation of a Reaction Pathway for Catalytic Methane Oxidation

1. Motivation

Narsimhan et al. demonstrated the first instance of a continuous, gas phase catalytic process for the direct conversion of CH_4 to methanol.[91] The system used Cu-exchanged zeolites to produce methanol using exclusively CH_4, H_2O, and O_2 at 473 K. Importantly, this process featured high selectivity across a wide range of zeolite topologies, albeit at very low conversion (0.001%). Because this process is continuous, fundamental understanding on the conversion of CH_4 to methanol over Cu-exchanged zeolites can be elicited with kinetic experiments. This fundamental understanding can then be used for catalyst and process improvement.[1] Primarily, open questions center on the reaction pathway for product formation. Within this context, of particular interest are the role of each reactant, the rate-controlling step(s), and process conditions and catalyst requirements to facilitate CH_3OH formation. This work, thus, for the first time, details the kinetics of Cu-exchanged zeolites for the continuous catalytic partial oxidation of methane to methanol using dioxygen in the presence of water.

Herein, advanced synthesis techniques coupled with rigorous kinetic analysis served to identify the reaction pathway for the direct, steady state catalytic conversion of CH_4 to methanol in copper-exchanged zeolites. Kinetic experiments were performed on zeolites with the chabazite (CHA) topology, composed of 8 x 8 x 12 Å cages interconnected by windows with a maximum pore diameter of 3.8 Å[111]. Although H_2O and zeolitic protons are kinetically inconsequential, they are necessary for the desorption of CH_3OH. Excess Cu (Cu/cage > 0.3) resulted in nanoparticle formation and unselective oxidation of CH_4 to CO_2. The fundamental examination of CH_4 activation kinetics and conversion pathways provides a roadmap for the optimization of low-temperature CH_4-to-methanol technologies.

2. Reaction Pathway Elucidation via Kinetic Experiments

Elucidation of a reaction pathway for the direct conversion of CH_4 to methanol necessitates control of Cu ion speciation, and therefore aluminum distribution, within the zeolite. We employed select synthetic methods to create a suite of catalysts with varied Cu content and Al speciation to study the effects of Cu distribution on C–H activation.[112, 113] Synthesis, characterization, and catalyst compositional details are given in II.6 Supporting Informati and summarized in Table II-1. In this chapter and Chapter III, catalysts designated as Cu-CHA(x) are copper-exchanged SSZ-13 zeolites with x Cu atoms per 8 x 8 x 12 Å cage.

Reaction rates were measured under kinetic control (Figure II-10, Figure II-11, Figure II-12). Reaction conditions were chosen to produce CH_3OH, CH_3OCH_3 (DME), and CO_2 in yields large enough to aid in reaction pathway analysis, even though over 95% selectivity to CH_3OH can be achieved via reaction conditions and catalyst choice (Figure II-13). A first-order delplot constructed from a kinetic study of a representative catalyst (Cu-CHA(0.11), Figure II-1A) indicates a sequential reaction pathway in which CH_4 can be first partially oxidized to CH_3OH before secondary downstream oxidation to CO_2.

Accordingly, the total rate of C–H activation was analyzed as the sum of all products formed ($r_{total}=r_{CH3OH}+2r_{DME}+r_{CO2}$). Kinetic analysis revealed a near first-order dependence of the C–H activation rate on P_{CH4} (Figure II-1B, implying weak binding of CH_4 to the active site. The near second-order dependence of DME formation rates on P_{CH4} is consistent with a bimolecular dehydration of methanol over bare Brønsted acid sites. C–H activation rates exhibited a near zero-order dependence on P_{O2} while CO_2 formation rates exhibited a linear dependence on O_2 partial pressure at P_{O2} < 0.1 kPa (Figure II-1C), suggesting that the overoxidation process involves direct reaction of a C_1 intermediate with either unbound O_2 or with a low-coverage of O_2-derived species. The weak dependence of C–H activation on P_{O2} indicates that the reoxidation of Cu-active sites prior to C–H activation in the redox cycle is not rate-limiting. Total C–H activation rates were unaffected by H_2O partial pressure (Figure II-1D and Figure II-2), and the partial oxidation selectivity decreased with decreasing water partial pressure to the limit of 0% in the absence of a H_2O co-feed (Figure II-2).

Table II-1. Composition and synthesis method for SSZ-13 zeolites.

Catalyst	Composition			Cu Content (wt%)	Cu/cage	Synthesis Method
	Si/Al	Cu/Al	Na/Al			
H-CHA	8.8	-	-	-	-	2-6MR[b]
Cu-CHA(0.05)	8.8	0.04	-	0.41	0.05	2-6MR, Cu-IE[c]
Cu-CHA(0.10)	8.8	0.08	-	0.76	0.10	2-6MR, Cu-IE
Cu-CHA(0.12)	8.8	0.10	-	0.90	0.12	2-6MR, Cu-IE
Cu-CHA(0.20)	8.8	0.16	-	1.6	0.20	2-6MR, Cu-IE
Cu-CHA(0.23)	8.8	0.19	-	1.9	0.23	2-6MR, Cu-IE
Cu-CHA(0.42)	8.8	0.34	-	3.3	0.42	2-6MR, Cu-IE
NH_4-Cu-CHA(0.16)	8.8	0.13	-	1.3	0.16	2-6MR, NH_4[d], Cu-IE
Cu-CHA(0.11)	23	0.22	-	0.92	0.11	1-6MR[e]
Cu-CHA(0.04)	21	0.07	-	0.33	0.04	1-6MR
Na-Cu-CHA(0.12)	26	0.27	0.51	1.0	0.12	2-6MR-Cu[f]
Cu-CHA(0.13)	11	0.13	-	1.1	0.13	1-6MR
Cu-CHA(0.72)	12	0.76	-	5.7	0.72	1-6MR, 2x Cu-IE
1Al-Cu-CHA	76	0.23	-	0.31	0.04	F-[g]
0Al-Cu-CHA	∞			1.0		IWI[h]

[a]Catalyst nomenclature is defined by extraframework cations present and composition where Cu-CHA(*x*) denotes an SSZ-13 catalyst with *x* Cu atoms per 8 x 8 x 12 Å cage.

[b]2-6MR denotes a SSZ-13 synthesis with Na in the synthesis gel, following which the zeolite was ion-exchanged twice with NH4NO3 to remove Na

[c]Cu-IE denotes Cu was introduced via aqueous copper ion-exchange

[d]NH4 denotes that following ion-exchange with NH4NO3, the zeolite was not calcined to remove NH3

[e]1-6MR denotes a SSZ-13 synthesis without Na in the synthesis gel and the direct incorporation of Cu using TEPA

[f]2-6MR-Cu denotes a SSZ-13 synthesis with Na present in the synthesis gel and the direct incorporation of Cu using TEPA

[g]F- denotes a SSZ-13 synthesis using fluoride media

[h]IWI denotes preparation via incipient wetness impregnation of a defect-free SSZ-13

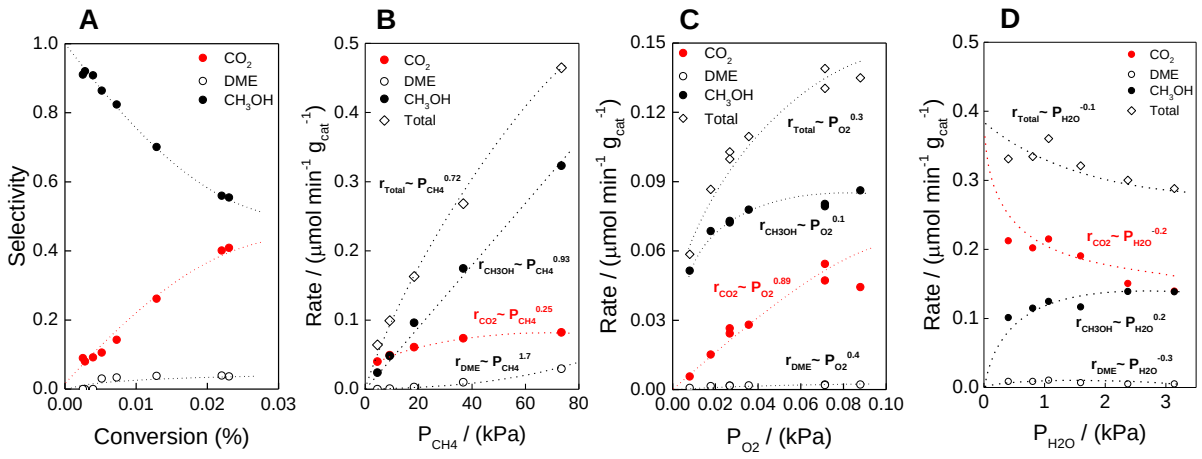

Figure II-1. A. Product selectivity as a function of conversion. Product formation rates as a function of **B.** P_{CH4}, **C.** P_{O2}, and **D.** P_{H2O} variations over Cu-CHA(0.11). $r_{Total}=r_{CH3OH}+2r_{DME}+r_{CO2}$, T = 543 K, 0.25 gcat, 25 - 200 sccm total flow, P_{CH4} = 18 kPa, P_{O2} = 0.09 kPa, P_{H2O} = 3.14 kPa, bal He except as noted.

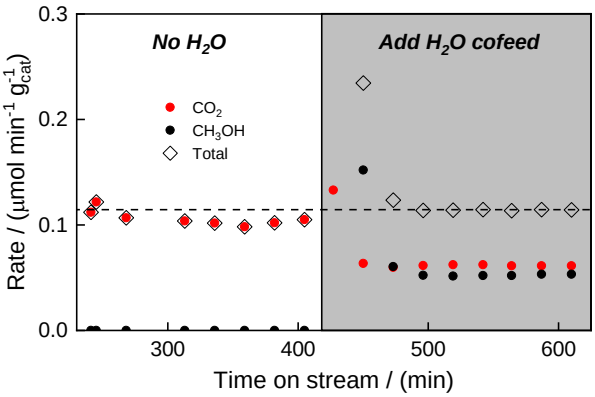

Figure II-2. Product formation rates in the absence and presence of H_2O co-feed. Cu-CHA(0.23), 0.25 g_{cat}, 543 K, 25 sccm, P_{CH4} = 18 kPa, P_{O2} = 0.09 kPa, P_{H2O} = 3.14 kPa, bal He. In the absence of water, He constituted the makeup gas.

These results, thus, implicate a reaction pathway where a rate-determining C–H scission event catalyzed by an oxidized copper-oxygen species is followed by either (i) H_2O-facilitated methanol desorption or (ii) secondary oxidation of a C_1 intermediate to CO_2. Previous reports have hypothesized that H_2O substantially decreases the desorption energy of surface-bound methoxy species to form methanol after initial C–H scission events.[83, 100 87, 114-115] Lower partial pressures of H_2O decrease the probability of methanol desorption events, resulting in more frequent interactions of activated C_1 intermediates with gas phase O_2 and increased total oxidation (Figure II-1D).

The apparent activation energy of C–H scission was 97 kJ mol^{-1} (Figure II-3). This barrier, indicative of the energetic difference between gas phase reactants and the transition state due to measurement in the P_{CH4} first-order regime, is in close accordance with the 99 kJ mol^{-1} C–H activation barrier calculated by Zhao et. al.[100] over Cu active sites in mordenite zeolites and other similar computational work.[86, 100] The observed rate-determining C–H scission is in agreement with the previously reported primary kinetic isotope effect during steady state methane-to-methanol reactions using CD_4 over Cu-ZSM-5 catalysts.[91] These observations are summarized schematically in a catalytic cycle in Figure II-4 and highlights C-H scission of CH_4 as rate-determining and the necessity of water for CH_3OH desorption**.** Discussion and evidence for the depicted active site structure are provided in Chapter III.

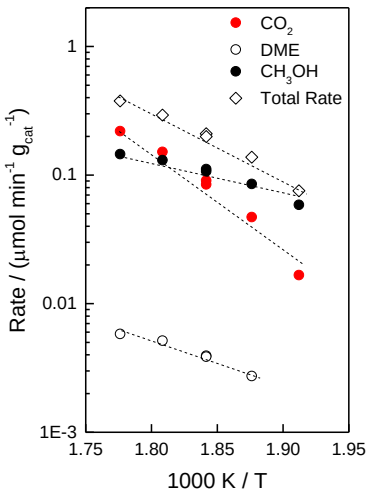

Figure II-3. Product formation rates versus temperature. Measured E_a was 97 kJ mol^{-1}. Cu-CHA(0.11), 0.25 g_{cat}, 523-563 K, 25 sccm, P_{CH4} = 18 kPa, P_{O2} = 0.09 kPa, P_{H2O} = 3.14 kPa, bal He.

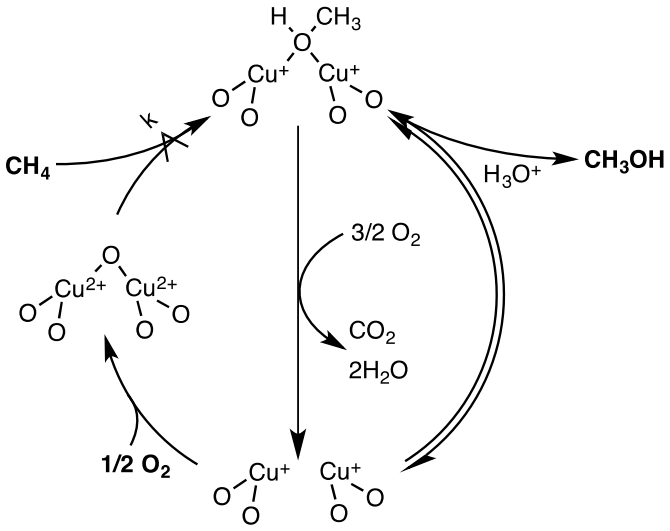

Figure II-4. Depiction of proposed hypothesized Cu-CHA. C-H scission of CH_4 is rate-determining, re-oxidation of the active site is not rate-determining and water is required for desorption of CH_3OH. In the absence of water, CO_2 is the only product. Discussion of the active site structure is provided in Chapter III.

3. Comparison of Kinetic Dependences Across Cu-SSZ-13 Compositions

Similar kinetic experiments were performed using the 14 Cu-CHA samples listed in Table II-1, whose Al speciation and Cu/Al compositions were controlled synthetically to probe the impacts of metal loading and Cu site speciation upon kinetics and product selectivity. Kinetic dependences for all samples are provided in Table II-2.

Table II-2. Reactant order dependencies and apparent activation energies of all catalysts. 0.25 g_{cat}, baseline conditions were 543 K, 25 sccm, P_{CH4} = 18 kPa, P_{O2} = 0.09 kPa, P_{H2O} = 3.14 kPa, bal He. E_a was measured from 523 – 563 K.

Catalyst	H^+ / Cage[a] Max (*min*)	Reactant Order Dependency			E_a (kJ mol^{-1})
		CH_4	O_2	H_2O	
Cu-CHA(0.05)	1.17 (*1.12*)	0.74	0	-	99
Cu-CHA(0.10)	1.12 (*1.02*)	-	-	-	92
Cu-CHA(0.12)	1.10 (*0.98*)	0.73	-	-	99
Cu-CHA(0.20)	1.02 (*0.82*)	0.66	0.35	-	84
Cu-CHA(0.23)	0.99 (*0.76*)	0.65	-	-	92
Cu-CHA(0.42)	0.80 (*0.38*)	0.59	0.37	-	110
NH_4-Cu-CHA(0.16)	1.09 (*0*)[b]	0.82[d]	0.2	-	100
Cu-CHA(0.11)	0.39 (*0.28*)	0.72	0.3	-0.1	97
Cu-CHA(0.04)	0.51 (*0.47*)	0.75	-	-	94
Na-Cu-CHA(0.12)	0.10 (*0*)	-	-	-	-
Cu-CHA(0.13)	0.87 (*0.74*)	-	-	-	-
Cu-CHA(0.72)	0.20 (*0*)	-	-	-	128
1-Al-Cu-CHA	0.16 (*0*)[c]	0.32	0.95	-	-
0Al-Cu-CHA	0 (*0*)	0.85	0.39	-	140

[a]Theoretical maximum and minimum free H^+ content of the zeolite normalized per CHA cage (12 T-sites per cage where a T-site is either a SiO_4 or AlO_4 tetrahedron). Maximum was calculated assuming every Cu resides as Cu(I) and is charge-balancing one Al T-site, and min was calculated by assuming every Cu resides as Cu(II) and is charge-balancing two proximate Al T-sites.

[b]Maximum was calculated assuming that NH_3 did not bind to any single free proton, and min is assuming that every single free proton has a strongly-bound NH_3.

[c]Maximum was calculated assuming that all Cu species reside as charge-neutral CuO_x nanoparticles and do not charge balance any Al T-sites, whereas min was calculated knowing that the number of Cu atoms exceeds the total framework Al content.

[d]Reactant order dependences were measured following removal of NH_3 from the zeolite.

All catalysts generally exhibited an increasing degree of undesirable downstream oxidation events with increasing conversion (Figure II-6A) as expected from the hypothesized sequential conversion pathway. Catalysts with Cu/cage > 0.3 exhibited lower partial oxidation selectivity than expected based on sequential conversion, suggesting that higher Cu loadings direct the formation of active sites that are unselective towards CH_4 partial oxidation. The purely siliceous 0Al-Cu-CHA sample, which lacked $[AlO_4]^-$ T-sites necessary for directing Cu ion exchange, only contained CuO_x nanoparticles within the CHA pores. This Al-free sample displayed broad UV-vis features in the 20,000 and 40,000 cm^{-1} regions that are associated with copper oxide nanoparticles (Figure II-5).[116-117] This catalyst also exhibited the highest apparent activation energy (140 kJ mol^{-1}, Figure II-14) of all measured catalysts and near 0% selectivity to CH_3OH. Al-containing catalysts with increasing catalyst Cu content above Cu/cage>0.3 also exhibited increasing apparent activation energies, similar UV-Vis features to those observed in 0Al-Cu-CHA (Figure II-5, Table II-2), and low partial oxidation selectivity, implicating the onset of CuO_x nanoparticle formation when exceeding a copper loading of Cu/cage=0.3.

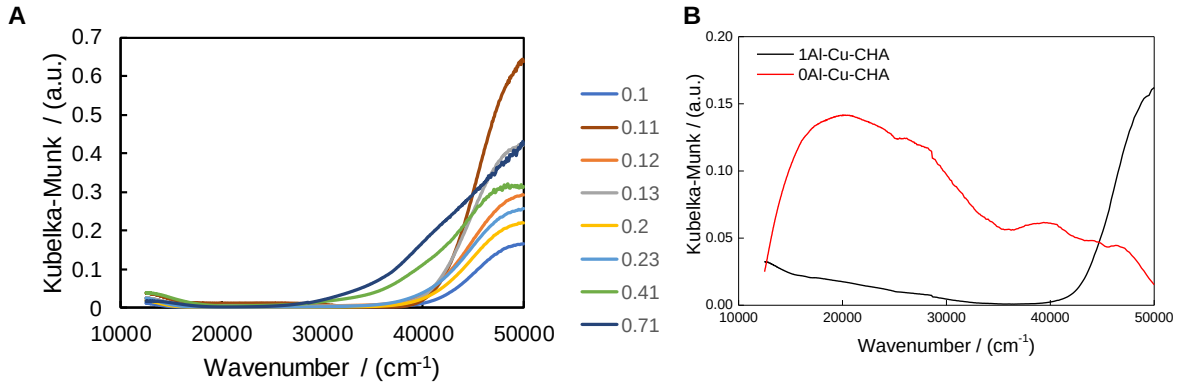

Figure II-5. DRUV of Cu-SSZ-13 catalysts at ambient conditions. **A.** Catalysts with Si/Al < 30. K-M units normalized to mass loading. Legend refers to Cu-CHA(x), where x is the Cu/cage as defined in the main text. **B.** 1Al-Cu-CHA and 0Al-Cu-CHA catalysts. The broad 20,000 – 30,000 cm^{-1} feature and the feature centered around 40,000 cm^{-1} for 0Al-Cu-CHA are consistent with previously reported DRUV of Cu_xO_y.[116-118] Cu-CHA(0.41) and Cu-CHA(0.71) display the same 40,000 cm^{-1} feature consistent with small CuO_x nanoparticles.

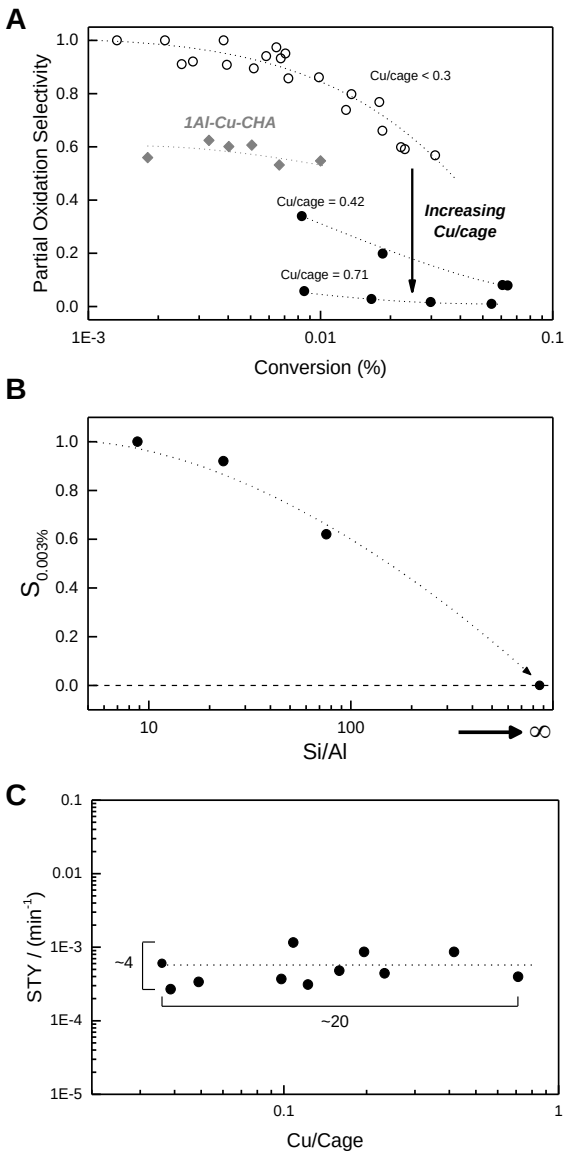

Figure II-6. A. Selectivity as a function of CH_4 for separate catalyst samples. All catalyst properties are listed in Table II-1. **B.** Partial oxidation selectivity at 0.003% conversion versus decreasing Al content for four catalyst samples. **C.** Cu-normalized total product formation rates (Site time yield, STY) as a function of Cu/cage Reaction conditions: 0.25 g_{cat}, 543 K, 25 - 200 sccm total flow, P_{CH4} = 18 kPa, P_{O2} = 0.09 kPa.

In addition, a sample with a low Al content (1Al-Cu-CHA, Si/Al = 76) was synthesized to isolate, on average, 1 Al T-site for every ~3 cages (one CHA cage consists of 36 T-sites that are each shared between three cages). This sample featured only ~50% selectivity to methanol at Cu/cage<0.2, a sub-first order dependence on P_{CH4}, and a first order dependence on P_{O2} (Figure II-6A, Figure II-7A, and Figure II-7B), differing significantly from all other Cu-CHA zeolites investigated. Spectroscopic studies of 1Al-Cu-CHA under working conditions indicated the presence of isolated Cu sites (*vide infra*). To further illustrate the effect of Si/Al ratio, Figure II-6B compares partial oxidation selectivity of four catalysts of differing Al content and similar Cu loadings below 0.2 Cu/cage at isoconversion (0.003%). Decreasing available Al content resulted in decreased selectivity to partial oxidation (Figure II-15 presents the effect of reducing available Al by the introduction of Na^+ ions), underscoring the importance of zeolitic H^+ species in the turnover cycle (*vide infra*). Moreover, a fully siliceous zeolite without ion-exchanged Cu species present displayed 0% selectivity towards methanol (0Al-Cu-CHA, Figure II-14), suggesting that partial oxidation of methane requires ion-exchanged Cu species within the zeolite.

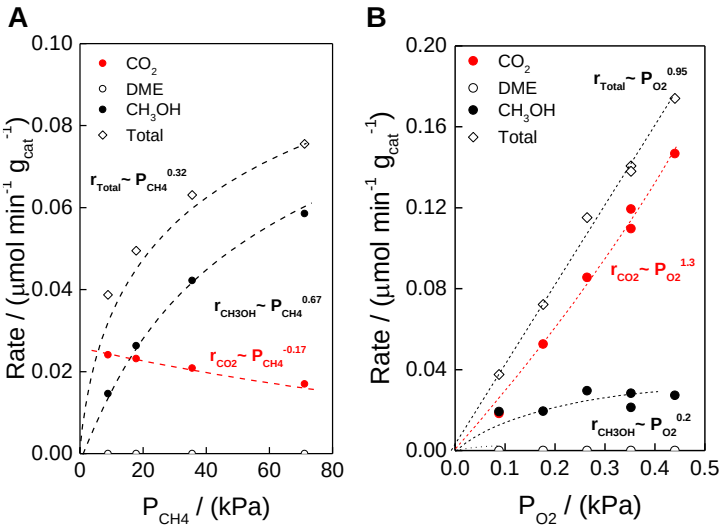

Figure II-7. Product formation rates as a function of **A.** CH_4 partial pressure and **B**. O_2 partial pressure. 1Al-Cu-CHA, 0.25 g_{cat}, 543 K, 25 sccm, P_{O2} = 0.09 kPa, P_{H2O} = 3.14 kPa, bal He.

Figure II-6C shows the overall site time yield across all catalysts (STY; the total rate of C–H activation normalized by Cu content) varied by a factor of 4 over a span of Cu-loading that varied by a factor of 20. This minimal variation in STY across a large range of Cu loadings in conjunction with similar kinetic pressure dependences and energetic barriers (Table II-2) implies the mechanisms and energetics of C–H activation are similar across numerous Cu-centric active sites, excluding 1Al-Cu-CHA. Slight variations in STY and kinetic dependences may be indicative of a small subset of Cu species in some catalyst samples that are either inactive for C-H activation or distinct from the selective partial oxidation sites present in Cu/Cage < 0.3 samples. These results highlight the necessity of moderate Cu loadings and high Al content to direct the synthesis of well-dispersed partial oxidation active sites.

4. Conclusions

The reaction pathway for the direct conversion of CH_4 to CH_3OH was elucidated with kinetic experiments. Low Cu loadings (Cu/cage < 0.3) with sufficiently high Al content are critical for catalyzing selective partial oxidation of CH_4. Higher Cu loadings resulted in the formation of Cu_xO_y nanoclusters that promote complete CH_4 oxidation to CO_2. CH_4 activation proceeds via rate-determining C-H scission to form a surface-bound C1 intermediate that can either be desorbed as methanol in the presence of H_2O/H^+ or completely oxidized to CO_2 by gas phase O_2. O_2 is required for active site re-oxidation but this process is not rate-limiting. H_2O is not kinetically relevant but required for CH_3OH desorption. High partial oxidation selectivity can be targeted by utilizing (1) reaction conditions of high CH_4 partial pressure in the presence of H_2O, and (ii) catalysts containing a high density of Brønsted acid sites and moderate Cu loadings (Cu/cage < 0.3). This work highlights the importance of mechanistic understanding to guide reaction condition selection and catalyst composition for process optimization

5. *Acknowledgements*

The authors gratefully acknowledge the financial support of ExxonMobil. K.D. acknowledges the partial support from the National Science Foundation Graduate Research Fellowship under Grant No. 1122374. Any opinion, findings, and conclusions or recommendations expressed in this material are those of the author(s) and do not necessarily reflect the views of the National Science Foundation. This work made use of the MRSEC Shared Experimental Facilities at MIT, supported by the National Science Foundation under award number DMR-14-19807. The authors thank Z. Wang for help in ICP data collection, M. Stone and T. Gani for comments on the manuscript, and A. Stubbs and X. He for helpful discussion.

6. *Supporting Information*

6.1. Methods

6.1.1. Catalyst Synthesis

Synthesis of H-CHA (Si/Al = 8.8)

To 22.7 g of colloidal silicon dioxide (Ludox® LS-30), 1.1 g of aluminum hydroxide (80.3 wt % $Al(OH)_3$, SPI Pharma 0250) was dissolved. Following, 6.0 g of aqueous sodium hydroxide (23.3 wt%) was added to the solution. 48.9 g of H_2O and finally 29.3 g of N,N,N-trimethyl-1-adamantanamine hydroxide solution (TMAdaOH, 25 wt % in H_2O, Sachem) were added. The final composition of the solution was 1 SiO_2: 0.1 $Al(OH)_3$: 0.3 NaOH: 0.3 TMAdaOH: 45 H_2O. The solution was stirred at room temperature for 6 h, transferred to six 23-mL Teflon-lined stainless steel autoclaves (No. 4749, Parr Instruments) and subjected to hydrothermal treatment at 433 K for 5 days in an oven under autogenous pressure and rotation (60 rpm). After hydrothermal treatment, the product was separated from the mother liquor by centrifugation, washed several times with distilled H_2O and dried at 393 K. The zeolite was calcined under dry air (Dry Size 300, Airgas) with the following temperature profile: heat 1 K min^{-1} to 423 K and hold for 1 h at 423 K, heat 1 K min^{-1} to 623 K and hold for 1 h at 623 K, and lastly heat 1 K min^{-1} to 853 K and hold for 10 h.

Synthesis of 1-6MR Cu-SSZ-13

1-6MR Cu-SSZ-13 was synthesized in a similar manner as H-CHA and is a modification of the works of Di Iorio et al.[113] and Martinez-Franco et al.[119] One-pot methods have been reported for the synthesis for Cu-SSZ-13 via the use of tetraethylenepentamine (TEPA).[120] TEPA acts as both a structure-directing agent and a chelating agent for Cu. Simulations have demonstrated that Cu-TEPA localizes one Cu per cage.[120] However, reported syntheses indicate a prevalence of copper oxides due to the amount of Cu incorporated into the zeolite when TEPA is used. To limit the presence of copper oxides, we utilized a cooperative SDA synthesis method; $^{-}$OH and TMAdaOH content was maintained constant and Cu content was controlled by Cu^{2+} loading in the synthesis gel. TEPA was added in 10% excess of the stoichiometric quantity (1 TEPA:1 Cu^{2+}). To obtain a catalyst with only isolated Al, synthesis gels were entirely devoid of Na^{+} and ionic charge was instead balanced with $TMAda^{+}$. The combination of these methods affords control over the fraction of paired framework Al and zeolite composition (Al, Na, and Cu contents) in a one-step method without the need for additional metal incorporation via ion exchange. Si/Al ratios between 10 and 25 were attainable with Cu loadings ranging from 0 to 0.60.

Copper sulfate pentahydrate (98% trace metals basis, Sigma-Aldrich) was first dissolved in water followed by the addition of tetraethylenepentamine (TEPA, technical grade, Sigma-Aldrich) and stirred for an hour before the addition of TMAdaOH. Following, aluminum hydroxide was dissolved in the solution before fumed silica (Sigma-Aldrich, 99.8%) was added. The final composition of the mixture was 1 SiO_2: x $Al(OH)_3$: 0.4 TMAdaOH: 44 H_2O: z $CuSO_4$: 1.1z TEPA where $0.1 \leq x \leq 0.03$ and $0 \leq z \leq 0.6$. The solution was subjected to the same aging, thermal, purification and calcination treatments as described for H-CHA.

Ammonium exchange

To remove Na from the synthesized SSZ-13 catalyst, 1 g of zeolite was stirred in 60 mL of a 1.0 M solution of ammonium nitrate (≥ 99%, Sigma-Aldrich) for 16 h at room temperature. The suspension was filtered at room temperature, rinsed with 300 mL of deionized H_2O, and the recovered zeolite was immediately subjected to a second ion exchange under the same conditions. Following, the zeolite was dried overnight at 393 K in stagnant air and calcined following the same profile described above.

Copper exchange

1 g of zeolite was stirred in 150 mL of 0.0005 - 0.05 M solutions of copper (II) acetate monohydrate (> 99%, Sigma-Aldrich) at room temperature for between one to two days. The suspension was then either filtered at room temperature and rinsed with 400 mL of deionized H_2O or recovered and washed via centrifugation. The zeolite was dried overnight at 393 K in a drying oven and subsequently calcined using the same procedure as described above. If needed, some catalysts were subjected to one to two additional Cu exchanges to achieve a targeted Cu loading.

Synthesis of Na-Cu-CHA(0.12)

Na-Cu-CHA(26, 0.27) was synthesized in the same manner as the 1-6MR Cu-SSZ-13 samples except NaOH was added to the solution following addition of TMAdaOH. The final composition of the mixture was 1 SiO_2: 0.03 $Al(OH)_3$: 0.2 NaOH: 0.2 TMAdaOH: 44 H_2O: 0.01 $CuSO_4$: 0.011 TEPA.

Synthesis of 1Al-Cu-CHA

1Al-Cu-CHA was synthesized based on the work of Eilertsen, et al.[121] Briefly, copper sulfate pentahydrate, TEPA, and TMAdaOH were stirred for 30 min in a PTFE jar. Following, aluminum hydroxide was added to the solution and stirred until the solution was clear. In a separate container, ethanol (200 proof, Koptec) and tetraethylorthosilicate (>99.0% (GC), Sigma-Aldrich) were stirred uncovered for 30 min. The ethanol and tetraethylorthosilicate solution was added to the copper solution and stirred uncovered until the target water ratio was obtained. Hydrofluoric acid (48 wt% in H_2O, >99.99% trace metals basis, Sigma-Aldrich) was then added and the gel was homogenized by hand. **Caution: HF Use proper personal protective equipment, ventilation, and additional safety measures.** The final composition of the mixture was 100 SiO_2: 1.33 $Al(OH)_3$: 50 TMAdaOH: 300 H_2O: 50 HF: 0.51 $CuSO_4$: 0.56 TEPA. The gel was transferred to a 23-mL Teflon-lined stainless steel autoclave and subjected to hydrothermal treatment at 428 K for 40 h in an oven under autogenous pressure and rotation (60 rpm). The zeolite was subjected to the same purification and calcination treatments as described for H-CHA.

Synthesis of Cu_xO_y in defect-free SSZ-13 (0Al-Cu-CHA)

Defect-free SSZ-13 was synthesized according to the method of Díaz-Cabañas et al.[122] Copper (II) nitrate trihydrate (Sigma-Aldrich, puriss. p.a., 99-104%) was incorporated into the zeolite via incipient wetness impregnation to achieve a 1 wt% Cu loading. To 0.5 of defect-free SSZ-13, 0.29 g of 0.27 M $Cu(NO_3)_2 \cdot 3\ H_2O$ (aq) was added dropwise. The catalyst was calcined with the same temperature profile as previously described.

6.1.2. Catalyst Characterization Techniques

Elemental analysis

Copper, sodium and aluminum contents were determined using inductively coupled plasma atomic emission spectroscopy (ICP-AES, Agilent 5100) or inductively coupled plasma mass spectrometry (ICP-MS, Agilent 7900). 5 – 10 mg of zeolite were placed in a polyethylene microfuge tube (1.5 mL) and digested in 20 µL hydrofluoric acid (48 wt %, trace metals basis, Sigma-Aldrich) for 2 h. The hydrofluoric acid solution was diluted to a total mass of 10.0 g using 2 wt % aqueous nitric acid (HNO_3) (veritas purity, GFS Chemicals). When using ICP-MS, 1 mL of these solutions were diluted once more to 10 mL solution total. A six point calibration curve was built using ICP standard solutions of 1,000 ppm Cu in 2 wt% HNO_3, 1,000 ppm Al in 2 wt% HNO_3 and 1,000 ppm Na in 2 wt% HNO_3. All standard solutions were purchased from Sigma-Aldrich (TraceCERT).

Calculations of molar ratios Si/Al$_{tot}$ and Cu/Al$_{tot}$.

The unit cell of a zeolite is given by:

$$H_x^+ Na_y^+ Cu_z^{2+} (AlO_2)_n^- (SiO_2)_m (H_2O)_k$$

where subscripts refer to the molar ratios of each component within the unit cell of a zeolite. Local charge balance was assumed to occur within the zeolite, requiring $x = n - 2z - y$.

From the unit cell given above, the mass balance of the unit cell is given by the following equation on a per gram zeolite basis:

$$1 = a\frac{g\ SiO_2}{g\ zeolite} + b\frac{g\ [AlO_2]^-}{g\ zeolite} + c\frac{g\ Cu^{2+}}{g\ zeolite} + d\frac{g\ Na^+}{g\ zeolite} + e\frac{g\ H^+}{g\ zeolite} + f\frac{g\ H_2O}{g\ zeolite}$$

where each coefficient represents the weight percent of each species. The weight percent of Al, Cu and Na were directly calculated using ICP-AES, allowing b, c, and d to be determined. Converting the weight percentages of Al, Cu and Na to mole percentages per gram zeolite, e was then calculated using the local charge balance of cations on the zeolite framework. The weight percentage of H_2O (f) was assumed to be equal to the weight percentage of H_2O in the zeolite framework unit cell (2 – 7 wt %).[123] The mass balance was then solved for the weight percentage of SiO_2 (a).

Si/Al$_{tot}$ was calculated by $\frac{Si}{Al_{tot}} = \frac{a}{b}\frac{m_{AlO2}}{m_{SiO2}} \times \frac{1\ mol\ Si}{1 mol\ SiO_2} \times \frac{1\ mol\ AlO_2}{1\ mol\ Al}$

where m_i is the molar mass of element i.

Cu/Al$_{tot}$ was calculated by $\frac{Cu}{Al_{tot}} = \frac{c}{b}\frac{m_{AlO2}}{m_{Cu}} \times \frac{1\ mol\ AlO_2}{1\ mol\ Al}$

Powder X-Ray Diffraction

The crystal structures of zeolite catalysts were determined from powder x-ray diffraction patterns collected using a Bruker D8 diffractometer using Cu-Kα radiation (λ = 1.5418 Å, 40 kV, 40 mA). Data were recorded in the range of 3-40 2θ with an angular step size of 0.02° and a rate of 4° min^{-1}.

UV-Vis-NIR Spectroscopy

UV-Vis-NIR spectroscopy was performed on a Cary 5000 UV-Vis-NIR spectrometer (Agilent Technologies) equipped with a DiffusIR diffuse reflectance accessory (PIKE Technologies). Gas phase flow conditions and temperature were maintained to mimic those obtained during steady state catalysis: T=543 K, ambient pressure, 0.09 kPa O_2, 3 kPa H_2O, 18 kPa CH_4, balance Helium, total flow of 25 sccm. Absolute reflectance was measured at ambient conditions from 11,100 cm^{-1} to 52,600 cm^{-1} with a scan rate of 11,700 cm^{-1} min^{-1}. All spectra were normalized with respect to a background spectra of hydrated H-SSZ-13 (Si/Al = 8.8).

Surface Area and Pore Volume Quantification

Nitrogen adsorption and desorption isotherms were measured on a Quantachrome Autosorb iQ apparatus at liquid nitrogen temperature (77 K). Prior to the adsorption analysis, all samples were degassed under vacuum for 12 h at 623 K. Micropore volume was calculated using the t-plot method.

6.1.3. Catalytic CH_4 Oxidation Reactions

CH_4 oxidation reactions were conducted in a continuous, tubular flow reactor (stainless steel tube, O.D. 6.35 mm, I.D. 4.57 mm). The reactor tube was mounted inside of a single-zone furnace (850W / 115V, Applied Test Systems Series 3210). Temperature was controlled using a thermocouple (Omega, model TJ36-CASS-116U) mounted slightly downstream of the catalyst bed connected to a temperature controller (Digi-Sense model 68900-10). 0.25 g of zeolite particles (pelletized and sieved into 250–420 μm particles) were packed between quartz wool plugs and rested on the thermocouple in the middle of the furnace heating zone. Void volume above and below the catalyst bed was filled with borosilicate glass beads to reduce homogeneous combustion. The flow of gases, including He (ultra high purity, Airgas), 1% O_2 in He (ultra high purity, Airgas), and CH_4 (research grade, Airgas) were controlled with independent mass flow controllers (Brooks Instruments LLC). H_2O (typically 3.2 kPa) was introduced into the gas stream using a syringe pump with a heated liquid injection port. Stainless steel gas transfer lines were heated with resistive heating tape from the point of liquid injection until the gas chromatographic analysis unit. Typical reaction pretreatment involved heating under ~50 mL min^{-1} flowing 1% O_2/He from ambient temperature up to a reaction temperature of 543 K unless otherwise specified.

CH_3OH, dimethyl ether (DME), CO_2, and alkane partial pressures evolved during catalytic CH_4 oxidation were quantified using a gas chromatograph (Agilent Technologies, 7890B). The gas chromatograph was equipped with a methanizer, flame ionization detector, and thermal conductivity detector. Three columns were used for product separation: two HP-PLOT Q PT (30 m x 0.53 mm x 40 μm, Agilent #19095P-QO4PT) and HP PLOT Molsieve (30 m x 0.53 mm x 50 μm, Agilent #19095P-MS0E).

Once steady-state CH_3OH production was achieved at 543 K, kinetic experiments were conducted. Contact time variations were performed by proportional alterations of all gas and liquid flow rates in order to maintain contact gas phase partial pressures. Titration experiments were performed by additional flow of 1% NH_3/He (ultra high purity, Airgas) and simultaneous removal of an equimolar flow of helium to maintain a constant space velocity. All reported values for selectivity, rates of product formation, and site time yield were averaged over three data points upon reaching steady-state.

Product quantification

Calibration curves for CH_3OH were constructed using a known vapor pressure of CH_3OH taken into a CH_4 stream. CH_3OH vapor pressure was controlled by immersing the saturator containing CH_3OH into cooling baths at several temperatures (e.g. ice water at 273 K, dry ice in ethanol at 201 K, etc). Relative response factors were calculated using the gas chromatograph between known CH_4 and CH_3OH partial pressures. Calibration curves for CO_2 and DME were constructed by flowing known mixtures of 1% CO_2/He or 10% DME/He and He to a gas chromatograph.

The large partial pressure of CH_4 in the gas stream during catalytic CH_4 oxidation reactions prevented the accurate quantification of CH_4 consumption. As such, CH_4 conversion was assumed to be equal to the total molar flow rate of carbon of all observed products divided by the initial molar flow rate of CH_4:

$$X_{CH4} = \frac{\sum_{i=1}^{N} C_i F_i}{F_{CH4,0}}$$

where X_{CH4} is the conversion of CH_4, F_i is the molar flow rate of product i, C_i is the number of carbon atoms in product i, $\Sigma\ C_iF_i$ is the total molar flow rate of carbon of all products, and $F_{CH4,0}$ is the initial molar flow rate of CH_4.

Product selectivity for catalytic CH_4 oxidation was defined as:

$$S_i = \frac{C_i F_i}{\sum_{i=1}^{N} C_i F_i}$$

where S_i is the selectivity of product *i* on a C-atom basis, C_i is the number of carbon atoms in product *i*, F_i is the molar flow rate of product *i*, and $\Sigma C_i F_i$ is the total molar flow rate of carbon of all products.

Site-time yield (STY) for catalytic CH_4 oxidation was defined as:

$$STY = \frac{\sum_{i=1}^{N} C_i F_i}{N_{Cu}}$$

where N_{Cu} is the number of moles of Cu within the zeolite determined by ICP.

6.2. Referenced Figures and Tables

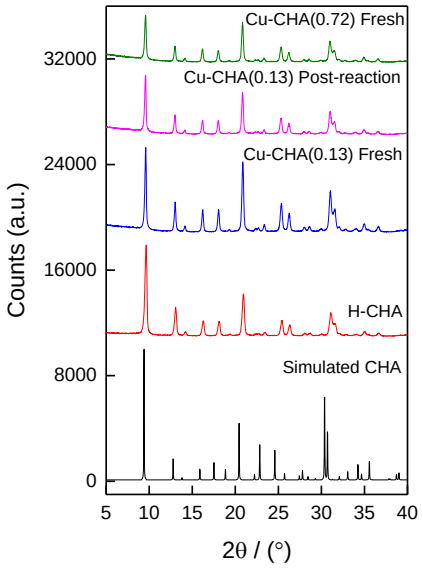

Figure II-8. Powder x-ray diffraction of as-synthesized and post-reaction catalysts. Catalysts displayed expected reflections of CHA and no loss in crystallinity was observed following exposure to methanol synthesis flows.

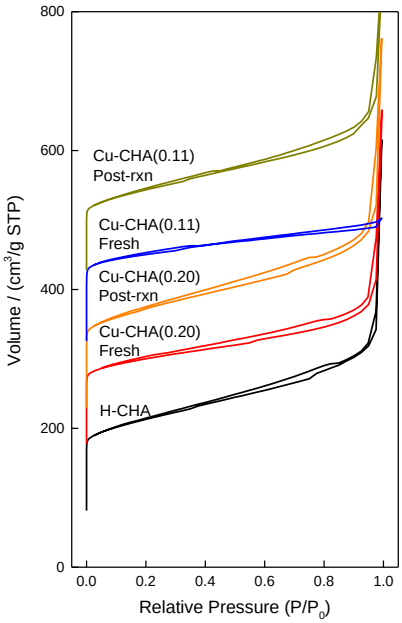

Figure II-9. N_2 physisorption isotherms of as-synthesized and post-reaction catalysts.

Table II-3. Micropore volumes of as-synthesized and post-reaction catalysts, calculated using t-plot method.

Catalyst	Micropore volume (cm^3/g)
Cu-CHA(0.11) Post-reaction	0.20
Cu-CHA(0.11) Fresh	0.23
Cu-CHA(0.20) Post-reaction	0.24
Cu-CHA(0.20) Fresh	0.23
H-CHA	0.23

Kinetic experiments were performed in the absence of heat or mass transfer limitations (Figure II-10 and Table II-4). Under typical reaction conditions, the steady state production of methanol was extremely stable with CH_4 conversion values below 0.1% with no observable deactivation over the course of 100 h on stream (Figure II-11). Methane conversion was negligible when exposing a non-Cu exchanged, Brønsted acid form H-SSZ-13 catalyst to typical reaction conditions. O_2 conversion was typically <10%. Quantifiable products consisted primarily of methanol, CO_2, and DME. CO and ethylene were observed as minor products under some higher temperature reaction conditions. Homogeneous combustion was measured in a blank reactor and accounted for <5% of all products formed (Figure II-12).

Table II-4. Parameters used for verification of absence of heat and mass transfer gradients. GradientCheck for Heterogeneous Catalysis was used.[124] Gaseous properties were obtained from the NIST WebBook's Thermophysical Properties of Fluid Systems.[22]

max r_{obs} (mol kg_{cat}^{-1} s^{-1})	$7.24 \cdot 10^{-6}$
ΔH_{rxn} (kJ mol^{-1})	-127
E_a (kJ mol^{-1})	100
Fractional conversion	0.001
n	1
ρ_{bulk} (kg m^{-3}) (Assumed ε=0.4)	750

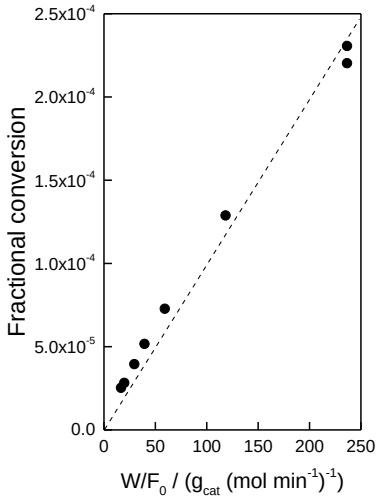

Figure II-10. Fractional conversion versus contact time demonstrates operation in differential conditions. Cu-CHA(0.11), 0.25 g_{cat}, 543 K, 25-200 sccm, P_{CH4} = 18 kPa, P_{O2} = 0.09 kPa, P_{H2O} = 3.14 kPa, bal He.

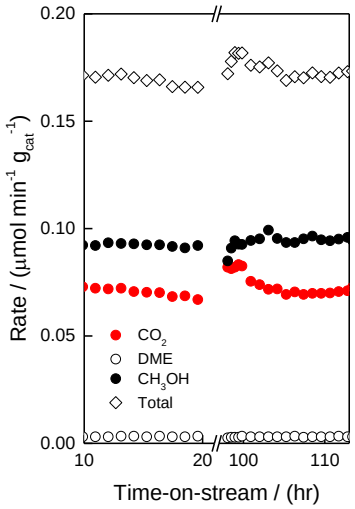

Figure II-11. Product formation rates versus time-on-stream, demonstrating catalyst stability for >4 days on stream. Cu-CHA(0.11), 0.25 g_{cat}, 543 K, 25 sccm, P_{CH4} = 18 kPa, P_{O2} = 0.09 kPa, P_{H2O} = 3.14 kPa, bal He

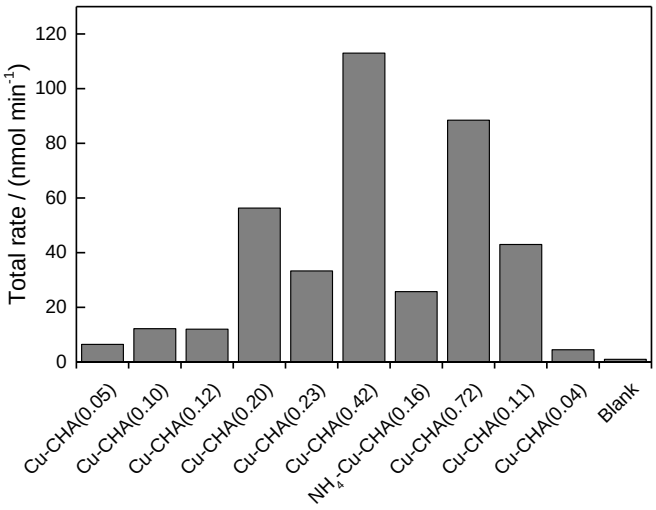

Figure II-12. Total rates of C-H scission calculated as the carbon-weighted sum of all reaction products at steady state. Total flow of 25 sccm, P_{CH4} = 18 kPa, P_{O2} = 0.09 kPa, P_{H2O} = 3.14 kPa, bal He. T = 543 K, 0.25 g_{cat} when applicable for all runs except blank. Blank reactor was packed in the same fashion as the typical reactor, replacing the bed of catalyst with a quartz wool plug. Catalyst nomenclature listed in Table II-1.

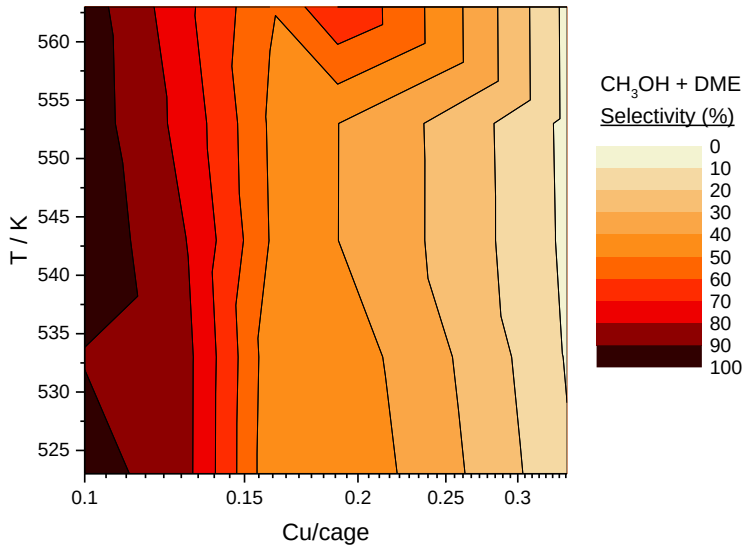

Figure II-13. Total CH_3OH and DME selectivity versus temperature and Cu loading from kinetic experiments. Reaction conditions were 0.25 g_{cat}, 25 sccm, P_{CH4} = 18 kPa, P_{O2} = 0.09 kPa, P_{H2O} = 3.14 kPa, bal He.

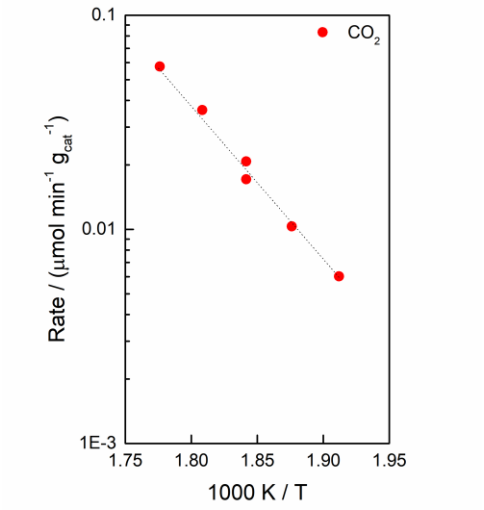

Figure II-14. CO_2 formation rate versus temperature of 1 wt% Cu_xO_y in defect-free SSZ-13 (0Al-Cu-CHA). 0.21 g_{cat}, 523-563 K, 21 sccm, P_{CH4} = 18 kPa, P_{O2} = 0.09 kPa, P_{H2O} = 3.14 kPa, bal He. Calculated apparent activation energy: E_a = 140 kJ mol^{-1}

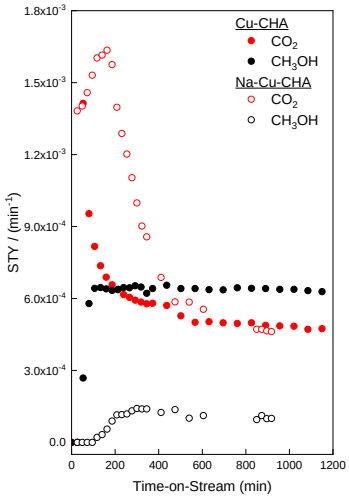

Figure II-15. Effect of Na and removal of Brønsted acidity on Cu-normalized product formation rates. Cu-CHA(0.11), Na-Cu-CHA(0.12), 0.25 g_{cat}, 543 K, 25 sccm, P_{CH4} = 18 kPa, P_{O2} = 0.09 kPa, P_{H2O} = 3.14 kPa, bal He. Direct comparison of methane oxidation rates between two zeolites with similar aluminum and Cu loadings but different proton contents as modified by Na^+ incorporation demonstrated the rate of methanol formation is markedly reduced. The large fraction of catalytically inactive charge-balancing Na^+ ions present in Cu-Na-SSZ-13 was partially responsible for the 85% lower rate of catalytic methanol production, supporting the necessity for Brønsted acidity in the catalytic production of methane.

III. Identification of a $[Cu\text{-}O\text{-}Cu]^{2+}$ Motif for Catalytic Methane Oxidation

Adapted with permission from Dinh, K. T.; Sullivan, M. M.; Narsimhan, K.; Serna, P.; Meyer, R. J.; Dincă, M.; Román-Leshkov, Y. Continuous Partial Oxidation of Methane to Methanol Catalyzed by Diffusion-Paired Copper Dimers in Copper-Exchanged Zeolites. *J. Am. Chem. Soc.* 2019, 141, 11641-11650.[110] Copyright 2019 American Chemical Society.

1. Motivation

In the previous chapter, a reaction pathway and catalyst and process requirements were identified to enable selective CH4 oxidation. Also of interest is the nature and genesis of the active sites involved in catalytic C–H activation and whether this site differs from those proposed for stoichiometric CH_4 oxidation over Cu-exchanged zeolites.[38] While similarities between stoichiometric CH_4 oxidation and catalytic CH_4 oxidation systems may exist, it is uncertain if the well-characterized active sites of stoichiometric oxidation systems[84, 88, 111, 115] are related to those active in a catalytic process. In fact, the notable differences between the activity and water-tolerance of the active sites in Cu-exchanged zeolites under stoichiometric versus catalytic oxidation reaction conditions[1] suggest that the active sites for the two processes may be entirely different from each other. This work, thus proposes an active site for the first time for the continuous catalytic partial oxidation of methane to methanol using dioxygen in the presence of water over Cu-exchanged zeolites.

Herein, chemical titration experiments and *in situ* spectroscopic characterization served to identify the active sites responsible for the direct, steady state catalytic conversion of CH_4 to methanol in copper-exchanged zeolites. These experiments uncovered a $[Cu–O–Cu]^{2+}$ dimeric motif as the active site for selective C–H activation that can be reversibly destroyed and generated upon introduction and complete desorption of NH_3, respectively. We hypothesize that these Cu dimers form under reaction conditions by hydrated ionic diffusion along a protonic highway, highlighting the importance of zeolite H^+ content.

2. Effects of Pretreatment, Brønsted Acidity, and Ammonia on Methane Oxidation

Inspired by reports on the mobilization of ammonia-solvated $[H_3N–Cu–NH_3]^+$ species to form multinuclear copper active sites in SSZ-13 at 473 K under NO_x reduction conditions,[125-127 128-129] we applied similar reductive and oxidative pretreatments to gain insight into the nature of the formation and turnover of active sites for CH_4 oxidation on Cu-CHA(0.23). Synthesis, characterization, and catalyst composition details are given in Section II.6 and summarized in Table II-1. In this chapter, catalysts designated as Cu-CHA(x) are copper-exchanged SSZ-13 zeolites with x Cu atoms per 8 x 8 x 12 Å cage. As shown in Figure III-1A, oxidative and reductive pretreatments had minimal effects on steady-state rates with one notable exception: NH_3 severely decreased rates of C–H activation whether introduced during pretreatment or as a co-feed, and rates could not be entirely recovered upon removal of the NH_3 co-feed (Figure III-1A). These inhibitive effects can be attributed to the favorable adsorption of NH_3 to both Brønsted acid sites and extraframework Cu ions within the zeolite pores.[112, 130-132]

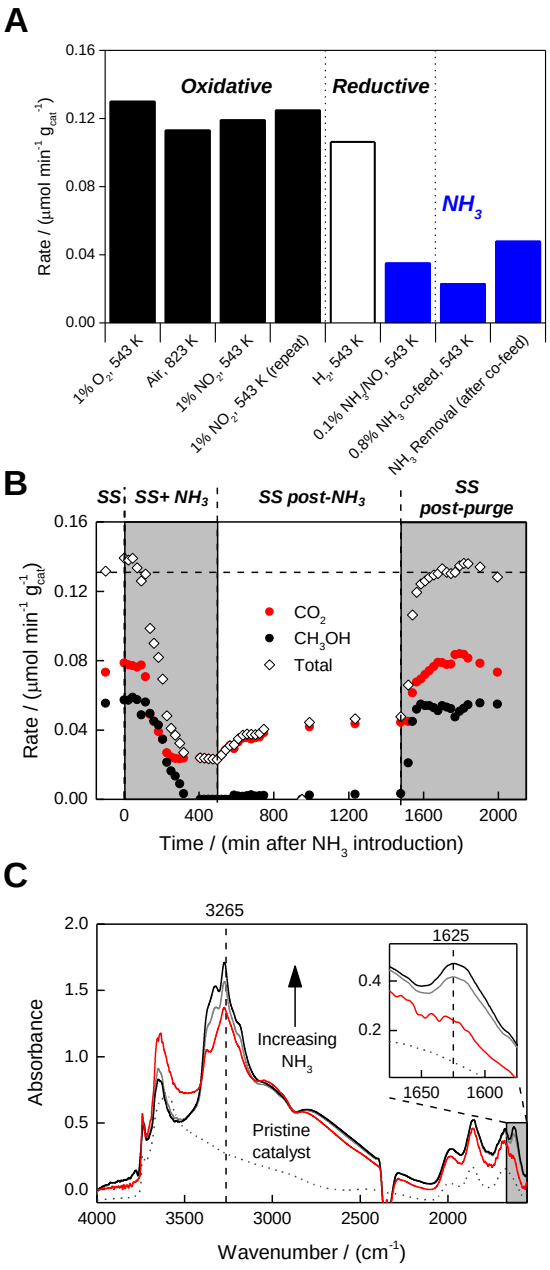

Figure III-1. Effect of NH_3 on catalytic methanol formation and Cu speciation for Cu-CHA(0.23). **A.** Product formation rates versus pretreatment conditions and NH_3 co-feed as listed. **B.** Effect on methanol formation. **C.** Ex situ FTIR of two catalyst samples: (i) "Fresh" Cu-CHA(0.23), never exposed to reaction conditions, only exposed to helium at 543 K, and (ii) Cu-CHA(0.23) exposed to methanol synthesis flows, NH_3 co-feed, and removal of NH_3 co-feed, before being removed from the reactor, pelletized, placed in the IR cell, and treated with subsequent *in situ* dosing with NH_3. CH_4 activation conditions were 0.25 g_{cat}, 543 K, 25 sccm, P_{CH4} = 18 kPa, P_{O2} = 0.09 kPa, P_{H2O} = 3.14 kPa, bal He. P_{NH3} = 0.08 kPa when co-feeding NH3. Spectra were collected in transmission of a 10 mg, 7 mm self-supporting catalyst wafer at 543 K.

To probe the effects of NH_3 on C–H activation, we performed an *operando* NH_3 titration (Figure III-1B) over Cu-CHA(0.23) under the following conditions: (i) baseline steady state flows (SS), (ii) NH_3 co-feed with steady state flows (SS+NH_3), (iii) steady state flows after removal of the NH_3 titrant (SS post NH_3), and (iv) baseline steady state flows after heating the catalyst to 673 K and holding for >10 h under pure helium flow (SS post-purge). Upon introduction of an NH_3 co-feed, methanol synthesis was almost entirely suppressed and CO_2 formation rates were substantially decreased (Figure III-1B, SS + NH_3). Removal of the NH_3 co-feed resulted in a moderate increase in CO_2 formation rates, but methanol production rates did not recover to the original values (Figure III-1B, SS post-NH_3). Di Iorio et al. reported that upon adsorption of NH_3 to both Brønsted acid sites and Cu, treatment with a wet He flow at 433 K selectively desorbed NH_3 from Cu without perturbing NH_3 coordinated to zeolitic protons.[130] Upon removal of the NH_3 co-feed in our system, the $CH_4/O_2/H_2O$ stream contacted the NH_3-titrated catalyst for ~1000 min at 543 K—conditions that selectively removed NH_3 only from Cu sites. This result is a strong indication that the persistent, significant inhibition of C–H activation rates after NH_3 removal was due to the blocking of Brønsted acid sites rather than a complete blockage of the Cu centers. An extended 12 h treatment under flowing helium at 673 K, known to induce NH_3 desorption even from zeolitic protons,[130] resulted in full recovery of CH_4 conversion rates and selectivity values (Figure III-1B, right), further evincing the deleterious effects of proton-blocking.

The necessity of protons to methanol production was inferred from the negligible selectivity to methanol shown in the center of Figure III-1B (SS post-NH_3), conditions under which NH_3 inhibits protons but not Cu as discussed above. Moreover, increasing the extent of NH_3 titration (leading to decreasing conversion) did not result in increasing selectivity to methanol as expected from Figure II-6A. Thus, we hypothesize that the absence of H^+ on Al sites impedes either (i) the formation of selective active sites or (ii) the desorption of methanol from selective active sites (if these sites remain). A combination of these two factors is also possible. Rapid regeneration of methanol synthesis rates upon NH_3 purging (Figure III-1B, SS post-purge) and the partial similarities of spectroscopic features of Cu species under SS and SS post-NH_3 conditions (*vide infra*) imply some fraction of selective partial methane oxidation active sites were present under SS post-NH_3 conditions, implicating the importance of H^+ for CH_3OH desorption.

Cu-CHA(0.23) was also characterized *ex situ* by FTIR spectroscopy following exposure and subsequent removal of an NH_3 co-feed under reaction conditions (Figure III-1C, red trace, SS post-NH_3). A strong signal from NH_3 adsorbed to Brønsted acid sites (3265 cm ^{1}) was observed while a signal from NH_3 adsorbed to Cu (1635 cm^{-1}) was entirely absent (Figure III-1C). Neither of the 3265 cm^{-1} and 1635 cm^{-1} features were observed on a fresh Cu-CHA(0.23) that was not exposed to reaction conditions or NH_3 dosing (Figure III-1C, dotted trace, Pristine catalyst). The SS post-NH_3 Cu-CHA(0.23) sample was then subjected to a series of 0.4 µmol NH_3 in He pulses, resulting in the appearance of both Cu–NH_3 signatures and more prominent NH_4^+ features (Figure III-1C), confirming the selective desorption of NH_3 from Cu and minimal desorption from Brønsted acid sites after NH_3 co-feed removal under reaction conditions.

These relevant FTIR peaks were identified by adsorption of NH_3 on Cu-CHA(0.20) as displayed in Figure III-2. Notable spectral features are of NH_3 on Brønsted acid sites (3278 cm^{-1}) and Cu (3190 and 1625 cm^{-1})[132-136]. The feature at 3325 cm^{-1} has been associated with both NH_3 adsorption to Brønsted acid sites and Cu. The Cu feature at 1625 cm^{-1} was used for further characterization due to the lack of any overlapping features.

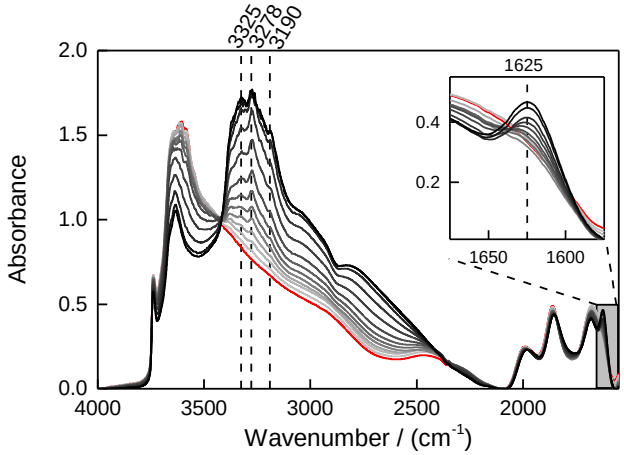

Figure III-2. *In situ* FTIR spectroscopy of NH_3 adsorption on Cu-CHA(0.20) demonstrating features of NH_3 adsorption to Cu and zeolitic protons. Spectra were collected in transmission of a 10 mg, 7 mm self-supporting catalyst wafer at 543 K.

The importance of zeolitic protons on C–H activation was also highlighted when testing catalysts where framework acid sites were ion-exchanged with NH_4^+ or Na^+ (discussion of the effect of Na^+ was provided earlier: Figure II-15 and Figure III-3). FTIR analysis of NH_4-Cu-CHA(0.16), a zeolite synthesized to contain simultaneously NH_4^+ and Cu^{2+} ions, showed that the NH_4^+ features of the as-synthesized catalyst were significant, whereas the Cu-NH_3 features were nonexistent. Subsequent NH_3 dosing moderately increased the NH_4^+ features, demonstrating the presence of some Brønsted acid sites either due to incomplete NH_3 exchange or partial desorption during Cu-ion exchange or FTIR experimentation. Upon exposure to methanol synthesis conditions, NH_4-Cu-CHA(0.16) facilitated C-H activation with a nearly 75% selectivity towards CO_2 formation. Importantly, treating the catalyst with a 673 K purge of helium resulted in a nearly 50% increase in the total rate of C-H activation and a shift in selectivity towards methanol and away from complete CH_4 oxidation, demonstrating the necessity of H^+'s for selective methanol synthesis. Both Na^+ and NH_4^+ ions inhibit methanol formation and appear to decrease the total rate of C-H activation. Although all of the effects of NH_4^+ and Na^+ ions on partial methane oxidation rates and selectivity cannot be conclusively proven to be identical, both ions cause similar effects to those observed from NH_3 co-feed-induced H^+ inhibition.

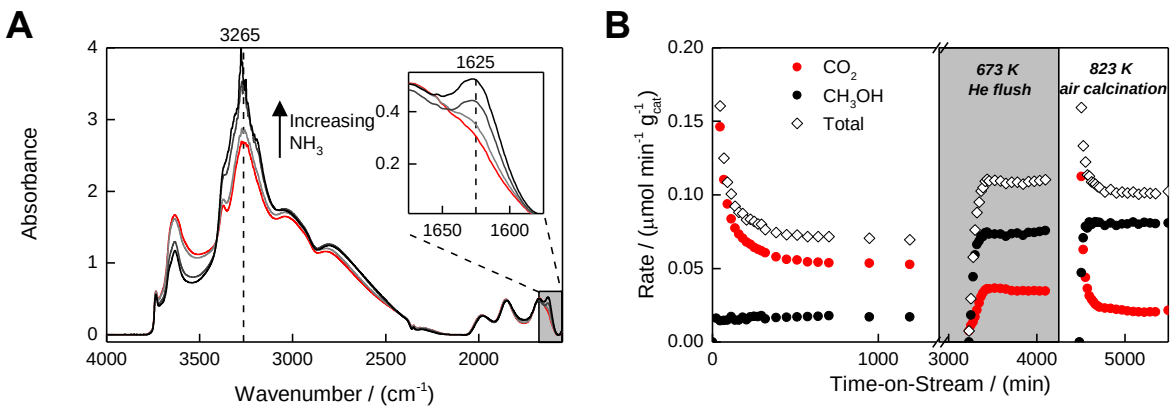

Figure III-3. A. *In situ* FTIR of NH_4-Cu-CHA(0.16) **B.** Product formation rates on NH_4-Cu-CHA(0.16) and after desorption of NH_3 from Brønsted acid sites (middle and right). Methane activation conditions were 0.25 g_{cat}, 543 K, 25 sccm, P_{CH4} = 18 kPa, P_{O2} = 0.09 kPa, P_{H2O} = 3.14 kPa, bal He. P_{NH3} = 0.8 kPa when co-feeding NH_3. Spectra were collected in transmission of a 10 mg, 7 mm self-supporting catalyst wafer at 543 K.

Taken together, these data show Brønsted acid site blocking has a twofold effect: (i) near complete inhibition of methanol formation pathways and (ii) significant inhibition of either C–H or O_2 activation processes. Figure II-6C shows that the rate of C–H activation is relatively invariant across samples of varying Al content (8.8 < Si/Al < 76). Therefore, we posit that protons are not kinetically relevant to the rate-determining C–H activation step. (Brønsted acid site content estimates are provided in Table II-2.) However, given the suppression of total CH_4 conversion due to H^+-inhibition, Brønsted acid sites are necessary for the completion of a C–H activation catalytic cycle, possibly by enabling active site formation or reoxidation.

The interrelation between Cu speciation, Brønsted acid sites, and NH_3 was then investigated by *in situ* X-ray absorption spectroscopy (XAS) during an identical NH_3 titration experiment to that shown in Figure III-1B. The effects of Al-density within the zeolite framework were also probed using two representative catalysts of similar Cu content: (i) high Al content (Cu-CHA(0.11)), and (ii) low Al content (1Al-Cu-CHA). Figure III-4A and Figure III-4B show the XAS spectra of the high-Al content Cu-CHA(0.11) during an entire NH_3 titration experiment. Fitting of the extended X-ray absorption fine structure (EXAFS) of Cu-CHA(0.11) upon exposure to steady state methanol synthesis conditions agrees with a $[Cu–O–Cu]^{2+}$ motif (fits of all spectra provided in Figure III-8 and Table III-1). The XANES spectra indicated the presence of both Cu(I) (8983 eV[137]) and Cu(II) (8978 and 8987 eV[137]), consistent with a Cu(II)/Cu(I) redox cycle during C–H activation. The first shell scattering peak fit to a Cu-O coordination number (CN) of 3.1 ± 1.1 (R_{Cu-O} = 1.90 ± 0.02 Å) and the second shell scattering peak fit to a Cu-Cu CN of 1.1 ± 0.6 (R_{Cu-Cu} = 2.94 ± 0.05 Å). These values are consistent with a moiety where each Cu atom coordinates to two framework O atoms or coordinating H_2O molecules, one extraframework O atom, and an additional Cu atom, represented in Figure III-4E. The observed interatomic distances for both Cu-O and Cu-Cu are also consistent with distances calculated for Cu dimers in SSZ-13,[138] yet we also recognize that the uncertainty of the Cu-O CN does not preclude the presence of either a Cu dimer coordinating to 2 extraframework O's or a subset of non-dimeric Cu species. Fitting of the second shell EXAFS peak with a T-site resulted in a negative CN (Table III-2). However, given the overlap of Cu-T-site and Cu-Cu scattering, small contributions by a T-site cannot be ruled out.

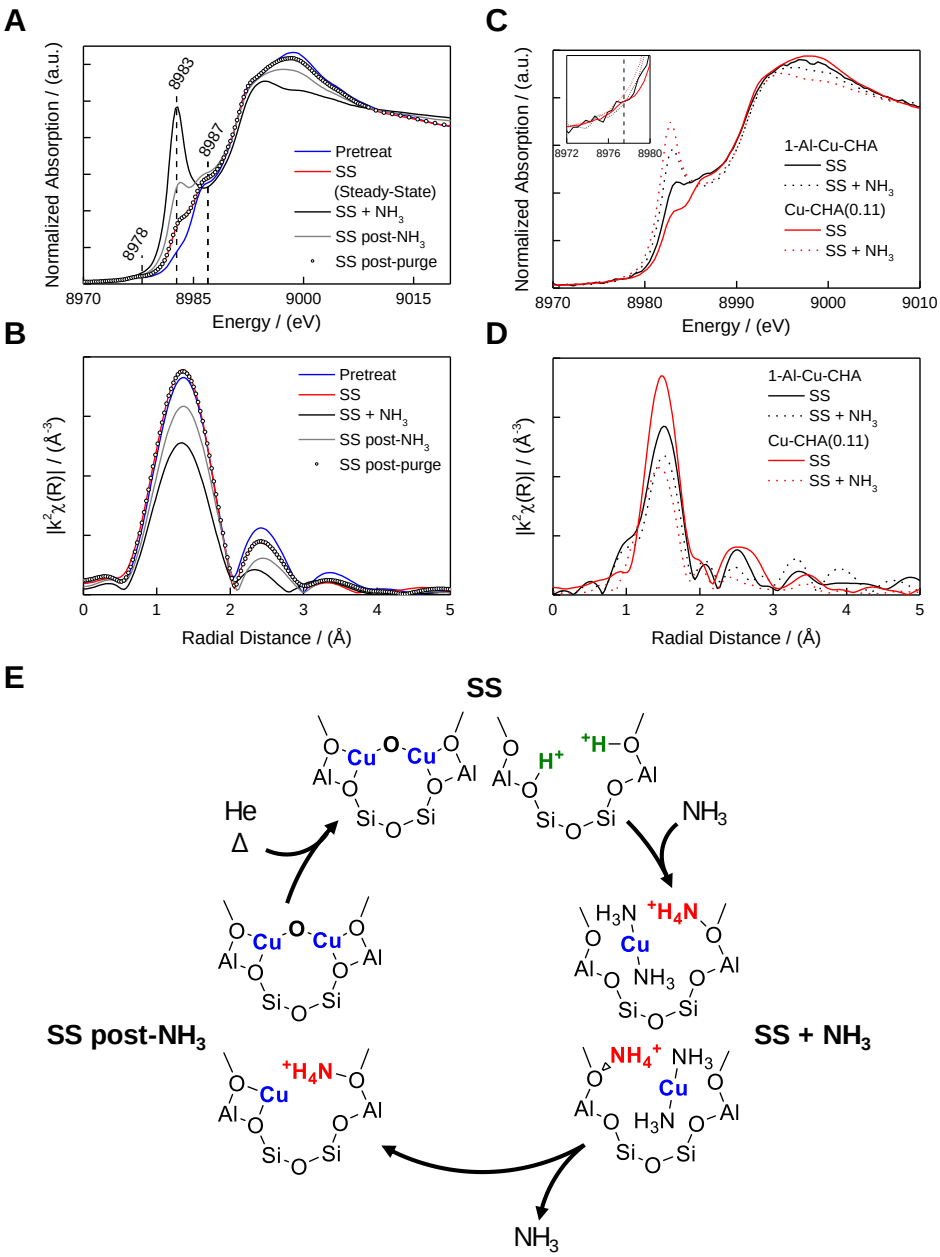

Figure III-4. A. XANES and **B.** EXAFS of Cu-CHA(0.11) and **C**. XANES and **D**. EXAFS of 1Al-Cu-CHA and Cu-CHA(0.11) under methanol synthesis and NH_3 flows. **E**. Hypothesized schematic representations of the average states of charge balancing Cu, NH_4^+, and H^+ species as a function of reaction flows and treatments. Single O atoms may correspond to framework zeolite O atoms or coordinating H_2O molecule. All spectra were collected at 543 K. The catalyst was pretreated in 1 kPa O_2, bal He from 298 K to 543 K at 5 K min^{-1} (Pretreat). At 543 K, the catalyst was exposed to methanol synthesis flows of P_{CH4} = 18 kPa, P_{O2} = 0.09 kPa, P_{H2O} = 3.14 kPa, bal He (SS), an additional NH_3 co-feed of P_{NH3} = 0.16 kPa (SS + NH_3), and then the removal of NH_3 (SS post-NH_3). Following NH_3 removal, the catalyst was brought to 673 K at 6 K min^{-1} and held in dry He before cooling to 543 K and exposure to methanol synthesis flows (SS post-purge).

Based upon the observation of a $[Cu\text{-}O\text{-}Cu]^{2+}$ motif via XAS, UV-vis was also employed because it has been used to identify Cu dimers in zeolites active for stoichiometric partial CH_4 oxidation.[47, 88, 139] *In situ* UV-vis of Cu-CHA(0.11) display a feature centered around 37,500 cm^{-1} that is present under methanol synthesis flows and not present upon titration with NH_3 (Figure III-5). The band at 37,500 cm^{-1} can be associated with Cu dimers[140] or simply the ligand-metal charge-transfer of Cu^{2+}.[88] Li et al. calculated features in this region can be from Cu dimers in SSZ-13.[140] Definitive assignment of this band is inconclusive, however, as features in this region may simply be related to reduction and oxidation of Cu ions.[88] Evidence of Cu dimer motifs were not observed at 22,700 cm^{-1}, which has been assigned to Cu dimers within zeolites active for the stoichiometric conversion of CH_4 to methanol.[47, 88, 139] The results from XAS and UV-vis, thus, fall in line with an abundant, oxidized dimeric Cu-active site at steady state prior to a rate-determining C–H activation event.

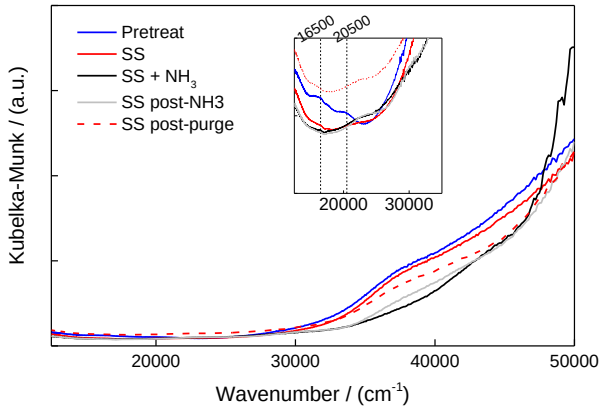

Figure III-5. *In situ* DRUV of Cu-CHA(0.11). All spectra were collected at 543 K and H-SSZ-13(Si/Al = 15) was used as a baseline. Evidence of Cu dimer motifs were not observed at 22,700 cm^{-1}. The band at 37,500 cm^{-1} can be associated with Cu dimers[140] or simply the ligand-metal charge-transfer of Cu^{2+}.[88] The catalyst was pretreated in 1 kPa O_2, bal He from room temperature to 543 K at 5 K min^{-1} (Pretreat). At 543 K, the catalyst was exposed to methanol synthesis flows of P_{CH4} = 18 kPa, P_{O2} = 0.09 kPa, P_{H2O} = 3.14 kPa, bal He (SS), an additional NH_3 co-feed of P_{NH3} = 1.6 kPa (SS + NH_3), and then the removal of NH_3 (SS post-NH_3). Following NH_3 removal, the catalyst was brought to 673 K at 6 K min^{-1} and held in dry He before cooling to 543 K and exposure to methanol synthesis flows (SS post-purge).

An NH_3 co-feed (SS+NH_3) resulted in the generation of a strong Cu(I) pre-edge feature, the disappearance of both Cu(II) pre-edge features (Figure III-4C inset), the disappearance of the Cu-Cu scattering signal, and a decrease in the first shell coordination number (CN) from 3.1 ± 1.1 to 1.8 ± 0.3. These changes are consistent with the destruction of Cu-dimers and the formation of mobile $[H_3N–Cu–NH_3]^+$ species similar to those previously reported by Paolucci et al. and represented in Figure III-4E.[128] Removal of the NH_3 co-feed (SS post-NH_3) resulted in a partial recovery in both the Cu-O and Cu-Cu scattering signals and a partial decrease in the intensity of the Cu(I) pre-edge feature. As discussed previously, NH_3 remains bound to Brønsted acid sites under methanol synthesis conditions after removal of the NH_3 titrant, demonstrating that zeolitic protons are crucial for both Cu reoxidation and reformation of Cu dimers for a significant fraction of Cu ions. In the final step of the titration experiment, initial steady state Cu speciation was restored after purging NH_3 from zeolitic protons under helium flow at 673 K and subsequently reintroducing methanol synthesis flows.

Figure III-4C and Figure III-4D compare the effects of NH_3 titration on low- and high-Al content samples via *in situ* XAS under the same methanol synthesis and NH_3 titration conditions. 1Al-Cu-CHA exhibits a stronger Cu(I) pre-edge feature under steady state methanol synthesis conditions versus Cu-CHA(0.11). A fit of the EXAFS of 1Al-Cu-CHA (Figure III-4D, Figure III-9, Table III-3) under these same conditions provided a Cu-O CN of 1.8 ± 0.5 (R_{Cu-O} = 1.94 ± 0.02 Å) and a smaller Cu-Cu CN of 0.6 ± 0.3 (R_{Cu-Cu} = 2.9 ± 0.1 Å) compared to Cu-CHA(0.11). Due to the nature of XAS as a bulk averaging technique, a Cu-Cu coordination number less than 1 is indicative of a mixture of isolated Cu-O species and multinuclear Cu-oxo species. An NH_3 co-feed to 1Al-Cu-CHA yielded similar results as with Cu-CHA(0.11): only Cu(I) was observed, Cu-O scattering intensity was reduced, and Cu-Cu scattering was eliminated. These results imply that an increasingly sparse Al population decreases the likelihood of multinuclear Cu species even at a moderate Cu/Al loading, and that isolated Cu species cannot be facilely aerobically oxidized.

Because of its bulk sampling nature, EXAFS alone cannot identify the active site for selective partial methane oxidation. However, EXAFS in combination with the reactivity measurements and NH3 titration experiments indicate a Cu dimer active site is likely to achieve selective catalytic partial oxidation of methane to methanol. Therefore, these combined reactivity and *in situ* spectroscopic data support the hypothesis that a $[Cu–O–Cu]^{2+}$ motif acts as the active site for catalytic partial CH_4 oxidation in SSZ-13, the dimer is formed at low Cu loadings (Cu/cage<0.3), and free zeolitic protons are critical for Cu dimer formation as evinced from selective synthesis, spectroscopic, and NH_3 titration results.

3. Proposed mechanism for $[Cu-O-Cu]^{2+}$ formation

The formation of a $[Cu–O–Cu]^{2+}$ species as CH_4 oxidation active sites is puzzling given C–H activation was observed at Cu densities as low as 0.04 Cu/cage where the probability of having two Cu ions within the same cage is prohibitively small. Further, while the partial methane oxidation selectivities of Cu-CHA(0.05 and Cu-CHA(0.04) were near unity (Figure II-6A), the selectivity for methanol of 1Al-Cu-CHA was much lower despite similar Cu/cage values among the three catalysts (0.05, 0.04, and 0.04 respectively), demonstrating that the active sites for selective partial oxidation form when the zeolite Al-content is sufficiently high even when the Cu loading is low. However, we stress that the high Cu loadings lead to non-selective active species regardless of Al-content as depicted above. *In situ* NH_3 titrations and concurrent spectroscopic data clearly show that Brønsted acid sites are involved in the formation of the $[Cu–O–Cu]^{2+}$ motif. We posit that these results can be rationalized by considering the proton-aided diffusion of hydrated Cu ions within the CHA framework schematically represented in Figure III-6; this hypothesized process is fundamentally analogous to the putative mechanism that allows hydrated Cu ions to diffuse into and out of CHA cages during aqueous ion exchanges.

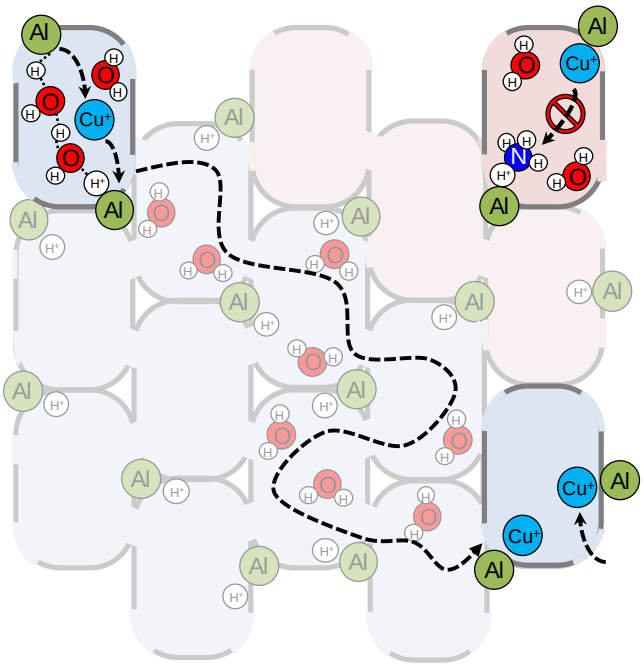

Figure III-6. Depiction of hypothesized H^+/H_2O-aided diffusion of Cu^+ and NH_3 inhibition within SSZ-13 to form Cu dimers relevant to the proposed catalytic methane oxidation cycle. Single O atoms may correspond to framework zeolite O atoms or coordinating H_2O molecules.

Each framework T-site in CHA is shared amongst three neighboring cages, and extraframework cations (e.g., H^+, Cu^+, Cu^{2+}) coordinated to Al T-sites can readily access each of these cages via the 8-MR windows with a minimal energetic penalty.[128] Psofogiannakis et al. used force field/molecular dynamics simulations to demonstrate that tetra-hydrated Cu ions are fully desorbed from the SSZ-13 framework and mobile on the picosecond timescale at temperatures relevant to this work (500-700 K). Further, Paolucci et al. calculated an energetic barrier of ~35 kJ mol^{-1} for the rotation of $[H_3N\text{-}Cu\text{-}NH_3]^+$ species through an 8MR window to an adjacent cage.[128, 141] Assuming a Cu ion can be mobilized and transferred to a proximate $[AlO_4]^-$ T-site, charge balance can be maintained by water-assisted proton hopping (Figure III-6, top-left). A zeolite with a high enough Al content, combined with the H^+/H_2O/Cu ion exchange process and Cu ion rotation between CHA cages would effectively allow Cu ions to access the entirety of the zeolite framework and facilitate Cu ion pairing even in low Cu-content zeolites. This Cu ion mobility, thus, enables formation of thermodynamically favorable Cu dimer species in the presence of water..[112, 141]

The low energetic barrier for this ion exchange across a single CHA cage and the facile shifting of Cu ions and protons between neighboring cages provide a means for Cu ions to access the entire microporous zeolite when a sufficiently high Al content allows for Cu ion exchange between nearby $[AlO_4]^-$ T-sites.[142] The introduction of NH_3 into the zeolite disperses Cu species as mobile $[H_3N–Cu–NH_3]^+$ and simultaneously blocks protons by NH_4^+ formation. Upon removal of NH_3 co-feed, Cu ions are deposited on $[AlO_4]^-$ T-sites, but now NH_4^+ (and not H^+) ions are coordinated to $[AlO_4]^-$ sites that lack Cu ions. These NH_4^+ ions are too energetically stable to desorb from $[AlO_4]^-$ T-sites to facilitate Cu ion mobility (Figure III-4, Figure III-6).

Aerobic oxidation of Cu to selectively produce methanol necessitates dimeric species in contrast to the complete oxidation of both monomeric and dimeric Cu(I) achieved by an NO_2 pretreatment (Figure III-7).[112] *In situ* XANES was collected while exposing Cu-CHA(0.11) to different oxidizing atmospheres. Cu-CHA(0.11) was first exposed to a 1 kPa NH_3, 1 kPa NO, bal He gas treatment, conditions similar to those used in the NH_3 titration experiments described previously to obtain entirely isolated Cu(I) sites (Figure III-4). Following, Cu-CHA(0.11) was treated with NO_2, a known oxidant,[129] resulting in only the presence of a Cu(II) pre-edge feature (8987 eV) and the absence of any Cu(I) pre-edge feature (8983 eV). The presence of a Cu(II) pre-edge feature along with the absence of a Cu(I) pre-edge feature demonstrates the complete oxidation by NO_2 of isolated Cu(I) sites. Separately, Cu-CHA(0.11) was exposed to methanol synthesis flows (SS), and both Cu(I) and Cu(II) pre-edge features were evident. An additional NH_3 co-feed and then the removal of NH_3 (SS post-NH_3) to destroy Cu dimer sites resulted in the persistence of Cu(I) and the absence of Cu(II) under methanol synthesis conditions, demonstrating dilute O_2 cannot oxidize isolated Cu(I) sites. These results, thus, demonstrate isolated Cu(I) sites can be oxidized by an appropriate oxidant but under aerobic conditions, dimeric Cu sites are required for the re-oxidation of Cu(I) to Cu(II) to complete the catalytic cycle for selective CH_4 oxidation.

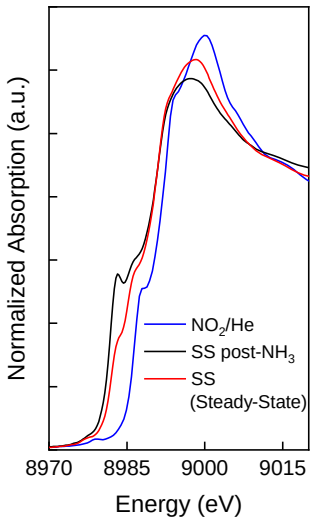

Figure III-7. Cu K-edge XANES of Cu-CHA(0.11) following exposure to NO_2 and O_2. 1 kPa NO_2, bal He exposure followed exposure to a 1 kPa NH_3, 1 kPa NO, bal He gas treatment at 493 K. At 543 K, the catalyst was exposed to methanol synthesis flows of P_{CH4} = 18 kPa, P_{O2} = 0.09 kPa, P_{H2O} = 3.14 kPa, bal He (SS), an additional NH_3 co-feed of P_{NH3} = 1.6 kPa, and then the removal of NH_3 (SS post-NH_3). Cu(I) persists upon exposure to dilute O_2.

Thus, catalytic CH_4 partial oxidation is greatly hindered without Cu dimer formation via an available ion diffusion pathway. The increased presence of Cu(I) following removal of the NH_3 co-feed observed in Figure III-4A (SS post-NH_3) compared to the original methanol synthesis flows (SS) is explained by the inability of O_2 to oxidize all isolated Cu(I) when the latter is trapped by NH_4^+ (Figure III-6, top-right cage of left scheme). The fraction of isolated Cu species oxidized by O_2 are thought to account for the non-zero rate of CO_2 formation in the presence of NH_3 and following NH_3 removal. Only upon complete NH_3 desorption and re-introduction of methanol synthesis flows is this significant fraction of Cu(I) re-oxidized and C–H activation rates are restored. This coincides with the opening of ionic diffusive channels that result in reformation of dimeric Cu active sites.

This theory is corroborated by the results in Figure III-4C and Figure III-4D of the isolated Al 1Al-Cu-CHA sample; this sample exhibits predominantly isolated Cu-O species that cannot diffuse due to a sparse population of $[AlO_4]^-$ T-sites. In line with this assumption, EXAFS analysis of the 1Al-Cu-CHA sample revealed limited Cu-Cu scattering (Figure III-4D). Cu dimer formation in a zeolite with low Al content can be accounted for by pockets of proximate Al sites, resulting from either (i) a random Al distribution (The average Al-Al distance at this Si/Al is 1.7 nm, close enough to permit Cu dimer formation via the 0.9 nm maximum diffusion radius of a Cu ion[128]), or (ii) Al zoning formed during zeolite synthesis as previously observed in other frameworks.[143-144] Furthermore, the increased intensity of the Cu(I) pre-edge feature of 1Al-Cu-CHA (Figure III-4C) is consistent with a greater population of isolated Cu-O species. However, partial methane oxidation activity over isolated Cu species cannot be ruled out. The Cu speciation and distinct kinetics of 1Al-Cu-CHA are still under investigation. While this mechanism is not unequivocally proven, the comprehensive and complex results reported in this work can be simply rationalized via an ionic diffusion pathway that facilitates the formation of $[Cu–O–Cu]^{2+}$ motifs that are active for selective partial oxidation of CH_4.

4. Conclusions

The active site for the direct conversion of CH_4 to methanol was elucidated with chemical titration experiments in combination with spectroscopic techniques. NH_3 titration and desorption uncovered a $[Cu–O–Cu]^{2+}$ motif that catalyzes selective CH_4 partial oxidation. Importantly, the $[Cu–O–Cu]^{2+}$ motif forms via the diffusion of hydrated Cu ions along a proton-paved highway. The necessity of protons was demonstrated by the introduction of Na^+ and NH_4^+ ions into separate zeolites, resulting in a decrease in the total rate of c-H activation and worse selectivity for methanol. Thus, catalysts containing a high density of Brønsted acid sites and moderate Cu loadings (Cu/cage<0.3) are required to maximize the presence of isolated dimeric Cu species. This work highlights the importance of mechanistic understanding to direct synthesis-driven active site speciation.

5. *Acknowledgements*

The authors gratefully acknowledge the financial support of ExxonMobil. K.D. acknowledges the partial support from the National Science Foundation Graduate Research Fellowship under Grant No. 1122374. Any opinion, findings, and conclusions or recommendations expressed in this material are those of the author(s) and do not necessarily reflect the views of the National Science Foundation. MRCAT operations are supported by the Department of Energy and the MRCAT member institutions. This research used resources of the Advanced Photon Source, a U.S. Department of Energy (DOE) Office of Science User Facility operated for the DOE Office of Science by Argonne National Laboratory under Contract No. DE-AC02-06CH11357. J. Katsoudas, T. Wu, and S. Aryal for help with XAS data collection, M. Stone and T. Gani for comments on the manuscript, and A. Stubbs and X. He for helpful discussion.

6. *Supporting Information*

6.1. Methods

Unless otherwise described below, remaining methods are described in Section II.6.1**.**

IR Spectroscopy

Infrared spectroscopic measurements were collected using a Vertex 80 spectrometer (Bruker Instruments) equipped with a liquid nitrogen cooled mercury-cadmium-telluride detector. Experiments were performed in a high temperature reaction cell for transmission acquisition (HTC-3, Harrick Scientific). 10 mg of a zeolite sample was pressed into a 0.7 cm diameter wafer. All spectra were collected under flowing He (ultra-high purity, Airgas) unless otherwise noted. All spectra were collected at 4 cm^{-1} resolution, averaged over 256 scans, and baseline corrected.

XAS Experiments

XAS was completed at Sectors 9-BM and 10-BM MRCAT of Argonne National Laboratory's Advanced Photon Source. Cu-CHA(0.11) was ground into a fine powder, and a loaded in a custom *in situ* fluorescence cell capable of gas flows and temperature control. In a separate experiment, Cu-CHA(0.11) and 1-Al-Cu-CHA were analyzed in transmission via a six shooter placed in a quartz tube inside a clamshell furnace equipped with a temperature controller.

EXAFS spectra were collected before heating under ambient conditions. Catalysts were calcined with 50 sccm 1% O_2 in He from ambient conditions to 543 K with a ramp of 5 K min^{-1} and XAS was collected. Methanol synthesis flows of 100 sccm P_{CH4} = 18 kPa, P_{O2} = 0.09 kPa, P_{H2O} = 3.14 kPa, bal He were introduced, followed by a 1.6 kPa NH_3 co-feed and an equimolar removal of He to maintain a 100 sccm total flow. NH_3 was removed and the gas flow was made up with He. Following NH_3 removal, the catalyst was brought to 673 K at 6 K min^{-1} and held in 100 sccm dry He before cooling to 543 K and exposure to methanol synthesis flows. XANES (~4.5 min/scan) were collected at each stage until no change in spectra were observed. Following, EXAFS was performed. All spectra were collected at 543 K.

XAS Data Fitting

XAS data was processed and fitted using the Athena and Artemis software from the Demeter package. Spectra were normalized using third-order polynomials in both the pre- and post-edge regions and were calibrated using the first zero-crossing of the second derivative of the Cu metal foil spectrum. EXAFS data were fit from k = 3 to ~ 8.5 $Å^{-1}$ and R = 1 – 3.2 Å with a Hanning window and dk = 2, unless otherwise noted. Reported uncertainties are taken from the diagonal of the covariance matrix and scaled by $\sqrt{\chi^2_v}$

6.2. Referenced Figures and Tables

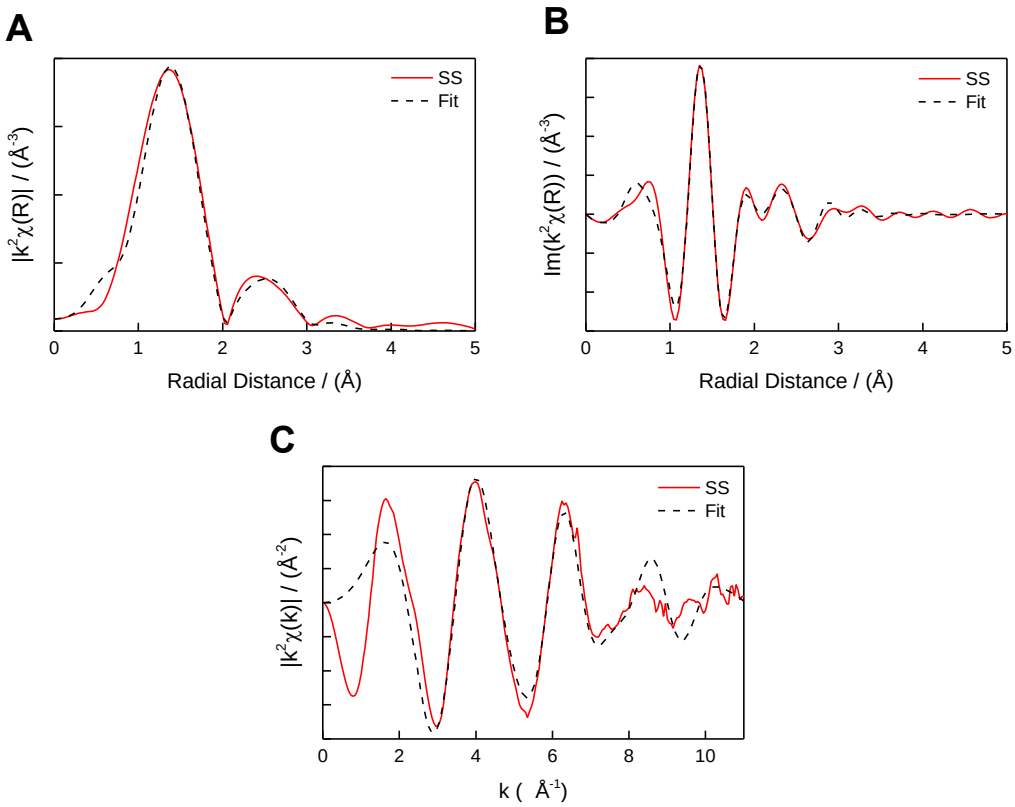

Figure III-8. EXAFS fitting of Cu-CHA(0.11) upon exposure to methanol synthesis flows at 543 K of P_{CH4} = 18 kPa, P_{O2} = 0.09 kPa, P_{H2O} = 3.14 kPa, bal He. **A.** Magnitude and **B.** Imaginary part of k^2 weighted Fourier transform **C.** Raw EXAFS spectrum with fit with k^2 weight.

Table III-1. EXAFS fitting results of Cu-CHA(0.11) under methanol synthesis and NH_3 flows. All spectra were collected at 543 K.

Gas Treatment	N_{Cu-O}	R_{Cu-O} (Å)	N_{Cu-Cu}	R_{Cu-Cu} (Å)	ΔE (eV)	σ^2_{Cu-O}	σ^2_{Cu-Cu}	R-factor
Pretreatment	2.9 ± 0.9	1.90 ± 0.02	1.6 ± 0.6	2.94 ± 0.04	-7 ± 3	0.004 ± 0.004	0.01	0.007
Steady State	3.1 ± 1.1	1.92 ± 0.03	1.1 ± 0.6	2.94 ± 0.05	-6 ± 4	0.006 ± 0.005	0.01	0.008
Steady State + NH_3	1.8 ± 0.3	1.90 ± 0.01	-	-	-4 ± 2	0.004 ± 0.003	-	0.003
Steady State post-NH_3	2.5 ± 0.4	1.90 ± 0.02	0.5 ± 0.2	2.96 ± 0.03	-5 ± 2	0.006 ± 0.002	0.006	0.004
Steady State post-purge	3.0 ± 0.8	1.91 ± 0.05	1.7 ± 0.7	2.96 ± 0.04	-7 ± 3	0.004 ± 0.003	0.015	0.004

The catalyst was pretreated in 1 kPa O_2, bal He from room temperature to 543 K at 5 K min^{-1}. At 543 K, the catalyst was exposed to methanol synthesis flows of P_{CH4} = 18 kPa, P_{O2} = 0.09 kPa, P_{H2O} = 3.14 kPa, bal He, an additional NH_3 co-feed of P_{NH3} = 1.6 kPa, and then the removal of NH_3. Following NH_3 removal, the catalyst was brought to 673 K at 6 K min^{-1} and held in dry He before cooling to 543 K and exposure to methanol synthesis flows. An amplitude factor of 0.86 was obtained by fitting a Cu foil reference. The range of fitting provided 7 independent points. Initial fits were obtained by fitting one σ^2 value for both scattering fits and then optimized by increasing $\sigma^2_{Cu\text{-}Cu}$ to minimize the R-factor. These values are similar to those reported by Pappas et al.[87] Correlations between $\Delta R_{Cu\text{-}O}$ and ΔE and $\sigma^2_{Cu\text{-}O}$ and $N_{Cu\text{-}O}$ were 0.93. All others were less than 0.6.

Table III-2. EXAFS fitting results of Cu-CHA(0.11) under methanol synthesis flows and fitting the second shell with a Cu-T-site scattering path.

Gas Treatment	$N_{Cu\text{-}O}$	$R_{Cu\text{-}O}$ (Å)	$N_{Cu\text{-}T}$	$R_{Cu\text{-}T}$ (Å)	ΔE (eV)	σ^2	R-factor
Steady State	2.9 ± 0.6	1.93 ± 0.01	**-1.1 ± 0.4**	3.00 ± 0.03	-4 ± 2	0.006 ± 0.003	0.003

An unphysical CN was obtained for the Cu-T-site scattering path.

Table III-3. EXAFS fitting results of 1Al-Cu-CHA under methanol synthesis and NH_3 flows. All spectra were collected at 543 K.

Gas Treatment	$N_{Cu\text{-}O}$	$R_{Cu\text{-}O}$ (Å)	$N_{Cu\text{-}Cu}$	$R_{Cu\text{-}Cu}$ (Å)	$\Delta E_{Cu\text{-}O}$ (eV)	$\Delta E_{Cu\text{-}Cu}$ (eV)	$\sigma^2_{Cu\text{-}O}$	$\sigma^2_{Cu\text{-}Cu}$	R-factor
Steady State	1.8 ± 0.5	1.94 ± 0.02	0.6 ± 0.3	2.9 ± 0.1	1 ± 3	-8 ± 15	0.002 ± 0.003	0.008	0.011
Steady State + NH_3	1.6 ± 0.8	1.93 ± 0.04	-	-	0.3 ± 5	-	0.003 ± 0.005	-	0.012

EXAFS was fit from k = 3 to ~ 10.5 $Å^{-1}$ and R = 1.45 – 3 Å. The catalyst was pretreated in 1 kPa O_2, bal He from room temperature to 543 K at 5 K min^{-1}. At 543 K, the catalyst was exposed to methanol synthesis flows of P_{CH4} = 18 kPa, P_{O2} = 0.09 kPa, P_{H2O} = 3.14 kPa, bal He, and an additional NH_3 co-feed of P_{NH3} = 1.6 kPa. An amplitude factor of 0.83 was obtained by fitting a Cu foil reference. The range of fitting provided 8 independent points. Initial fits were obtained by fitting one σ^2 value for both scattering fits and then optimized by increasing $\sigma^2_{Cu\text{-}Cu}$ to minimize the R-factor. These values are similar to those reported by Pappas et al.[87] Correlations between $\Delta R_{Cu\text{-}Cu}$ and $\Delta E_{Cu\text{-}Cu}$, $\Delta R_{Cu\text{-}O}$ and $\Delta E_{Cu\text{-}O}$, and $\sigma^2_{Cu\text{-}O}$ and $N_{Cu\text{-}O}$ were 0.93, 0.91, and 0.87, respectively. All others were less than 0.6.

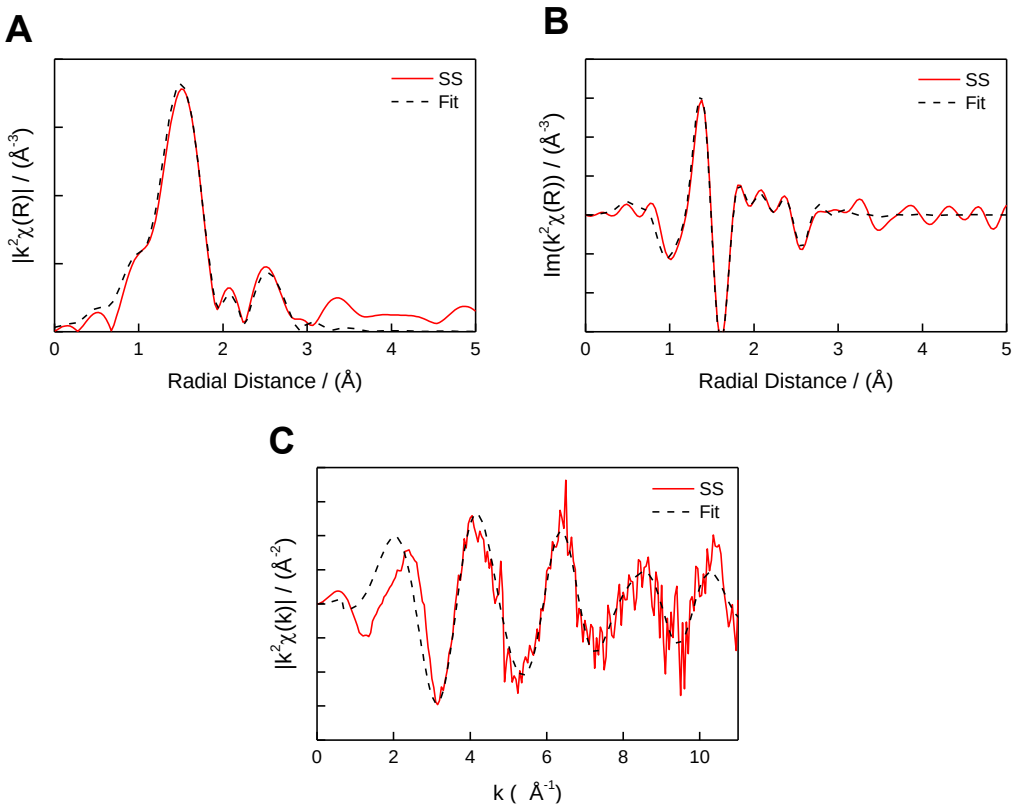

Figure III-9. EXAFS fitting of 1Al-Cu-CHA upon exposure to methanol synthesis flows at 543 K of P_{CH4} = 18 kPa, P_{O2} = 0.09 kPa, P_{H2O} = 3.14 kPa, bal He. **A.** Magnitude and **B.** Imaginary part of k^2 weighted Fourier transform **C**. Raw EXAFS spectrum with fit with k^2 weigh

IV. Characterization and Kinetics of Isolated Copper Sites for Partial Methane Oxidation

1. Motivation

In chemical looping partial methane oxidation systems, the active site has been experimentally identified as a Cu dimer[47, 139, 145] or trimer.[84] Recently, Dinh et al. identified a Cu dimer motif as active for catalytic partial methane oxidation and hypothesized that these dimers form via the diffusion of hydrated Cu ions between Al and Brønsted acid sites within a zeolite.[110] Kulkarni et al. used DFT calculations to suggest Cu monomers within the 8-membered rings of a SSZ-13 zeolite are capable of activating methane selectively.[83] However, to date, there have been no experimental reports on the activity of Cu monomers within zeolites for partial CH_4 oxidation. Based on these reports, we hypothesized Cu monomers can be studied for partial CH_4 oxidation in catalysts with sufficiently low Al content such that Cu ion diffusion is inhibited.

Herein, we report Cu-SSZ-13 zeolites (CHA crystal structure) with low Al content (Si/Al = 76 and 160) are active, but unselective, for partial methane oxidation. Kinetic experiments demonstrate CO_2 is a primary product, O_2 activation is a rate-determining step, and H_2O is required for the formation of methanol. X-ray absorption spectroscopy revealed a prominent Cu(I) pre-edge feature that coincides with the absence of Cu-Cu scattering under methanol synthesis conditions, suggesting Cu monomers can plausibly be obtained within these zeolites.

2. Kinetics of Low Al Cu-SSZ-13 Zeolites

Cu-CHA(76) and Cu-CHA(160) were synthesized to have decreasing Al content (Table IV-1), but similar Cu content. In this chapter, Cu-CHA(*x*) denotes a Cu-exchanged SSZ-13 zeolite where *x* is the Si/Al ratio of the catalyst. These catalyst were synthesized in a one-pot method based on modifications of syntheses reported by Dinh et al.[110] and Eilertsen et al.[121] Catalyst synthesis and catalyst characterization details are provided in Section IV.6 and Figure IV-6. These zeolites were chosen to attempt to observe the increasingly isolated nature of Cu ions as the reduction in Al content prevents facile Cu ion diffusion. These two zeolites represent a 60 and 80% decrease in Al content, respectively, compared to previously studied Cu-SSZ-13 zeolites (Si/Al ≈ 10 – 25) that are selective for partial methane oxidation.[87-88, 110]

Table IV-1. Catalyst composition of Cu-CHA and H-MFI

Catalyst	Composition		Cu Content (wt%)	Cu/cage[a]
	Si/Al	Cu/Al		
Cu-CHA(76)	76	0.23	0.31	0.04
Cu-CHA(160)	160	0.37	0.20	0.03

[a]Cu/cage is the number of Cu atoms per 8 x 8 x 12 Å CHA cage

Figure IV-1 demonstrates the impact that Al content has on the CH_4 partial oxidation reaction pathway at 543 K in the absence of heat and mass transfer limitations (Figure IV-7 and Table IV-2). In the absence of catalyst, CO_2 was the only observed product (Figure IV-8). The rates of CO_2 formation observed over Cu-CHA(76) and Cu-CHA(160) were all greater than this background rate of CO_2 formation under identical conditions. Due to the lack of data on homogeneous rates of CO2 formation across conditions, subtraction of CO2 was not completed. However, Figure V-15 suggests the background rate of CO_2 formation is not strongly affected by a change in reactant feed composition or temperature. Notably, selectivity for CH_3OH is less than 80% at 0.0001% CH_4 conversion (Figure IV-2) for both Cu-CHA(76) and Cu-CHA(160), which is significantly lower than the often observed >80% CH_3OH selectivity in Cu-exchanged zeolites active for partial CH_4 oxidation.[91, 110] As CH_4 conversion approaches 0% over Cu-CHA(76), the selectivity for CO_2 approaches a finite, nonzero value, indicating that both CH_3OH and CO_2 are primary reaction products. However, the increasing selectivity for CO_2 combined with the decreasing selectivity for CH_3OH with increasing conversion suggests a sequential reaction pathway. In the more Al-deficient Cu-CHA(160), the selectivity towards CH_3OH is invariant to increasing CH_4 conversion, indicating CH_3OH and CO_2 form from CH_4 as primary products in a parallel reaction pathway. In this way, by modifying the total reactant flow, we conclusively demonstrate a shift in the reaction network from a sequential process (CH_4 to CH_3OH to CO_2) to a parallel one (CH_4 to both CH_3OH and CO_2) with decreasing Al content. This parallel reaction network has not been reported in the literature.[1, 27, 38, 110] These results suggest inherent differences between the active site(s) of Cu-CHA(76) and Cu-CHA(160), and the Cu dimer motifs reported for selective CH_4 oxidation.

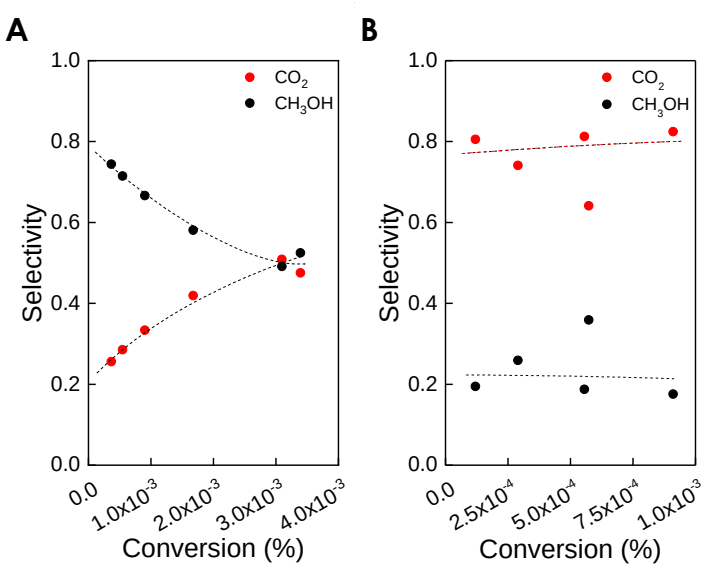

Figure IV-1. Product selectivity versus conversion for **A.** Cu-CHA(76) and **B.** Cu-CHA(160). T = 543 K, 0.25 g_{cat}, 25 - 200 sccm total flow, P_{CH4} = 18 kPa, P_{O2} = 0.09 kPa, P_{H2O} = 3.14 kPa, bal He except as noted.

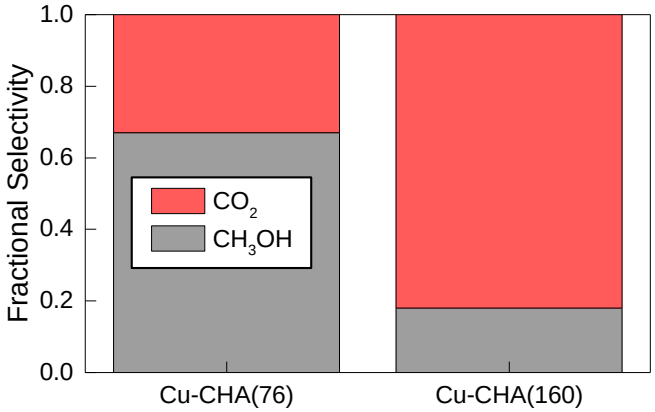

Figure IV-2. Product selectivity of Cu-CHA(76) and Cu-CHA(160) at 0.0001% CH_4 conversion. 0.25 g_{cat}, 543 K, P_{CH4} = 18 kPa, P_{O2} = 0.09 kPa, P_{H2O} = 3.14 kPa, bal He, total flow rate was altered to achieve target conversion.

As a result of a change in the active site(s) within Cu-CHA(76) and Cu-CHA(160), it is likely that the reaction orders would deviate from the previously identified reaction orders of -0.1, 0.72, and 0.3 for H_2O, CH_4, and O_2, respectively, for a Cu-CHA zeolite (Si/Al = 23, Cu/Al = 0.22, Cu/cage = 0.11) selective for partial CH_4 oxidation.[110] Similar to this previous report, H_2O appears to be kinetically irrelevant for partial methane oxidation, but necessary for methanol production with near-zero order dependences for both Cu-CHA(76) and Cu-CHA(160) (Figure IV-3A and Figure IV-3D).[83, 110] Upon returning to baseline methanol synthesis conditions, a reduced rate of CO_2 production was observed over Cu-CHA(160), suggesting deactivation may have occurred. This observation is also consistent with DFT calculations, which indicated water is necessary for methanol desorption over monocopper sites, but is not otherwise involved.[83, 146] In contrast to the near first order dependence on P_{CH4} observed for selective methane oxidation, we observed 0.51 and 0.2 P_{CH4} dependences over Cu-CHA(76) and Cu-CHA(160), respectively (Figure IV-3B and Figure IV-3E, $r_{total} = r_{CO2} + r_{CH3OH}$). The weakening P_{CH4} dependence of the total rate of C-H activation with decreasing Al content indicates C-H scission plays less of a rate-controlling role in these zeolites with low Al. The weakening dependence on P_{CH4} was expected to be accompanied by an increase in the reaction order of a different reactant that is indicative of its increased degree of rate control. This was observed with P_{O2} order dependences for the total rate of C-H activation of 0.42 and 0.60 for Cu-CHA(76) and Cu-CHA(160), respectively (Figure IV-3C and Figure IV-3F). The weak P_{CH4} and strong P_{O2} dependence are consistent with initial observations reported by Dinh et al for a zeolite with similar Al content.[110] The increase in the P_{O2} order dependence with decreasing Al content suggests O_2 activation, and re-oxidation of the Cu active site, is rate-controlling for zeolites with low Al content.

Temperature studies over these catalysts indicate an apparent activation energy ($E_{a,app}$) of 73 and 100 kJ mol^{-1} for Cu-CHA(76) and Cu-CHA(160), respectively (Figure IV-4). From Cu-CHA(76) to Cu-CHA(160), an increase in $E_{a,app}$ coincides with CO_2 becoming the major product and may be indicative of the E_a for complete oxidation of CH_4. Dinh et al. reported an $E_{a, app}$ of 140 kJ mol^{-1} for Cu_xO_y within SSZ-13 zeolites, which were only active for CO_2 formation.[110]

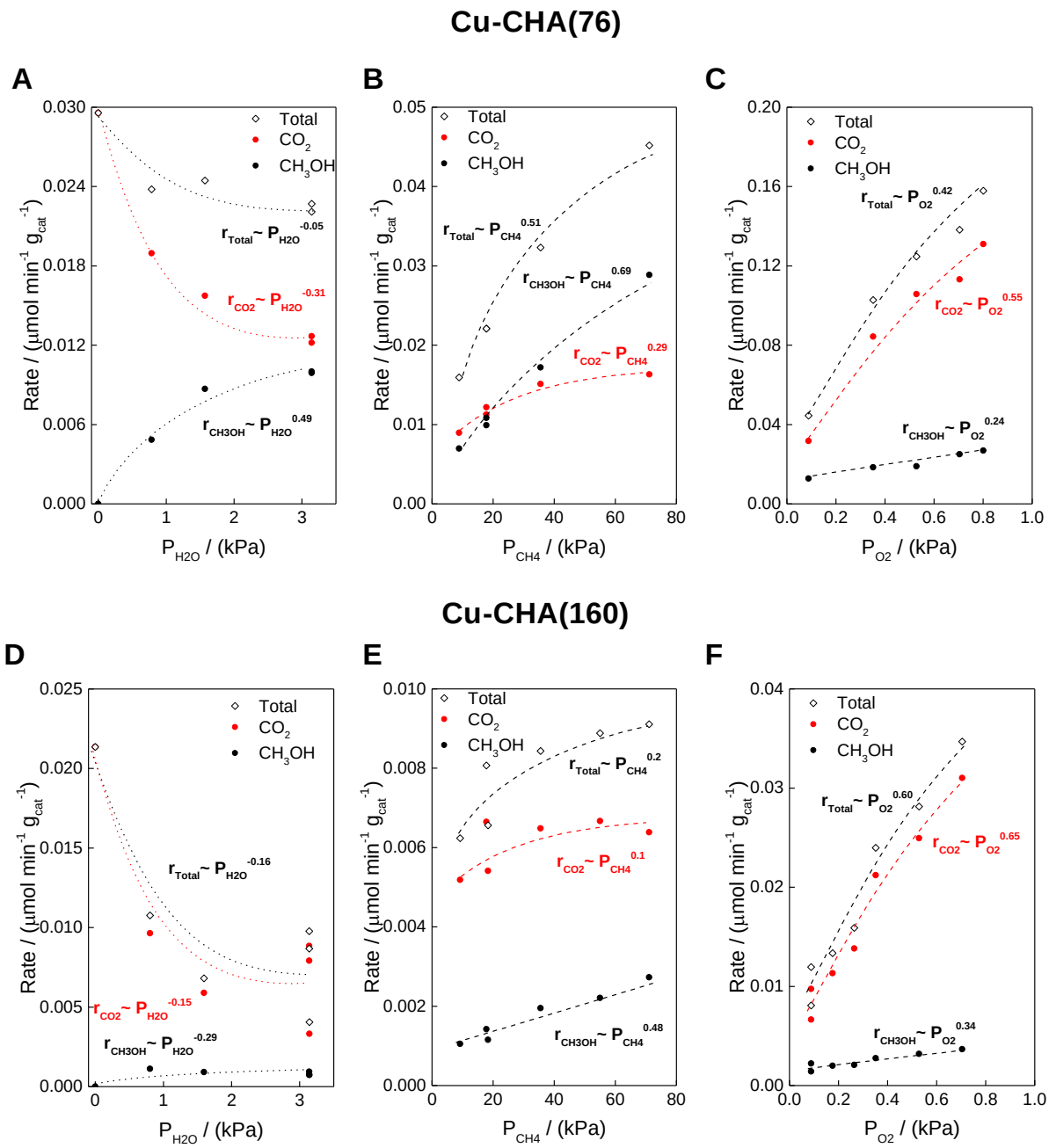

Figure IV-3. Partial pressure variations over Cu-CHA(76) and Cu-CHA(160). **A.** P_{H2O}, **B.** P_{CH4}, and **C.** P_{O2} over Cu-CHA(76). **D.** P_{H2O}, **E.** P_{CH4}, and **F.** P_{O2} over Cu-CHA(160). T = 543 K, 0.25 g_{cat}, 25 - 200 sccm total flow, P_{CH4} = 18 kPa, P_{O2} = 0.09 kPa, P_{H2O} = 3.14 kPa, bal He except as noted. $r_{total} = r_{CO2} + r_{CH3OH}$.

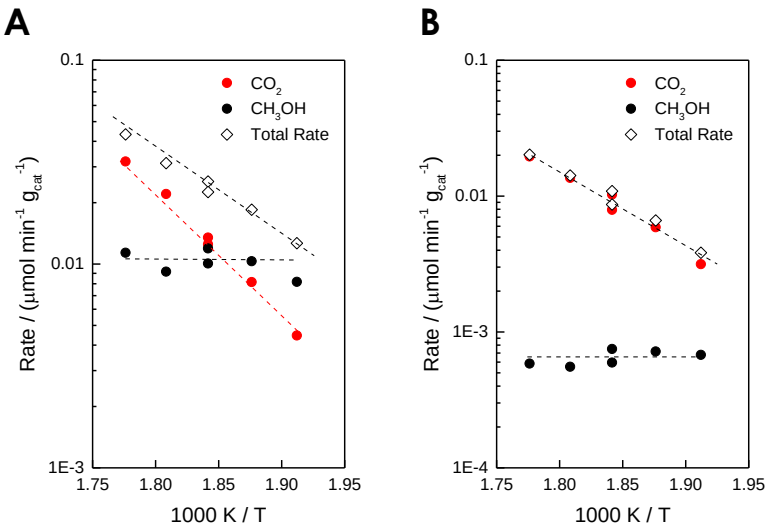

Figure IV-4. Product formation rates versus temperature over **A.** Cu-CHA(76) and **B.** Cu-CHA(160). Measured $E_{a,\ app}$ was 73 kJ mol^{-1} for Cu-CHA(76) and 100 kJ mol^{-1} for Cu-CHA(160). 0.25 g_{cat}, 523-563 K, 25 sccm, P_{CH4} = 18 kPa, P_{O2} = 0.09 kPa, P_{H2O} = 3.14 kPa, bal He.

3. Characterization of Low Al Cu-SSZ-13 Zeolites

While kinetic experiments over Cu-CHA(76) and Cu-CHA(160) demonstrate stark differences in the reaction pathway and the roles of CH_4 and O_2 versus a zeolite with an abundance of Al that is selective for partial CH_4 oxidation, detailed characterization methods in combination with chemical titration are required to elucidate the nature of the active site(s) within these two zeolites. Thus, these zeolites were characterized by *in situ* x-ray absorption spectroscopy (XAS) under methanol synthesis conditions (Figure IV-5). Notably, Cu-CHA(76) has a significant pre-edge feature at 8983 eV in the x-ray absorption near edge spectrum (XANES), indicative of an abundance of Cu(I) within the zeolite (Figure IV-5A). [137] This result is consistent with re-oxidation of the Cu active site as the rate-determining step for CH_4 oxidation. In the extended x-ray absorption fine spectrum (EXAFS), this catalyst does not exhibit a second-shell scattering peak (~2-3 Å), suggesting the existence of isolated Cu sites within Cu-CHA(76) (Figure IV-5B). The second-shell scattering peak is primarily assigned to Cu-Cu or Cu-T-site scattering,[87, 147-148] However, these results are different from those previously reported where under similar methanol synthesis flows, limited Cu-Cu scattering was observed over a Cu-CHA catalyst with the same Si/Al content (Si/Al = 76). In contrast to Cu-CHA(76), Cu-CHA(160) does not display such an intense Cu(I) pre-edge feature under methanol synthesis flows in the XANES (Figure IV-5A) and features a second shell scattering peak (Figure IV-5B). Both of these features are similar to previously studied Cu-CHA zeolites containing Cu dimers selective for partial CH_4 oxidation.[110] However, given the hypothesized disperse nature of Cu, the second shell scattering peak of Cu-CHA(160) can plausibly be from either Cu-Cu or Cu-T-site scattering, rendering a fit inconclusive. In both Cu-CHA(76) and Cu-CHA(160), the presence of a second shell scattering feature in the EXAFS may be a result of inhomogeneities in Al distribution allowing for the formation of small Cu clusters.[143-144] Because the local Cu structure was not readily assigned, we probed the nature of the Cu in greater detail by using NH_3 titration in combination with XAS.

Introduction of an NH_3 co-feed to methanol synthesis flows is known to destroy Cu dimers[110] and enable diffusion of ammoniated Cu ions between proximate Al.[128] Following complete desorption of NH_3, Cu dimers can then be reformed upon the re-introduction of methanol synthesis flows by the diffusion of hydrated Cu ions.[110] In the limit of dispersed Al sites, the introduction and removal of NH_3 is not expected to enable Cu diffusion and Cu speciation should be unaffected. Thus, Cu-CHA(76) and Cu-CHA(160) were treated with NH_3 and, upon complete desorption, exposed to methanol synthesis flows to probe the possibility of the existence of mobile Cu ions within these zeolites. Accordingly, following treatment with NH_3, Cu-CHA(76) showed minimal changes in the XANES and EXAFS, consistent with the inhibition of Cu ion diffusion due to the lack of an Al pathway. In contrast, Cu-CHA(160) now featured a significant Cu(I) pre-edge feature in the XANES and the absence of a second-shell scattering peak in the EXAFS, markedly different than prior to NH_3 treatment and quite similar to Cu-CHA(76). The change in the XANES and EXAFS of Cu-CHA(160) following NH_3 treatment is confusing given Cu diffusion was not expected to occur facilely with minimal Al content. Consequently, while the second shell scattering peak observed for Cu-CHA(160) prior to an NH_3 treatment may be from Cu-Cu scattering, the absence of this second shell scattering following NH_3 treatment is also not readily rationalized. Consequently, while the exact nature of Cu speciation within Cu-CHA(76) and Cu-CHA(160) cannot be easily determined, we can conclude Cu speciation within both Cu-CHA(76) and Cu-CHA(160) is not the same as the reversibly formed Cu dimers observed in catalysts with an abundance of Al.

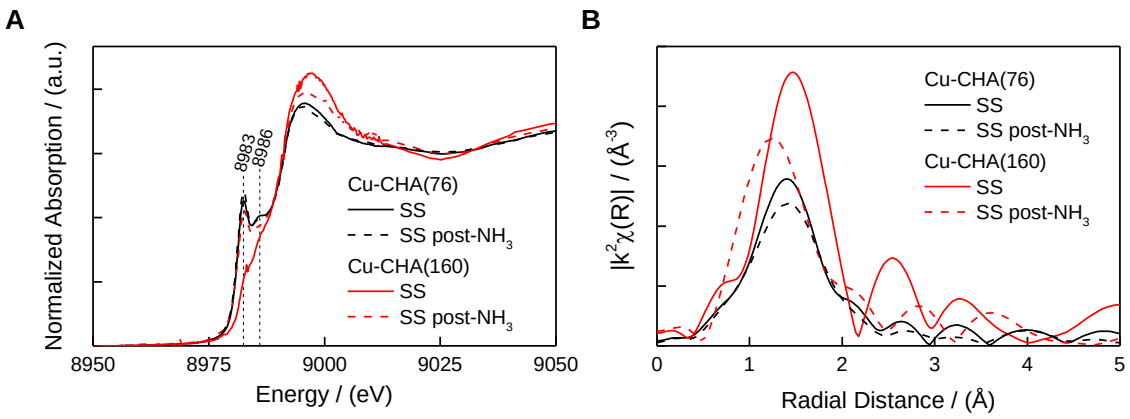

Figure IV-5. A. XANES and **B.** EXAFS under methanol synthesis flows and following NH_3 titration and complete desorption of Cu-CHA(76) and Cu-CHA(160). T = 543 K, 25 sccm, 3.2 kPa H_2O, 8 kPa O_2, 18 kPa CH_4, bal He; SS: steady-state methanol synthesis flows, SS post-NH_3: steady-state methanol synthesis flows following NH_3 poisoning (1 kPa NH_3, bal He, 543 K) and desorption at 673 K under dry He.

4. Conclusions

Two zeolites with decreasing Al content were synthesized to disrupt hydrated Cu ion diffusion and promote formation of isolated Cu sites. We demonstrated that the reaction pathway at dilute Al is a sequential pathway where O_2 activation is a rate-controlling step and there is less rate control by C-H scission of CH_4. Decreasing Al content results in worsening selectivity for CH_3OH. *In situ* XAS suggests isolated Cu ions can be obtained but other species are also present. These species are destroyed by NH_3 titration and do not reform, unlike those active for selective partial CH_4 oxidation. These results demonstrate zeolites with dilute Al promote formation of Cu sites that are active, but unselective, for partial CH_4 oxidation.

5. *Acknowledgements*

This research used resources at beamline 8-ID (Inner Shell Spectroscopy) of the National Synchrotron Light Source II, a U.S. Department of Energy (DOE) Office of Science User Facility operated for the DOE Office of Science by Brookhaven National Laboratory under Contract No. DE-SC0012704.The authors gratefully acknowledge the financial support of ExxonMobil. K.D. acknowledges the partial support from the National Science Foundation Graduate Research Fellowship under Grant No. 1122374. Any opinion, findings, and conclusions or recommendations expressed in this material are those of the author(s) and do not necessarily reflect the views of the National Science Foundation. The authors thank Z. Wang for help with ICP-MS data collection and M. Stone and M. Orella for feedback on the manuscript.

6. *Supporting Information*

6.1. Methods

Unless otherwise described below, remaining methods are described in Section II.6.1.

6.1.1. Catalyst Characterization Techniques

X-Ray Absorption Experiments

Cu-CHA(75) and Cu-CHA(160) were ground into a fine powder, and loaded in a Kapton capillary tube (SWPT-072-12-50, translucent amber miniature polyimide, 0.072” ID, 0.0745” OD) between two plugs of quartz wool and used in a Clausen cell with a thermocouple placed coaxially downstream of the catalyst.[149] XAS data collection was performed at NSLS-II on beamline 8-ID (Inner Shell Spectroscopy). Data was collected in fluorescence mode with a Cu foil as a reference.

EXAFS spectra were collected under ambient conditions prior to gas treatments. Catalysts were then heated to 543 K in 50 min under 25 sccm P_{O2} = 8 kPa, bal He. Following, methanol synthesis flows of 25 sccm P_{CH4} = 18 kPa, P_{O2} = 8 kPa, P_{H2O} = 3.14 kPa, bal He. The catalyst was then treated to 20 sccm P_{NH3} = 1 kPa, bal He, followed by complete desorption under 23 sccm He by ramping to 673 K in 15 min and holding until no change in XANES was observed. The cell was then cooled to 543 K under He and methanol synthesis flows were reintroduced. XAS (~60 s/scan) were collected at each stage until no change in spectra were observed. Ten spectra were then collected at these steady-state conditions. All spectra were collected at 543 K.

6.2. Referenced Figures and Tables

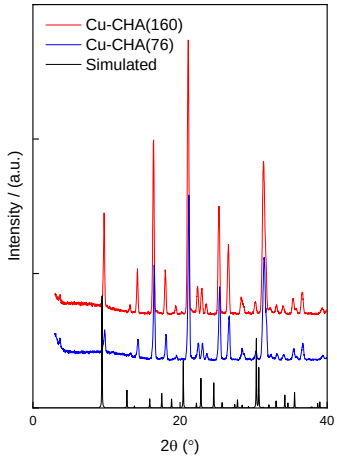

Figure IV-6. PXRD of Cu-CHA(76) and Cu-CHA(160). Simulated pattern was taken from the IZA Database of Zeolite Structures.[150]

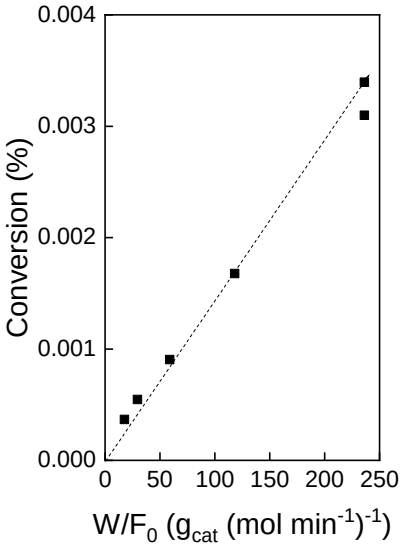

Figure IV-7. Fractional conversion versus contact time. Cu-CHA(76), 0.25 g_{cat}, 543 K, 25-200 sccm, P_{CH4} = 18 kPa, P_{O2} = 0.09 kPa, P_{H2O} = 3.14 kPa, bal He.

Table IV-2. Parameters used for verification of absence of heat and mass transfer gradients. GradientCheck for Heterogeneous Catalysis was used.[124] Gaseous properties were obtained from the NIST WebBook's Thermophysical Properties of Fluid Systems.[22]

max r_{obs} (mol kg_{cat}^{-1} s^{-1})	$7.24 \cdot 10^{-7}$
ΔH_{rxn} (kJ mol^{-1})	-127
E_a (kJ mol^{-1})	100
Fractional conversion	0.003
n	1
ρ_{bulk} (kg m^{-3}) (Assumed ε=0.4)	750

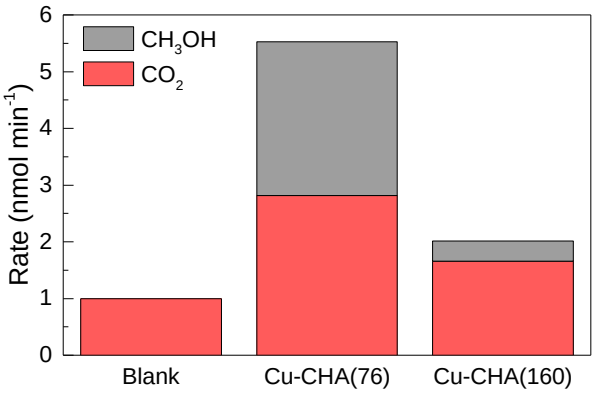

Figure IV-8. Product formation rates in the absence of catalyst and over Cu-CHA(76) and Cu-CHA(160). 0.25 g_{cat}, 543 K, P_{CH4} = 18 kPa, P_{O2} = 0.09 kPa, P_{H2O} = 3.14 kPa, bal He, 25 sccm

V. Breaking the Selectivity-Conversion Limit of Direct Methane to Methanol by Tandem Partial Oxidation and Alkylation with Size-Selective Zeolites

1. Motivation

Extensive study of catalytic partial oxidation of CH_4 over Cu-exchanged zeolites revealed > 75% CH_3OH selectivity can be attained by simply co-feeding readily available CH_4, H_2O, and O_2 at mild conditions (T < 573 K, P = 1 bar), but CH_4 conversion is limited to ~0.01%.[104, 151-152] Despite their attractiveness, at CH_4 conversion beyond 0.01%, selectivity for CH3OH drops precipitously due to the selectivity-conversion limit of CH_4 stemming from the relative ease of continued oxidation of partially oxidized CH_4-derived products.[38, 110] Consequently, ideas such as product capture or protection must be employed to move past this thermodynamic limit.[1, 27, 38, 152]

Norskov and coworkers suggested the introduction of a CH_3OH collector to limit gas phase over oxidation[38] while van Bokhoven and coworkers emphasized the use of a multicomponent catalyst to protect methanol as a solution.[27] As discussed previously in Chapter I (and Dinh et al.[1]), I highlighted an alternative solution of product protection combined with chemical scavenging, inspired by methane monooxygenases that utilize a gating mechanism to limit contact of CH_3OH with the active site to prevent continued oxidation. Importantly, the selectivity for CH_3OH of methane monooxygenases is not solely based on active site structure as the methane monooxygenase active site is more active for CH_3OH activation.[50] While this gating mechanism is not possible with synthetic catalysts due to their relatively rigid nature, we suggested chemical scavenging of the methoxy intermediate upon the activation of CH_4 to CH_3OH as a means to mimic this gating system. Chemical scavenging is particularly attractive as it avoids the necessity of reactant and temperature cycling to desorb CH_3OH and reactivate the catalyst.

To successfully implement a chemical scavenging system for partially oxidizing CH_4, the system must meet multiple requirements: (1) CH_4 activation is uninhibited by the scavenger molecule, (2) the scavenger molecule and product are more resistant than CH_3OH to undesirable oxidation to CO_2, (3) the rate of the scavenging reaction must not be rate-limiting, and (4) the diffusion distance of CH_3OH must be minimized to limit opportunities for over oxidation of CH_3OH to undesirable CO_2.

A system that has the potential to meet these requirements are Cu-exchanged zeolites, which produce CH_3OH continuously with >75% selectivity at ~0.01% CH_4 conversion[91, 110] by co-feeding readily available CH_4, H_2O, and O_2 at mild conditions (T < 573 K, P = 1 bar). Beyond 0.01% CH_4 conversion, selectivity for methanol decreases quickly with increasing conversion over Cu-exchanged zeolites.[38, 110] Thus, with product protection, this system has the potential to significantly increase CH_4 conversion while maintaining high product selectivity.

More specifically, chemical scavenging can be implemented by the combination of a Cu-SSZ-13 zeolite (CHA crystal structure) with H-ZSM-5 (MFI crystal structure) and an additional benzene co-feed with the methanol synthesis feed of CH_4, H_2O, and O_2 (Figure V-1). Cu-SSZ-13 is responsible for the continuous production of methanol and methanol is then captured as toluene by alkylation with benzene over the acid sites of H-ZSM-5.[153-154] Cu-SSZ-13 is particularly well-suited because benzene cannot access the pores of Cu-SSZ-13 to inhibit selective CH_4 activation (CHA pore window diameter of 3.72 Å[150] vs. kinetic diameter of benzene of 5.85 Å[155]).

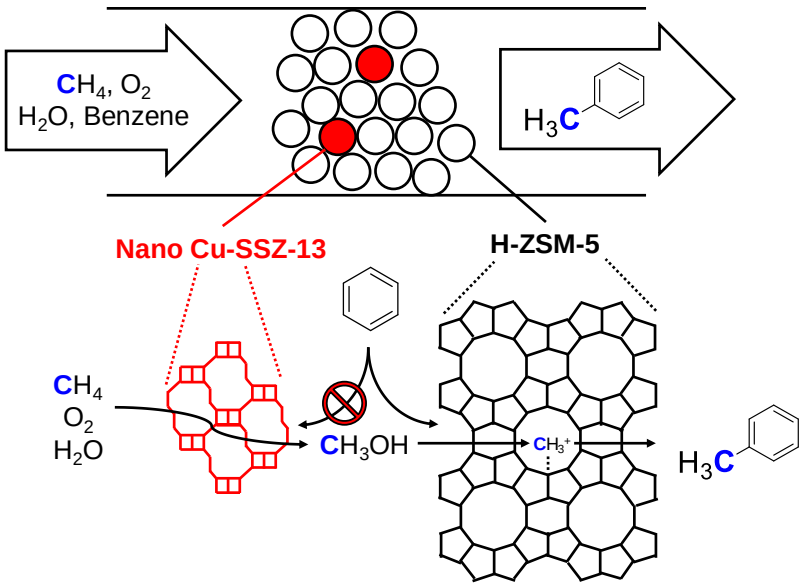

Figure V-1. Depiction of product protection using a copper-exchanged zeolite and a second proton-form zeolite of a different topology. The copper-exchanged zeolite produces an activated C_1 intermediate or methanol that is incorporated into an aromatic co-feed over the Brønsted acid sites of the second zeolite.

Therefore, we demonstrate the implementation of a tandem partial oxidation and alkylation process that maintains partial oxidation selectivity of >70% beyond 0.1% CH_4 conversion. This process effectively scavenges CH_3OH generated from Cu-catalyzed partial methane oxidation in Cu-SSZ-13. The partially oxidized intermediates are incorporated into aromatic products by acid-catalyzed alkylation pathways in H-ZSM-5,[153, 156-157] creating methyl-substituted aromatic products that are less susceptible than methanol to over oxidation reactions and enabling partial oxidation selectivities beyond the selectivity-conversion limit endemic to methane partial oxidation systems. 77% toluene selectivity at 663 K and 1 bar and 90% toluene selectivity at 543 K and 11 bar were obtained compared to only 2% and 48% CH_3OH selectivity, respectively, under identical conditions in the absence of benzene at isoconversion. A 100x improvement over current continuous processes was attained with a product yield 2.7 μmol min^{-1} g_{cat}^{-1} at 11 bar and 603 K (59% toluene and xylene selectivity, 0.7% CH_4 conversion). These findings provide a pathway towards achieving an industrially-relevant small-scale CH_4 conversion process.

2. Implementation of Tandem Partial Methane Oxidation and Alkylation

Based on the findings of Dinh et al.,[110] Cu-SSZ-13 catalysts (denoted Cu-CHA) were chosen to contain no Na, an abundance of Al to facilitate active site formation, and Cu/cage < 0.3 to avoid the formation of undesirable Cu oxides. H-ZSM-5 (denoted H-MFI) was synthesized to contain no Fe and an abundance of Al, and thereby protons, to enable benzene alkylation.[153, 157] Catalyst synthesis and catalyst characterization details are provided in Section V.6, Figure V-11, and Figure V-12. Compositions of all catalysts used in this study are summarized in Table V-1.

Table V-1. Catalyst composition of Cu-CHA and H-MFI used in this study

Catalyst	Composition		Cu Content (wt%)
	Si/Al	Cu/Al	
Cu-CHA-1	11	0.13	1.1
Cu-CHA-2	13	0.13	0.9
H-MFI-1	19	-	-
H-MFI-2	16	-	-
H-MFI-3	15	-	-

Dinh et al. also demonstrated CO_2 formation over Cu-exchanged zeolites is a result of a sequential pathway proceeding by CH_4 to CH_3OH to CO_2.[110] Thus, to minimize the number of downstream over oxidation events, we minimized the diffusion path of CH_3OH by combining Cu-CHA with H-MFI with a larger amount of H-MFI than Cu-CHA (e.g., 1:3 Cu-CHA:H-MFI by weight, denoted Cu-CHA/H-MFI). Cu-CHA and H-MFI were intimately mixed by vortexing the fine powders together prior to pelletizing.

Figure V-2 demonstrates the successful implementation of chemical scavenging to selectively produce toluene and circumvent the selectivity-conversion limit for direct partial oxidation of methane. Rates of product formation are presented as the absolute rates observed to enable direct comparison of H-MFI, Cu-CHA, and Cu-CHA/H-MFI. The catalyst loading of the individual H-MFI and Cu-CHA catalysts beds were the same as in the intimately mixed catalyst bed. Reaction rates were measured in the absence of heat and mass transfer limitations (Figure V-13 and

Table V-3). Stable and repeatable product formation rates were observed for at least 12 h on stream (Figure V-14). Toluene was not observed in the absence of catalyst under the same feed and reactor conditions (Figure V-15). Immediately apparent is the reduced rate of CO_2 formation and an increased rate of formation of partially oxidized products (CH_3OH, CH_3OCH_3, and toluene) with Cu-CHA/H-MFI in comparison to Cu-CHA despite an apparent increase in CH_4 conversion. This is in contrast to the expected selectivity-conversion trend. At 663 K and 1 bar, there is 58% selectivity for toluene over Cu-CHA/H-MFI in contrast to only 4% selectivity for partially oxidized products over Cu-CHA. This same effect is observed when pressure is increased. At 543 K and 11 bar, there is 89% selectivity for toluene over Cu-CHA/H-MFI versus only 40% selectivity for partially oxidized products over Cu-CHA. These results indicate the combination of partial CH_4 oxidation with a chemical scavenging system is a viable solution to improving CH_4 conversion while maintaining high product selectivity.

Importantly, significant toluene formation is only observed when both Cu-CHA and H-MFI are present with a co-feed of CH_4, O_2, H_2O, and benzene, indicating both catalysts are required for toluene formation. In the absence of either Cu-CHA or H-MFI, low rates of toluene formation were observed over H-MFI for $P > 1$ bar and over Cu-CHA for $T \geq 633$ K or $P > 1$ bar (Figure V-2). These rates of formation of toluene are much lower than those observed over Cu-CHA/H-MFI. We hypothesize that the observed toluene formation over Cu-CHA is a result of surface protons catalyzing aromatic alkylation since benzene cannot access the pores of Cu-CHA while direct formation of toluene from CH_4 over H-MFI has been reported.[158]

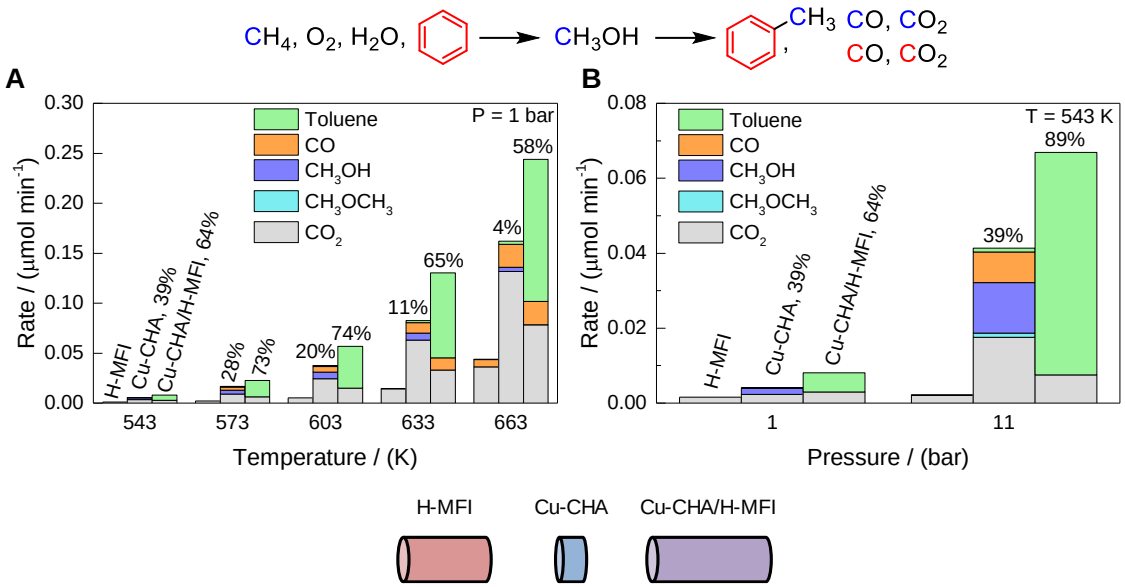

Figure V-2. Comparison of the total rates of product formation across **A.** Temperature and **B.** Pressure over different catalyst compositions with the alkylation feed mixture: 0.2625 g H-MFI-1, 0.0875g Cu-CHA-1, and (0.0875 g Cu-CHA-1 + 0.2625 g H-MFI-2), 26.1 sccm, x_{CH4} = 0.18, x_{C6H6} = 0.008, x_{O2} = 0.001, P_{H2O} = 3.1 kPa, bal He. When pressurizing, water partial pressure remains unchanged because it was introduced by a saturator, all other reactants increased proportionally (Section 6.1.2). Reaction schematic demonstrates potential sources of product formation where red and blue C's are indicative of source of C (CH_4 or benzene) for observed products.

Upon closer inspection of Figure V-2, the total rate of product formation is consistently higher over Cu-CHA/H-MFI than over either H-MFI or Cu-CHA or the addition of the rates of production formation over each of H-MFI and Cu-CHA (Figure V-16). We hypothesize the oxidation of benzene to CO and CO_2 contributes to these observed rates in addition to the already expected over oxidation of CH_4 to CO_2. Thus, while the rate of toluene formation over Cu-CHA/H-MFI is similar to the total rate of product formation over Cu-CHA (Figure S6), we cannot make a direct comparison due to differing amounts of CO and CO_2 stemming from benzene over these catalysts. To study complete CH_4 and benzene oxidation reactions in greater detail, the rates of product formation were observed over the same catalyst beds in the absence of benzene and CH_4, respectively.

Figure V-3A demonstrates in the absence of benzene (feeding $CH_4/H_2O/O_2$), the activation of the C-H bond of CH_4 originates primarily over Cu-CHA. Across all temperatures, the total rate of C-H activation is similar between Cu-CHA and Cu-CHA/H-MFI. Further, the rate of C-H activation over MFI is negligible over 543 – 663 K in comparison to the rates of C-H activation versus Cu-CHA, a necessary requirement with the introduction of a second catalyst for chemical scavenging to avoid other sources of unwanted CH_4 over oxidation. The absence of significant CH_3OH formation between Cu-CHA and Cu-CHA/H-MFI can be attributed to the added catalyst through which CH_3OH must travel, increasing the probability of over oxidation events occurring homogeneously or over H-MFI.

Figure V-3B then demonstrates benzene oxidation contributes to the rates of CO and CO_2 formation in the absence of CH_4 (feeding $C_6H_6/H_2O/O_2$). Across all three catalyst beds, CO and CO_2 are the primary products observed. Because these rates of product formation are on similar scales to those observed when co-feeding $CH_4/H_2O/O_2$ (Figure V-3), we must consider the contribution of benzene oxidation to CO and CO_2 product formation rates under tandem oxidation and alkylation conditions. It is unknown to what extent Cu-CHA and H-MFI each contribute to the observed rates of product formation over Cu-CHA/H-MFI because the sum of the rates over the individual catalyst beds of H-MFI and Cu-CHA is not equal to the rates over Cu-CHA/H-MFI.

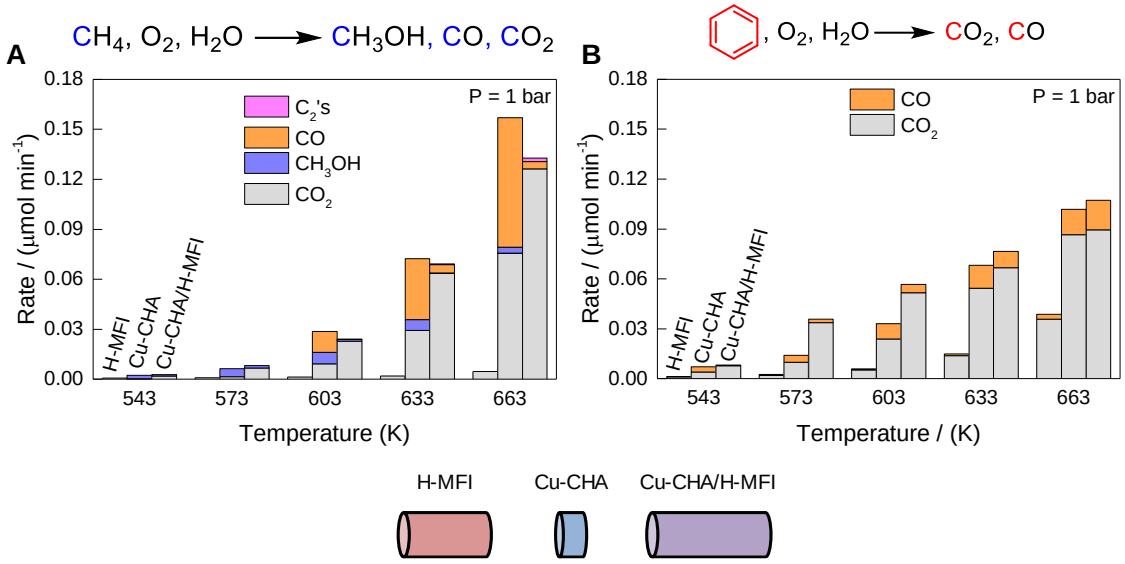

Figure V-3. Comparison of the total rates of conversion and product formation under **A**. Partial methane oxidation flows and **B**. Benzene oxidation flows over different catalyst compositions: 0.2625 g H-MFI-1, 0.0875g Cu-CHA-1, and (0.0875 g Cu-CHA-1 + 0.2625 g H-MFI-1), P = 1 bar, 26.1 sccm, P_{CH4} = 18 kPa, P_{O2} = 0.09 kPa, P_{H2O} = 3.1 kPa, P_{C6H6} = 0.80 kPa, bal He. Reaction schematic demonstrates potential sources of product formation where red and blue C's are indicative of source of C (CH_4 or benzene) for observed products.

Given the significance of benzene oxidation, an isotope switching experiment with $^{13}C_6H_6$ under tandem oxidation and alkylation conditions (co-feed of $CH_4/O_2/H_2O/C_6H_6$) over Cu-CHA/H-MFI revealed benzene oxidation accounts for more CO_2 as temperature increases (Section V.6.2.1,Table V-4, Figure V-17 and Figure V-18). Benzene accounts for 19% of CO_2 observed at 543 K and 1 bar and 42% of CO_2 at 603 K and 1 bar. Because benzene is fed in large excess compared to CO and CO_2 and its fragmentation pattern includes m/z = 28, we could not estimate the contribution of benzene oxidation to CO formation directly. These results were used to remove the contribution of benzene oxidation to CO_2 formation rates over Cu-CHA/H-MFI and enable direct comparison of the rates of product formation from CH_4-to-CH_3OH over Cu-CHA to the rates of product formation from tandem oxidation and alkylation over Cu-CHA/H-MFI (*vide infra)*. Kinetic data in combination with these results were used to estimate the contribution of benzene oxidation at conditions not specifically tested (*vide infra*, Section V.6.2.2 and Figure V-19).

To gain further insight into the origins of product formation and the role of each reactant during tandem partial oxidation and alkylation, kinetic experiments at 543 K were completed by varying the total flow and partial pressures of CH_4, O_2, and benzene fed to Cu-CHA/H-MFI (Figure V-4). Analysis of a plot of selectivity versus conversion demonstrates product formation proceeds by a combination of sequential and parallel reaction pathways (Figure V-4A). The parallel reaction pathway can plausibly be attributed to two sources: (1) parallel formation of CO_2 from benzene and (2) parallel formation of CO_2 and toluene from CH_3OH. The presence of a sequential pathway is consistent with CH_4 activation first proceeding to CH_3OH and then to toluene and CO_2, in line with what has been previously reported for CH_4 activation over Cu-SSZ-13.[110] The parallel reaction pathway can be attributed to the parallel formation of CO_2 from benzene alongside the formation of CO_2 and toluene from CH_3OH.

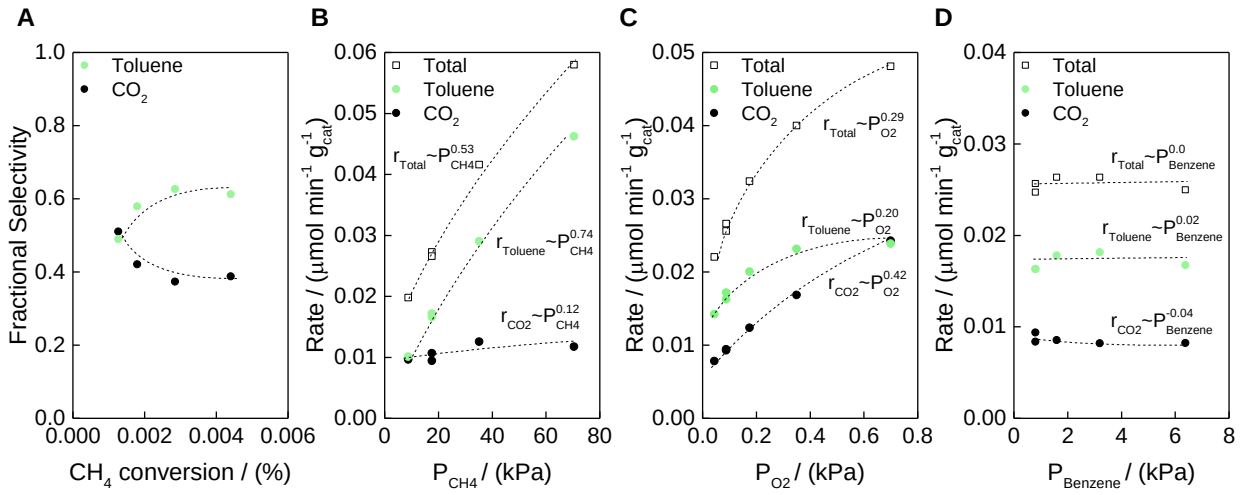

Figure V-4. A. Product selectivity versus conversion. Product formation rates versus **B.** P_{CH4}, **C.** P_{O2}, and **D**. $P_{benzene}$ over (0.0875 g Cu-CHA-1 + 0.2625 g H-MFI-2), T = 543 K, P = 1 bar, 26.1 sccm, 3.2 kPa H_2O, 0.09 kPa O_2, 18 kPa CH_4, 0.80 kPa benzene, bal He, except as noted.

The positive order dependence of toluene formation rate upon CH_4 pressure implies that C-H scission is rate determining in the methylation reaction sequence (Figure V-4B). This finding is consistent with the near first order P_{CH4} dependence previously reported for CH_4-to-CH_3OH formation over Cu-CHA.[110] The weak order dependence for the rates of product formation on P_{O2} are consistent with the dependences observed under methanol synthesis conditions over Cu-CHA (Figure V-4C). The lack of observed gaseous methanol in conjunction with zero-order dependence of all product formation rates upon benzene partial pressure implies rapid methanol interception and following alkylation reactions (Figure V-4D) are necessary to allow for the formation of toluene. The proposed reaction pathway in Figure V-5 summarizes these observations where initial CH_4 activation forms CH_3OH that can either alkylate benzene to form toluene or be over oxidized to form CO_2. CO_2 is also formed via benzene oxidation in a parallel pathway.

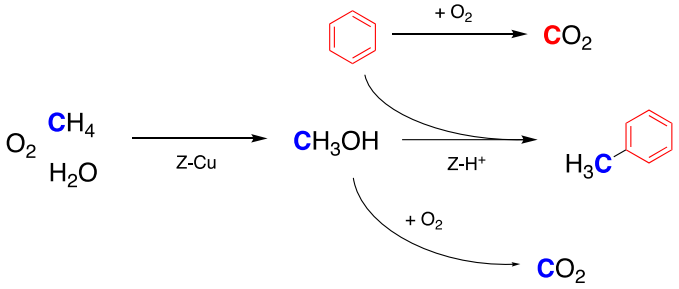

Figure V-5. Hypothesized reaction pathway at work in the reported methane partial oxidation/aromatic alkylation mixed system. Deleterious CO_2 formation from methanol oxidation is minimized by intermediate scavenging to form alkylated aromatics, thus decreasing CO_2 yields, and direct benzene oxidation pathways can be mitigated by modification of catalyst morphology and gas phase compositions. CO is hypothesized to form by the same reaction pathways as CO_2 and is omitted for clarity.

A separate set of experiments was conducted to investigate the effects of proximity and mixing of Cu-CHA and H-MFI upon rates of product formation and product selectivity (Figure V-6). The rates of production formation over separate beds in series are compared to intimately mixed Cu-CHA and H-MFI and to the simple addition of product formation rates from individual beds of Cu-CHA and H-MFI. Across a range of temperatures and pressures, two things stand out as the two catalyst beds are brought into closer contact: (1) the rate of toluene formation increases and (2) the rates of CO_2 and CO formation decrease. Consequently, intimately mixed Cu-CHA and H-MFI yielded the highest toluene selectivity of all catalyst configurations under identical conditions. These observations can be rationalized by the increased distance CH_3OH must be transported to be brought into contact with H-MFI with the separated beds, thereby increasing the number of homogeneous over oxidation events of CH_3OH and reducing the amount of CH_3OH available for benzene alkylation.

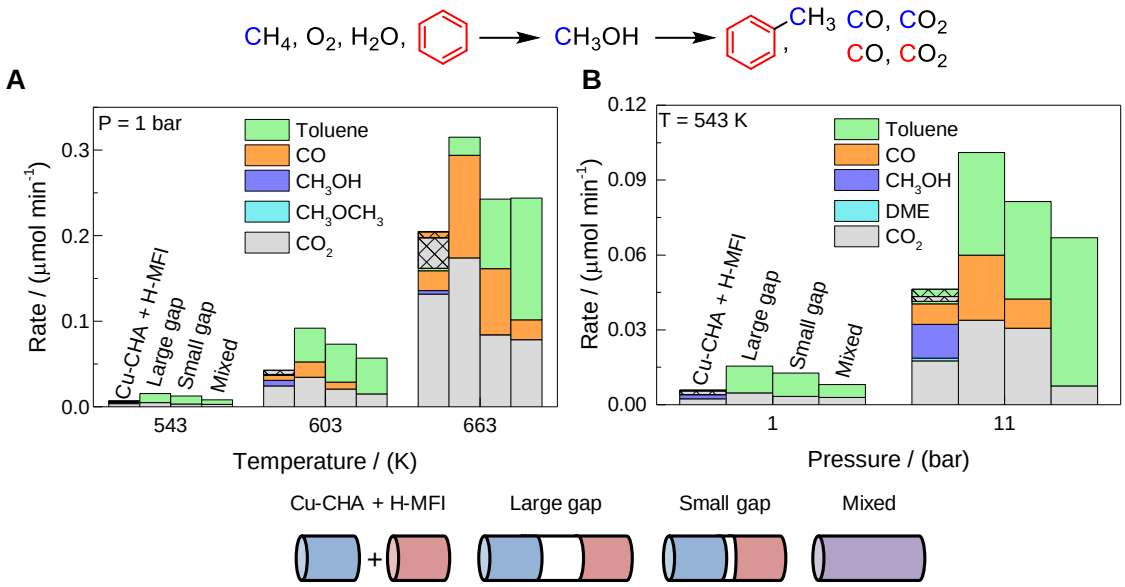

Figure V-6. Comparison of the total rates of product formation across **A.** Temperature and **B.** Pressure over catalyst configurations with tandem oxidation and alkylation feed mixture. “Cu-CHA + H-MFI” corresponds to addition of rates over separate beds of Cu-CHA and H-MFI, “Large gap” corresponds to a 3 cm quartz wool plug between beds, and “Small gap” corresponds to a 1 cm quartz wool plug. Bars with “x” are rates observed over H-MFI. (0.0875 g Cu-CHA-1 and 0.2625 g H-MFI-2), 26.1 sccm, x_{CH4} = 0.18, x_{C6H6} = 0.008, x_{O2} = 0.001, P_{H2O} = 3.1 kPa, bal He. When pressurizing, water partial pressure remains unchanged because it was introduced by a saturator, all other reactants increased proportionally (Section 6.1.2). Reaction schematic demonstrates potential sources of product formation where red and blue C’s are indicative of source of C (CH_4 or benzene) for observed products.

Based upon the necessity for intimate mixing of Cu-CHA and H-MFI and knowledge of the origins of each product, we can now compare CH_4-to-CH_3OH conversion over Cu-CHA to CH_4-to-CH_3OH-to-toluene conversion over Cu-CHA/H-MFI (Figure V-7) to demonstrate the efficacy of methanol scavenging. The results of the isotope labeling experiment plus kinetic experiments were used to remove the contribution of benzene to CO_2 formation rates in the tandem partial oxidation and alkylation system. First, Figure V-7A and Figure V-7B demonstrate there is good agreement between the total rates of product formation over Cu-CHA for the conversion of CH_4-to-CH_3OH and Cu-CHA/H-MFI for the conversion of CH_4-to-CH_3OH-to-toluene. Both catalyst beds contained the same loading of Cu-CHA but the bed used for tandem partial oxidation and alkylation contained additional H-MFI. These results are consistent with CH_4 activation occurring primarily over Cu-CHA as previously discussed, and enable facile observation of the improvement in desirable product selectivity under tandem partial oxidation and alkylation conditions. The slight differences in the total rate of C-H activation may be result of slight variations in Cu content between catalyst beds and being unable to account for the contribution of benzene oxidation to CO formation rates. The improvement in partial oxidation selectivity is highlighted at 663 K and 1 bar where there is 77% selectivity for toluene over Cu-CHA/H-MFI in contrast to 2% selectivity for CH_3OH over Cu-CHA. The high selectivity for toluene at increasing conversion is indicative of the relatively fast scavenging of CH_3OH by toluene versus thermodynamically favorable deleterious over oxidation events with free gaseous CH_3OH.

Increasing pressure for catalytic CH_4-to-CH_3OH conversion resulted in a small decrease in selectivity for CH_3OH (Figure V-7B), which is in contrast to stoichiometric processes where selectivity is often minimally affected.[89, 159] However, increasing pressure under tandem oxidation and alkylation conditions over Cu-CHA/H-MFI improves selectivity from 70 to 89%. This improved selectivity can be explained by analysis of the total dependence on reactant partial pressures for each product (e.g., with $r_{product} \sim P_{CH4}^{a} P_{O2}^{b}$, the total order dependence is a + b). Because toluene has a total dependence of 0.94 versus 0.54 for CO_2, increasing pressure increases the rate of toluene formation 75% more than the rate of CO_2 formation. In contrast, the rate of methanol formation has a total order dependence of 1.03 versus 1.14 for the rate of CO_2 formation under CH_4-to-CH_3OH conditions over Cu-SSZ-13, consequently slightly favoring CO_2 formation at elevated pressures. Thus, under tandem partial oxidation and alkylation conditions, pressure provides another variable for optimizing process conditions for selective CH_4 oxidation that would otherwise be unavailable.

Based on these favorable results, plotting partial oxidation selectivity versus conversion demonstrates the selectivity-conversion limit of CH_4 was circumvented by scavenging methanol (Figure V-7C). All data points presented from this work were generated by altering contact time, temperature, pressure, and catalyst loading and are summarized in Table V-5. Rates of product formation with increased catalyst loading are presented in Figure V-20. P_{O2} was increased by 3 and 5x for the points at 0.4 and 0.7% CH_4 conversion, respectively. Immediately apparent is above 0.01% CH_4 conversion, selectivity for toluene is at least 80% while selectivity for CH_4-to-CH_3OH over Cu-CHA has dropped to <60%. The low selectivity for toluene observed below 0.01% CH_4 conversion may be a result of underestimation of the contribution of benzene oxidation at these conversions and competition between over oxidation of CH_3OH to CO_2 versus its diffusion to Brønsted acid sites. Implementation of a tandem partial oxidation and alkylation system enabled us to surpass previously reported results for selectivity versus CH_4 conversion at mild conditions[110] while only requiring readily available O_2 and H_2O for CH_4 activation.

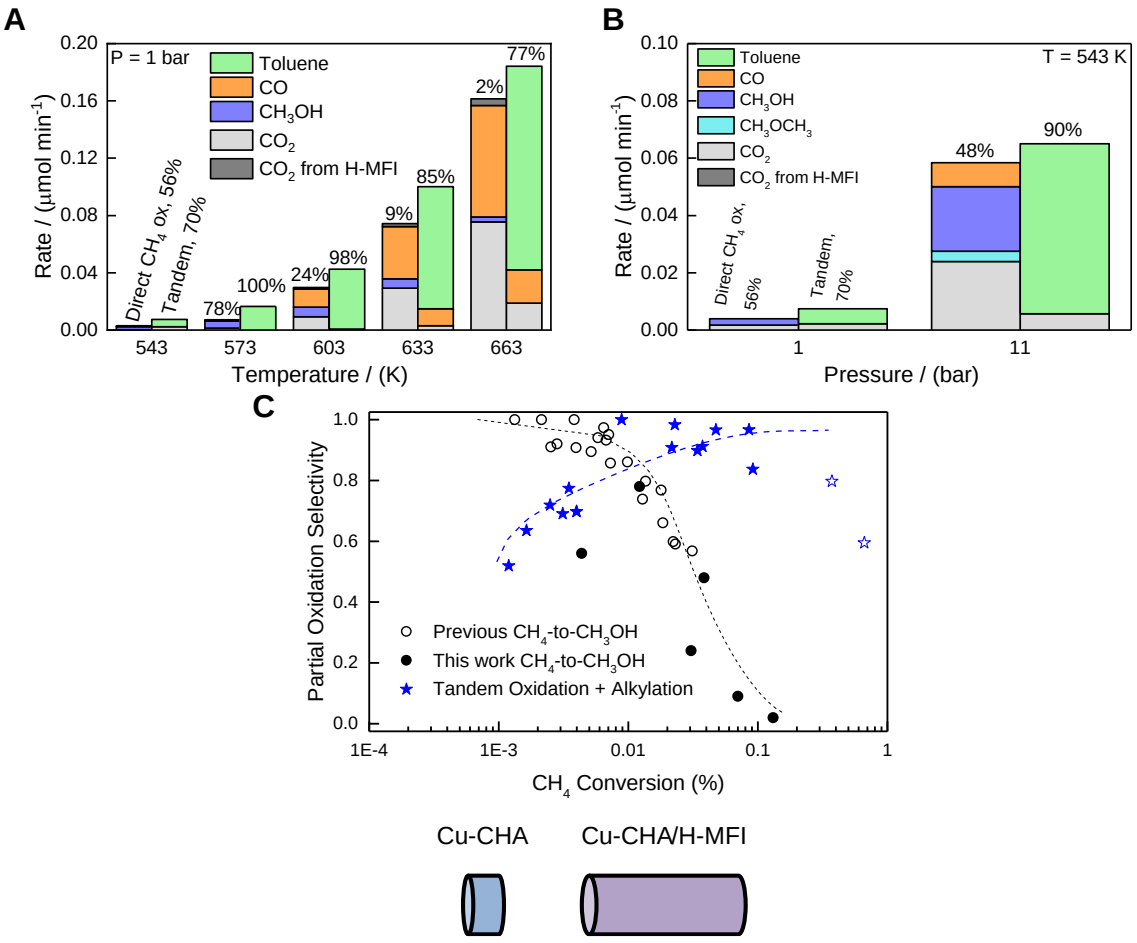

Figure V-7. Comparison of rates of CH_4-to-CH_3OH over Cu-CHA-1 to tandem oxidation and alkylation over Cu-CHA-1/H-MFI-2 across **A.** Temperature and **B.** Pressure. **C.** Selectivity for partially oxidized products versus conversion. Numbers above each bar are the carbon-weighted selectivities for partial oxidation products. "Open circles" were previously reported by Dinh et al.[110] "Black circles" were from this work and generated by varying temperature and pressure as in A and B over 0.0875 g Cu-CHA-1. Blue stars were generated by altering temperature, pressure, total flow rate, catalyst loading and P_{O2} over (0.0875 g Cu-CHA-1 + 0.2625 g H-MFI-1), (0.0875 g Cu-CHA-1 + 0.2625 g H-MFI-2), and (0.366 g Cu-CHA-2 + 1.097 g H-MFI-3). Open blue stars increased P_{O2} by 3 and 5x. Flow conditions: 26.1 sccm, x_{CH4} = 0.18, x_{C6H6} = 0.008, x_{O2} = 0.001, P_{H2O} = 3.1 kPa, bal He, When pressurizing, water partial pressure remains unchanged because it was introduced by a saturator, all other reactants increased proportionally (Section 6.1.2).

These results necessarily warrant comparison to the best performing stoichiometric processes for CH_4-to-CH_3OH conversion over Cu-exchanged zeolites and to other heterogeneous CH_4-to-CH_3OH systems. Sushkevich et al.[159] recently reported the optimization of an isothermal stoichiometric process over a Cu-FAU zeolite (Si/Al = 2.6, Cu/Al = 0.41, Cu wt% = 9.32) where the catalyst is first activated for 1 h under O_2 and then exposed to CH_4 for 1 h. Following, methanol is desorbed for 1 h at 633 K with water vapor. Taking this process as a 3 h cycle time, the optimized methanol yield was 2 $\mu mol_{CH3OH}\ min^{-1}\ g_{cat}^{-1}$ (~1400 $\mu mol_{CH3OH}\ mol_{Cu}^{-1}\ min^{-1}$, 93% selectivity). In comparison, we observed a greater yield for tandem oxidation and alkylation of 2.7 $\mu mol_{Toluene+Xylene}\ min^{-1}\ g_{Cu\text{-}CHA}^{-1}$ at 603 K and 11 bar (59% selectivity for toluene and xylene combined). We also highlight that our Cu loading was an order of magnitude lower than that used for the optimized stoichiometric process, giving a rate of formation of 19,000 $\mu mol_{CH3OH}\ mol_{Cu}^{-1}\ min^{-1}$ that far exceeds the 1400 $\mu mol_{CH3OH}\ mol_{Cu}^{-1}\ min^{-1}$ reported for the optimized stoichiometric process. Finally, our process was not optimized and these reported rates of product formation can be further enhanced by optimizing pressure, temperature, reactant partial pressures, and Cu loading in a similar fashion as was completed by Sushkevich et al.[159]

This conversion and yield for tandem oxidation and alkylation are also comparable to the best performing heterogeneous catalysts for CH_4-to-CH_3OH conversion. Greater than 75% CH_3OH selectivity has been reported for heterogeneous catalysts at < 2% CH_4 conversion.[27] However, with the exception of Cu-exchanged zeolites, the remaining heterogeneous catalysts require expensive oxidants such as H_2O_2[74] or N_2O[45] or extreme conditions (e.g., P > 140 bar).[30] but our system simply requires O_2, H_2O, and benzene as additional reactants and H-MFI as an additional catalyst at relatively mild conditions in comparison to these processes.

3. Kinetic Modeling of Tandem Partial Methane Oxidation and Alkylation Performance Limits

Based on the favorable results of methanol scavenging with benzene alkylation, these results necessarily raise the question of the performance limits of scavenging. Thus, to gauge performance limits, a macrokinetic model was developed based on the hypothesized pathways for product formation (Figure V-8). CO and CO_2 were assumed to form by the same pathway and are lumped together for ease of analysis. Rate laws were derived from kinetic data of CH_4 activation to CH_3OH over Cu-SSZ-13 (Figure II-1) and from those observed for tandem oxidation and alkylation over Cu-SSZ-13/H-ZSM-5 (Figure V-4).

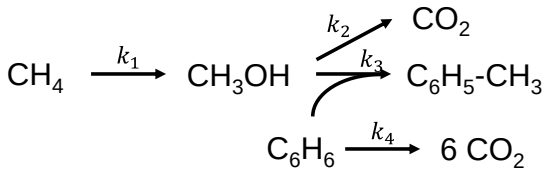

Figure V-8. Product formation reaction pathway used for macrokinetic modeling. CO and CO_2 were assumed to form by the same pathway and are lumped together as one product.

The rate laws are as follows:

$$r_1 = k_1 P_{CH4}^{0.72} P_{O2}^{0.3}$$

$$r_2 = k_2 P_{CH3OH}^{0.27} P_{O2}^{0.88}$$

$$r_3 = k_3 P_{CH3OH}$$

$$r_4 = k_4 P_{O2}^{0.4}$$

While water is necessary for the formation of methanol, it is not kinetically relevant, and thus, was not included in the rate laws. Rate constants and orders were estimated from fits of the partial pressure data. Importantly, r_1 was taken from the dependence of the total rate of C-H activation of CH_4 over Cu-SSZ-13. Rate constants and dependences of the rates of CO_2 and toluene formation on P_{CH3OH} were not collected and, thus, inferred from the rates of product formation on P_{CH4} because the reaction pathway for partial oxidation of CH_4 proceeds first to CH_3OH prior to any additional product formation.

Briefly, r_2 was estimated by plotting the rate of CO_2 formation on P_{CH3OH} from the kinetic results examining the dependence of product formation rates on P_{CH4} over Cu-SSZ-13 (Figure II-1). The order of P_{O2} was taken directly from the observed dependence for the rate of CO_2 formation on P_{O2} because O_2 is not rate-limiting on CH_4 activation and the near first order dependence suggests O_2 activation is rate-limiting for the conversion of CH_3OH to CO_2. r_3 was developed in a similar manner. However, because methanol was not observed when altering P_{CH4} over Cu-CHA/H-MFI, P_{CH3OH} was estimated based on the observed rates of CO_2 and toluene at 543 K where it was assumed $r_{CH3OH} = r_{toluene} + 0.81r_{CO2}$. The 0.81 was to account for the contribution of benzene oxidation to CO_2 formation rates as discussed previously. The rate law of r_3 is reasonable based on the mechanistic studies of aromatic alkylation over proton-form zeolites where the exact nature of the mechanism is still under investigation but the two main routes both require CH_3OH adsorption.[154] r_4 was taken from the observed rate dependence for benzene oxidation on P_{O2} in the absence of CH_4 (Figure V-19). Zero order dependences of the rates of CO_2 and toluene formation on benzene were observed and, thus, benzene is not included in the above rate laws. The rate constants and apparent activation energies are provided in Table V-2. Activation energies were estimated from the observed rates of formation of each product as a function of temperature (Figure II-3, Figure V-2A, Figure V-3A).

Table V-2. Fits of rate constants and $E_{a,app}$ for each reaction as presented in Figure V-8.

Reaction	*k* (543 K)	$E_{a,\,app}$ (kJ mol^{-1})
1	0.045 μmol min^{-1} g_{cat}^{-1} kPa$^{-1.02}$	97
2	2.4 μmol min^{-1} g_{cat}^{-1} kPa$^{-1.15}$	110
3	460 μmol min^{-1} g_{cat}^{-1} kPa$^{-1.}$	24.4
4	0.0266 μmol min^{-1} g_{cat}^{-1} kPa$^{-0.4}$	60.3

The reaction system was modeled as a plug flow reactor and all reactants and products behaved as an ideal gas with negligible change in volumetric flow rate. Molar flow rates were converted to partial pressures by the ideal gas law.

With these rate laws, differential equations, developed from the governing equation for a plug flow reactor operating at steady state, were written as:

$$\frac{d\dot{N_{CH4}}}{dV} = -r_1$$

$$\frac{d\dot{N_{O2}}}{dV} = -\frac{1}{2}r_1 - \frac{3}{2}r_2 - \frac{15}{2}r_4$$

$$\frac{d\dot{N_{C_6H_6}}}{dV} = -r_2 - r_4$$

$$\frac{d\dot{N_{CH3OH}}}{dV} = r_1 - r_2 - r_3$$

$$\frac{d\dot{N_{Toluene}}}{dV} = r_3$$

$$\frac{d\dot{N_{CO2}}}{dV} = r_2 + 6r_4$$

where $\dot{N}_x$ is the molar flow rate of species *x*, *V* is catalyst bed mass and the coefficients are derived from the stoichiometry of each reaction. This macrokinetic model was simulated in MATLAB using ode45.

Relevant definitions are:

$$CH_4\ Conversion = \frac{\dot{N_{CH4,\iota}} - \dot{N_{CH4}}}{\dot{N_{CH4,\iota}}}$$

$$Benzene\ Conversion = \frac{\dot{N_{C6H6,\iota}} - \dot{N_{C6H6}}}{\dot{N_{C6H6,\iota}}}$$

$$Selectivity = \frac{\dot{N_{CH3OH}} + \dot{N_{Toluene}}}{CH_4\ Conversion * \dot{N_{CH4,\iota}}}$$

$$Fraction\ of\ Benzene\ Wasted\ as\ CO_2 = 1 - \frac{\dot{N_{Toluene}}}{Benzene\ Conversion * \dot{N_{C6H6,\iota}}}$$

Figure V-9A demonstrates in the absence of benzene (CH_4-to-CH_3OH conditions), low O_2 concentration and low CH_4 conversion are required for high partial oxidation selectivity. As O_2 concentration increases, the maximum initial selectivity for CH_3OH decreases and overall selectivity drops rapidly with increasing CH_4 conversion. The concave up nature of selectivity versus conversion at increasing CH_4 conversion is a result of decreasing O_2 concentration as O_2 is consumed. The decreased O_2 concentration limits over oxidation of CH_3OH. Analysis of r_2 and r_1 (O_2 order dependences of 0.88 and 0.3, respectively) indicates increasing O_2 concentration favors over oxidation of CH_3OH over CH_4 conversion to CH_3OH, thereby resulting in poorer selectivity for CH_3OH. These results are also consistent with analysis completed by Latimer et al.[38] who analyzed this same selectivity-conversion limit for partial CH_4 oxidation. Their results differ, however, from these results because their analysis assumes there is a first order dependence on P_{CH4} for the conversion of CH_4 to CH_3OH and a first order dependence on P_{CH3OH} on deep oxidation of CH_3OH to CO_2 and O_2 concentration is not kinetically relevant.

The requirement for low CH_4 conversion to maintain partial oxidation selectivity can be removed with the introduction of a scavenging molecule (Figure V-9A). Beyond ~0.01% CH_4 conversion, CH_4-to-CH_3OH selectivity drops precipitously while tandem partial oxidation and alkylation selectivity does not worsen, consistent with experimentally observed results Figure V-7C). Importantly, Figure V-9C indicates at CH_4 conversion above ~0.01%, less than 20% of benzene is converted to undesirable CO_2. The majority of benzene is converted to CO_2 when x_{O2} = 0.05, but these conditions are generally unfavorable as there is almost no selectivity for toluene. Thus, these results demonstrate the benefits of the introduction of a scavenging molecule that is resistant to deep oxidation.

More generally, selection of an appropriate scavenging chemistry is dictated by the rate of reaction of the scavenging reaction and minimizing the diffusion pathway of CH_3OH. The idea of the diffusion pathway of CH_3OH can be explored computationally by altering k_3 such that the rate constant is very large or very small. A large k_3 is representative of perfect capture of CH_3OH by benzene and a small k_3 is representative of the reaction being limited by CH_3OH diffusion. Experimentally, this can be explored by varying the crystal sizes of SSZ-13 and ZSM-5. These ideas were beyond the scope of these simulations.

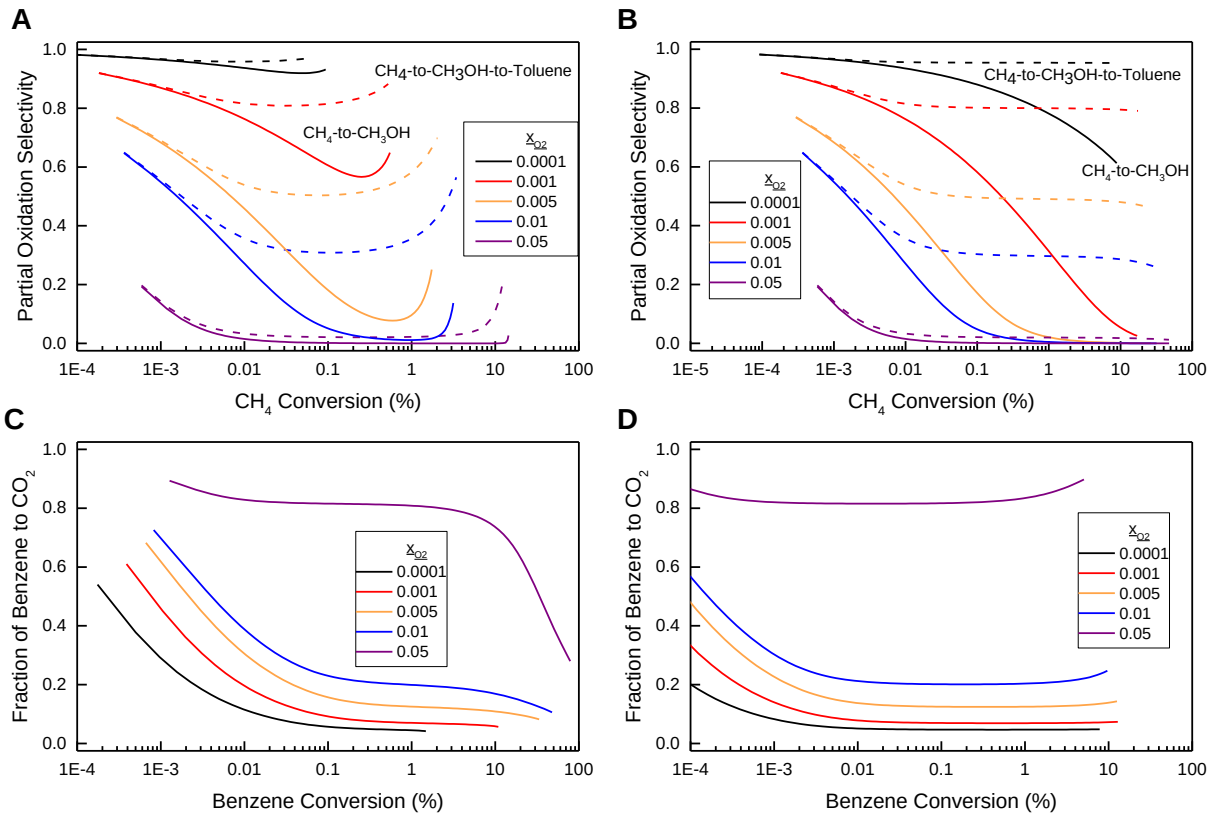

Figure V-9. Effect of O_2 concentration on partial oxidation selectivity versus CH_4 conversion in the presence and absence of benzene. **A.** Partial oxidation selectivity versus CH_4 conversion with O_2 consumption. The concave up nature is a result of a decrease in PO2, thereby favoring partial CH_4 oxidation over CO_2 formation. **B.** Partial oxidation selectivity versus CH_4 conversion assuming constant P_{O2} maintained throughout bed (x_{C6H6} = 0.20) **C.** Fraction of benzene wasted as CO_2 when O_2 is consumed. **D.** Fraction of benzene wasted as CO_2 when P_{O2} is maintained (x_{C6H6} = 0.20). Initial conditions unless otherwise noted: P = 1 bar, T = 543 K, x_{CH4} = 0.177, x_{C6H6} = 0.008, P_{H2O} = 3.14 kPa

To explore the effects of low O_2 concentration in greater detail, I assumed O_2 concentration could be maintained low and constant (Figure V-9B and Figure V-9D). This is modeled physically by a series of continuous stirred tank reactors. Partial oxidation selectivity is similar for both CH_4-to-CH_3OH and tandem partial oxidation and alkylation conditions when compared to same conditions but O_2 is consumed (Figure V-9A). However, this simulation removes the limit of O_2 concentration on CH_4 conversion. Again, while selectivity for CH_4-to-CH_3OH decreases above 0.01% CH_4 conversion, selectivity for toluene is not altered even as CH_4 conversion approaches 100%.

The effects of pressure (Figure V-10A and Figure V-10B), CH_4 concentration (Figure V-10C and Figure V-10D), and temperature (Figure V-10E and Figure V-10F) on partial oxidation selectivity were also simulated. Increasing pressure generally lowers selectivity for partial oxidation with the greatest change occurring from 1 to 11 bar. This again is rationalized by the rate laws employed where r_1 increases by 11.5x but r_2 increases by 13.5x, resulting in lower selectivity. This is in contrast to the experimentally observed results where improved selectivity was observed at increasing pressure. These differences may be a result of the estimation of the order dependences for CH_3OH oxidation and benzene alkylation. Over Cu-CHA/H-MFI, a 0.48 O_2 order dependence was observed (includes both benzene and methanol oxidation), weaker than the one used in kinetic simulations. This decrease would then account for the improved selectivity with increasing pressure observed experimentally. Increasing P_{CH4} favors selectivity for partial oxidation products as r_1 increases, beneficially aiding CH_3OH formation and benzene alkylation over undesired oxidation. Increasing temperature also negatively affects partial oxidation selectivity. While consistent with our observed results for CH_4-to-CH_3OH conversion, we have observed generally more favorable tandem partial oxidation and alkylation selectivity at elevated temperatures. These discrepancies are likely a result of error in the estimation of apparent activation energies as these were based on available temperature dependence data and not from specific temperature variation studies. In all cases, minimal benzene is wasted as CO_2.

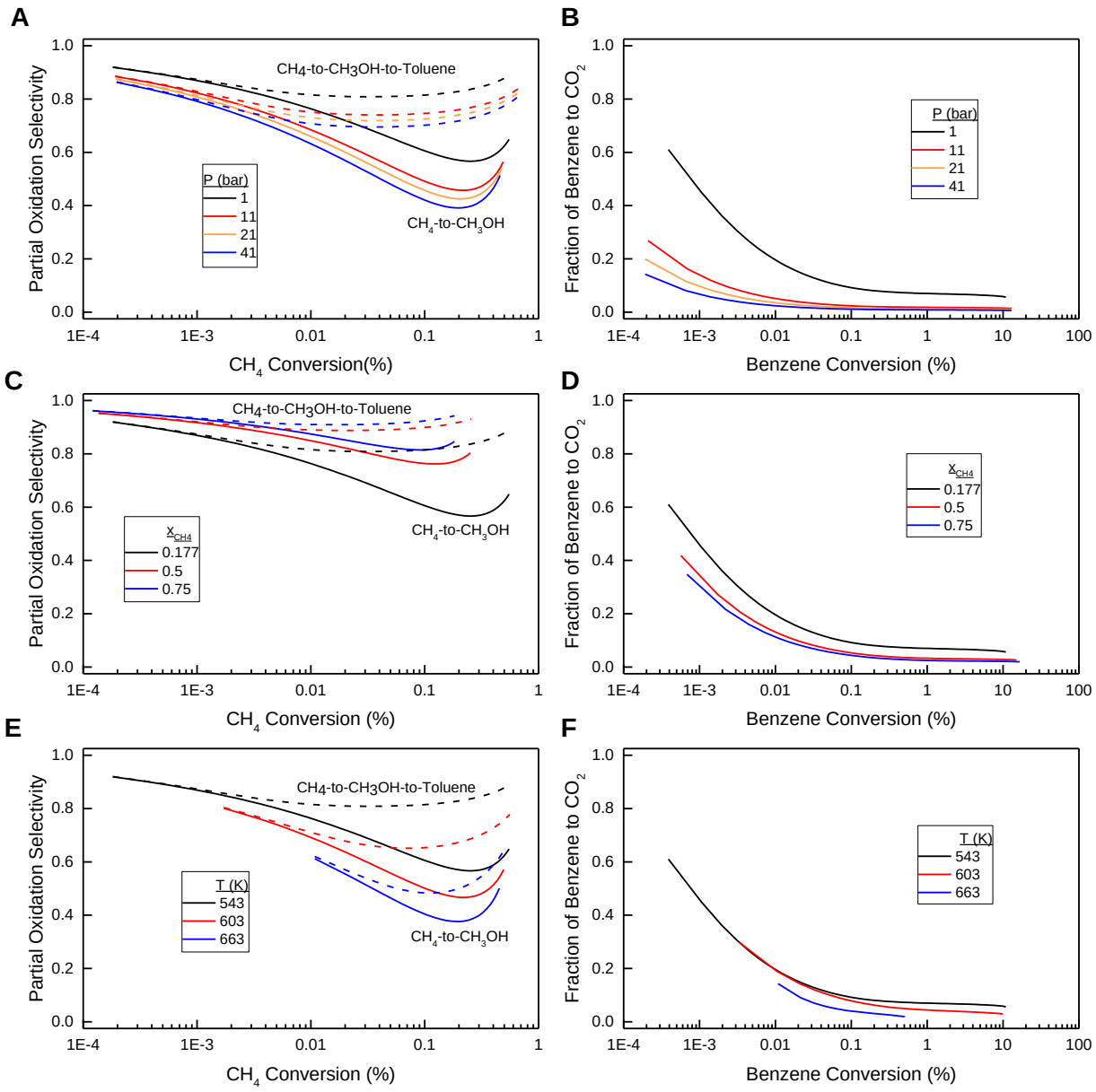

Figure V-10. Effect of **A.** Pressure, **C.** CH_4 concentration, and **E.** Temperature on partial oxidation selectivity versus CH_4 conversion. Fraction of benzene wasted as CO_2 due to **B.** Pressure, **D.** CH_4 Concentration, and **F.** Temperature. Initial conditions unless otherwise noted: P = 1 bar, T = 543 K, x_{CH4} = 0.177, x_{O2} = 0.001, x_{C6H6} = 0.008, P_{H2O} = 3.14 kPa, xO2 = 0.001

4. Conclusions

We have demonstrated the viability of product protection for CH_4 activation by first activating CH_4 over Cu-exchanged zeolites to produce CH_3OH and then capturing CH_3OH by aromatic alkylation over a proton-form zeolite. Control reactions and isotopically labeled benzene experiments demonstrate benzene oxidation occurs in parallel to methane activation and contributes to the observed CO and CO_2 formation rates. Upon accounting for benzene oxidation, the rates of CH_4 activation are comparable between Cu-CHA and Cu-CHA/H-MFI across all conditions but selectivity for desirable products is markedly improved by chemically scavenging methanol. High selectivity towards desirable products is maintained even above 0.1% CH_4 conversion where selectivity for CH_4-to-CH_3OH processes deteriorate. We report a toluene and xylene yield of 2.7 $\mu mol_{Toluene+Xylene}$ min^{-1} $g_{Cu\text{-}CHA}^{-1}$ at 603 K and 11 bar, greater than an optimized stoichiometric CH_4-to-CH_3OH system. Product protection is therefore an area of necessary research to enable CH_4 activation, especially in the area of process optimization and catalyst design. Of particular interest are designing catalysts to reduce benzene oxidation and further limit CH_3OH diffusion pathways.

We also developed a simple macrokinetic model to simulate the addition of a scavenging reaction with partial CH_4 oxidation chemistry. The model can be easily refined as kinetic data is refined and k_3 can be simply varied to study the effects of CH_3OH diffusion. Overall, the results of the modeling indicate low O_2 and high CH_4 concentration are desirable for high selectivity. Ideally, O_2 concentration should be maintained low and constant. Increasing pressure also minimally worsens selectivity for tandem partial oxidation and alkylation indicating there is an opportunity to optimize product yield and selectivity with pressure. While selectivity for partial oxidation drops markedly with increasing temperature, no firm conclusions can be drawn from these results.

Successful product protection processes must meet several requirements:

- Catalysts are designed to minimize the gaseous lifetime of CH_3OH
- Scavenging reaction reactants and products are resistant to complete oxidation and do not interfere with partial methane oxidation to methanol
- Complete CH_4 oxidation does not occur over the catalyst designed to scavenge methanol
- The rate of the scavenging reaction is greater than the rate of methanol formation so that the scavenging reaction is not rate-limiting

This work in total provides a pathway towards achieving industrially relevant product selectivities at desirable CH_4 conversions.

5. *Acknowledgements*

The authors gratefully acknowledge the financial support of ExxonMobil. K.D. acknowledges the partial support from the National Science Foundation Graduate Research Fellowship under Grant No. 1122374. Any opinion, findings, and conclusions or recommendations expressed in this material are those of the author(s) and do not necessarily reflect the views of the National Science Foundation. *This work made use of the MRSEC Shared Experimental Facilities at MIT, supported by the National Science Foundation under award number DMR-14-19807.* The authors thank Z. Wang for help with ICP-MS data collection and scientific discussion and S. Kwon for help with SEM data collection. The authors thank T. Wesley and Z. Wang for critical feedback on the manuscript.

6. *Supporting Information*

6.1. Methods

Unless otherwise described below, remaining methods are described in Section II.6.1.

6.1.1. Catalyst Synthesis and Characterization

Synthesis of H-MFI

To 41.343 g water, 6.663 g tetrapropylammonium hydroxide (TPAOH, 40 wt% in water, SACHEM) was added and stirred for 15 min. Following, 0.135 g aluminum hydroxide (SPI Pharma 250) was added followed by 2.25 g sodium hydroxide solution in water (NaOH, Sigma-Aldrich, 23.0 wt% in water). The mixture was stirred for at least 10 mins. 2.604 g fumed silica (Cab-o-Sil M5) was then slowly added and shaken vigorously. The final gel composition was 1 SiO_2: 0.04 $Al(OH)_3$: 0.3 TPAOH: 0.3 NaOH. The gel was allowed to homogenize and age with stirring for 16 h before being transferred to 23-mL Teflon-lined stainless steel autoclaves (No. 4749, Parr Instruments) and subjected to hydrothermal treatment under static conditions at 453 K for 2 days in an oven under autogenous pressure. After hydrothermal treatment, the product was separated from the mother liquor by centrifugation, washed several times with distilled H_2O until pH < 9 and dried overnight at 393 K. The zeolite was calcined under dry air (Dry Air Size 300, Airgas) with the following temperature profile: heat 1 K min^{-1} to 423 K and hold for 1 h at 423 K, heat 1 K min^{-1} to 623 K and hold for 1 h at 623 K, and lastly heat 1 K min^{-1} to 853 K and hold for 10 h.

Following calcination, to remove Na, 1 g of zeolite was stirred in 60 mL of a 1.0 M solution of ammonium nitrate (≥ 99%, Sigma-Aldrich) for 16 h at room temperature. The suspension was filtered at room temperature, rinsed with 300 mL of deionized H_2O, and the recovered zeolite was immediately subjected to the same ion exchange twice more under the same conditions. Following, the zeolite was dried overnight at 393 K in stagnant air and calcined following the same profile described above.

Scanning Electron Microscopy

Scanning electron microscopy was performed on a Zeiss Merlin High-resolution SEM. Samples were crushed into a fine powder and loaded on to carbon black tape. Micrographs were collected at 3.0 kV, 100 pA, and 6.7 mm WD with the HE-SE2 detector in High Resolution column mode.

6.1.2. Catalytic Partial CH_4 Oxidation and Alkylation Reactions

All reactions were conducted in a continuous, tubular flow reactor (304 stainless steel tube, O.D. 0.25 in, I.D. 0.18). The reactor tube was mounted inside a single-zone furnace (850W / 115V, Applied Test Systems Series 3210). Temperature was controlled using a thermocouple (Omega, model TJ36-CASS-116U) mounted slightly downstream of the catalyst bed connected to a temperature controller (Digi-Sense model 68900-10). The mixture of a copper-exchanged zeolite and a proton-form zeolite were mixed in a ratio of 1:3 by weight, ground with a mortar and pestle, and then vortexed to ensure a homogeneous catalyst mixture. 0.35 g of this zeolite mixture (pelletized and sieved into 250–420 μm particles) were packed between quartz wool plugs and rested on the thermocouple in the middle of the furnace heating zone. Control reactions were performed with the same absolute loadings of the individual catalysts and catalyst beds were pelletized to the same size distribution. Void volume above and below the catalyst bed was filled with borosilicate glass beads to reduce homogeneous combustion. Blank reactors were loaded in the same manner in the absence of catalyst. For testing with increased catalyst loading a 304 stainless steel, O.D. 0.5 in, I.D. 0.40 in. reactor was used.

The flow of gases, including He (ultra high purity, Airgas), 1% O_2 in He (ultra high purity, Airgas), and CH_4 (research grade, Airgas) were controlled with independent mass flow controllers (Brooks Instruments LLC). H_2O (typically 3.2 kPa) was introduced into the gas stream via a stainless steel saturator and benzene was introduced using a syringe pump (Harvard Apparatus) with a heated liquid injection port. Stainless steel gas transfer lines were heated with resistive heating tape from the point of liquid injection until the gas chromatographic analysis unit. Typical reaction pretreatment involved calcining the catalyst at 823 K for 8 h under 50 mL min^{-1} dry air.

CH_3OH, dimethyl ether (DME), CO, CO_2, benzene, toluene, and xylene partial pressures evolved during catalytic tandem oxidation and alkylation reactions were quantified using a gas chromatograph (Agilent Technologies, 7890B). The gas chromatograph was equipped with a methanizer, flame ionization detector, and thermal conductivity detector. Three columns were used for product separation: two HP-PLOT Q PT (30 m x 0.53 mm x 40 μm, Agilent #19095P-QO4PT) and HP PLOT Molsieve (30 m x 0.53 mm x 50 μm, Agilent #19095P-MS0E).

All reported values for selectivity and rates of product formation were averaged over three data points upon reaching steady-state.

Product quantification

Calibration curves for CO_2, CH3OH, CO, and DME were constructed by flowing known mixtures of 1% CO_2/He, 0.5% CH3OH/He, 90 ppm CO/N2 or 10% DME/He and He, respectively, to a gas chromatograph. Calibration curves for benzene and toluene were constructed by injecting known liquid flow rates into a flowing gas stream of known flow rate. A response factor for xylene was inferred from that of toluene by carbon weighting.

The large partial pressure of CH_4 in the gas stream during catalytic CH_4 oxidation reactions prevented the accurate quantification of CH_4 consumption. As such, CH_4 conversion was assumed to be equal to the total molar flow rate of carbon of all observed products divided by the initial molar flow rate of CH_4:

$$X_{CH4} = \frac{\sum_{i=1}^{N} C_i F_i}{F_{CH4,0}}$$

where X_{CH4} is the conversion of CH_4, F_i is the molar flow rate of product *i*, C_i is the number of carbon atoms incorporated from CH_4 into product *i*, $\Sigma C_i F_i$ is the total molar flow rate of carbon of all products, and $F_{CH4,0}$ is the initial molar flow rate of CH_4.

Product selectivity for catalytic CH_4 oxidation and tandem oxidation and alkylation was defined as:

$$S_i = \frac{C_i F_i}{\sum_{i=1}^{N} C_i F_i}$$

where S_i is the selectivity of product *i* on a C-atom basis, C_i is the number of carbon atoms incorporated from CH_4 into product *i*, F_i is the molar flow rate of product *i*, and $\Sigma C_i F_i$ is the total molar flow rate of carbon of all products.

Product yield for catalytic CH_4 oxidation and tandem oxidation and alkylation was defined as:

$$Y_i = \frac{C_i F_i}{N_{Cu} or\ g_{cat}}$$

where Y_i is the selectivity of product *i* on a C-atom basis, N_{Cu} is the number of moles of Cu within the zeolite determined by ICP, and g_{cat} is the catalyst loading.

6.2. Referenced Figures and Tables

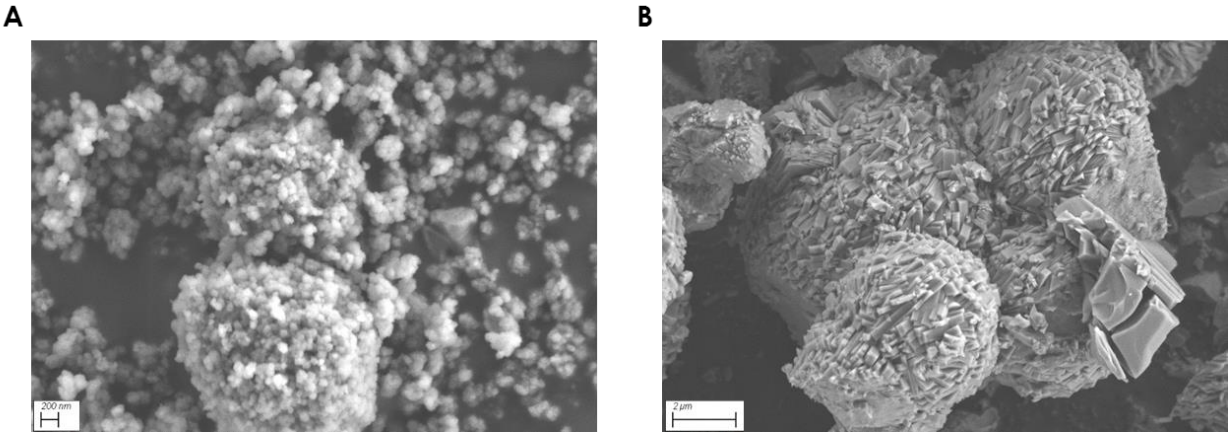

Figure V-11 Representative SEM of **A.** Cu-CHA-1 and **B.** H-MFI-1 demonstrating difference in particle size of the two zeolites.

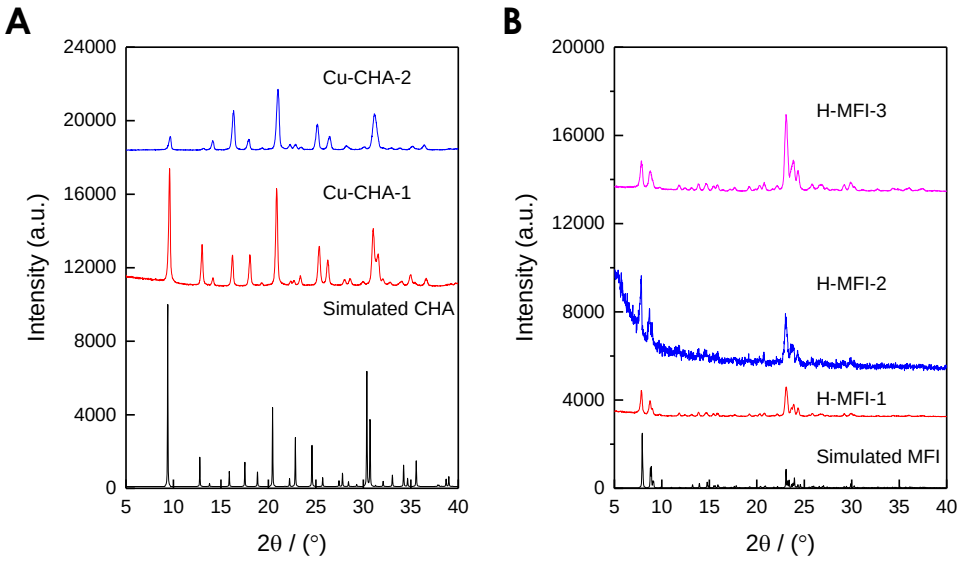

Figure V-12. PXRD of **A.** Cu-CHA and **B.** H-MFI. Simulated patterns were taken from the IZA Database of Zeolite Structures.[150]

Table V-3. Parameters used for verification of absence of heat and mass transfer gradients. GradientCheck for Heterogeneous Catalysis was used.[124] Gaseous properties were obtained from the NIST WebBook's Thermophysical Properties of Fluid Systems.[22]

max r_{obs} (mol kg_{cat}^{-1} s^{-1})	$1.30 \cdot 10^{-6}$
ΔH_{rxn} (kJ mol^{-1})	-300
E_a (kJ mol^{-1})	100
Fractional conversion	0.00004
n	1
ρ_{bulk} (kg m^{-3}) (Assumed ε=0.4)	750

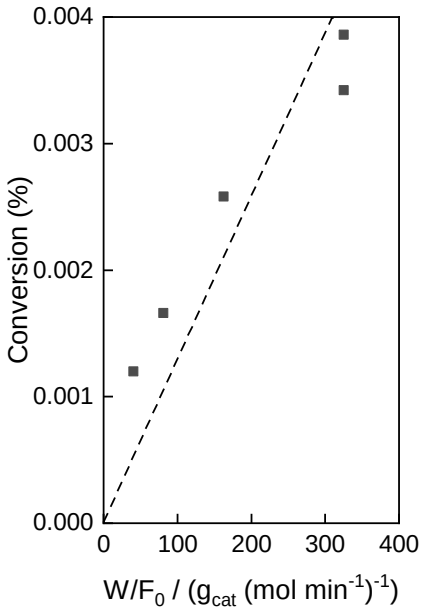

Figure V-13. CH_4 Conversion versus contact time for (0.0875 g Cu-CHA-1 + 0.2625 g H-MFI-2), 543 K, 1 bar, 26.1 - 209 sccm, P_{CH4} = 18 kPa, P_{O2} = 0.09 kPa, P_{H2O} = 3.1 kPa, P_{C6H6} = 0.80 kPa, bal He.

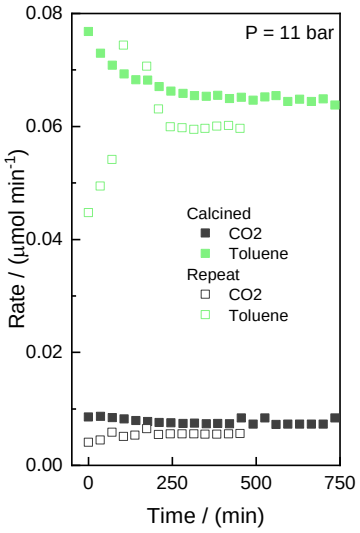

Figure V-14. Rates of product formation over Cu-CHA/H-MFI versus time-on-stream, demonstrating stable rates are observed for at least 12 hours. (0.0875 g Cu-CHA-1 + 0.2625 g H-MFI-2), 543 K, 26.1 sccm, x_{CH4} = 0.18, x_{C6H6} = 0.008, x_{O2} = 0.001, P_{H2O} = 3.1 kPa, bal He. Catalysts were calcined at 823 K under dry air for 8 h prior to testing.

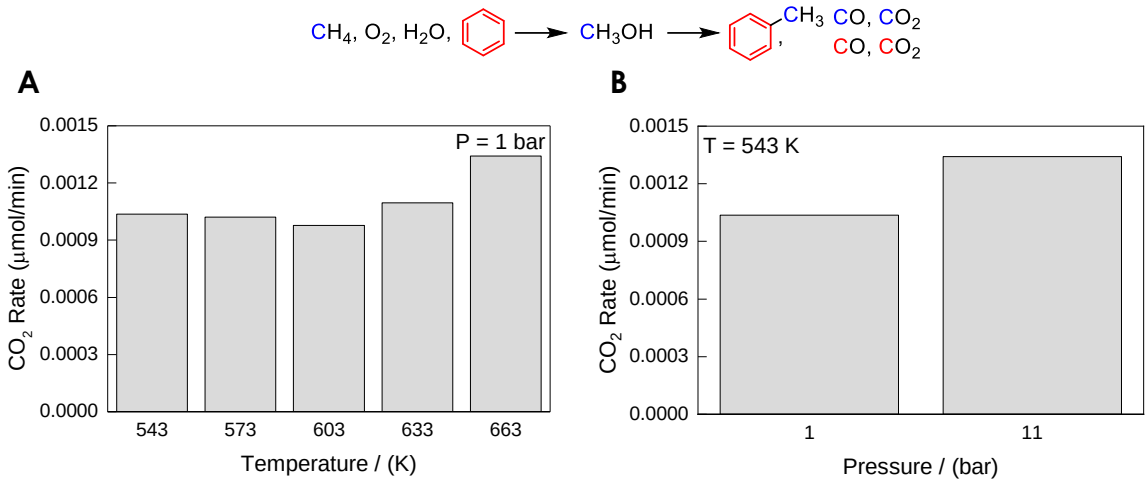

Figure V-15. Rates of CO_2 formation in the absence of catalyst across **A.** Pressure at 543 K, **B.** Temperature at 1 bar. CO_2 was the only observed product. Flow conditions: 26.1 sccm, x_{CH4} = 0.18, x_{C6H6} = 0.008, x_{O2} = 0.001, P_{H2O} = 3.1 kPa, bal He. When pressurizing, water partial pressure remains unchanged, all other reactants increased proportionally.

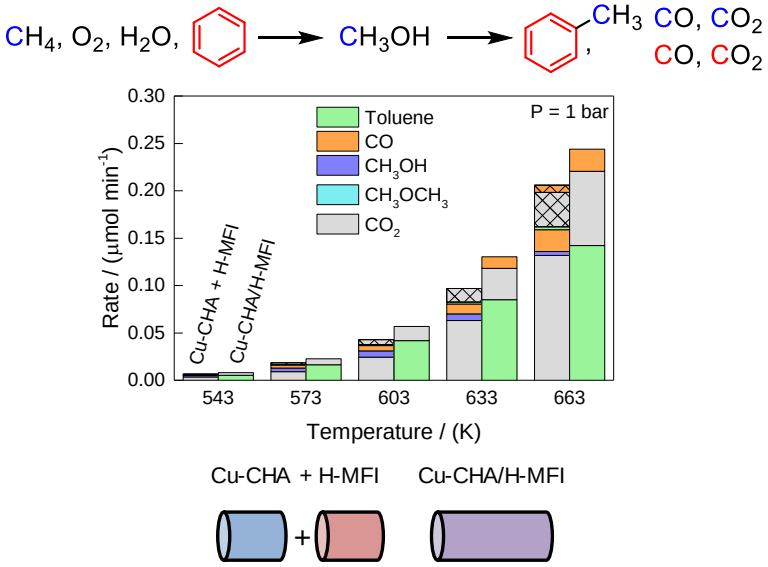

Figure V-16. Comparison of tandem oxidation and alkylation rates from the addition of individual beds of Cu-CHA and H-MFI to an intimately mixed bed of Cu-CHA/H-MFI. "x" denote the observed rates from H-MFI. 0.2625 g H-MFI-1, 0.0875g Cu-CHA-1, and (0.0875 g Cu-CHA-1 + 0.2625 g H-MFI-2), 26.1 sccm, xCH4 = 0.18, xC6H6 = 0.008, xO2 = 0.001, PH2O = 3.1 kPa, bal He.

Figure V-16 demonstrates that across all temperatures, there is a greater rate of product formation for Cu-CHA/H-MFI than from the addition of the rates of product formation over individual Cu-CHA and H-MFI beds.

6.2.1. $^{13}C_6H_6$ Isotope Switching Experiment

To quantify the contribution of benzene oxidation to the observed rates of CO and CO_2 formation, a $^{13}C_6H_6$ (Sigma Aldrich, 423637, 99 atom%) isotope switching experiment was completed. Prior to the experiment, the catalyst bed was calcined under 50 sccm dry air at 823 K for 8 h before cooling to 543 K. At 543 K and 1 bar, reactant flows were introduced with unlabeled benzene until steady-state was attained. Steady state was tracked by GC and an online mass spectrometer (Hiden Analytical HPR-20/QIC). CO, ^{13}CO, CO_2, $^{13}CO_2$, benzene, and $^{13}C_6$ benzene were tracked by MS. Upon reaching steady-state, the benzene feed was switched to $^{13}C_6H_6$ until a steady-state was reached. The feed was then switched back to unlabeled benzene. The catalyst bed was then heated to 603 K and the same experiment was repeated. The rates of CO and CO_2 formation were unchanged with the change in benzene isotope. The change in MS signal of each species was assumed to respond linearly to the gas phase concentration of each species. The natural abundance of ^{13}CO and $^{13}CO_2$ were accounted for in accounting for the contribution of benzene oxidation to the rates of CO and CO_2 formation as follows:

Prior to isotope switch:

$$x = \frac{^{12}CO\ signal}{^{13}CO\ Signal}$$

$$Rate\ of\ ^{13}CO\ formation\ pre-switch = \frac{Total\ Rate\ of\ CO\ Formation}{1+x}$$

Following isotope switch:

$$y = \frac{^{12}CO\ signal}{^{13}CO\ Signal}$$

$$Rate\ of\ ^{13}CO\ formation\ post-switch = \frac{Total\ Rate\ of\ CO\ Formation}{1+y}$$

$$Rate\ of\ CO\ formation\ from\ benzene = Rate\ of\ ^{13}CO\ formation\ post-switch - Rate\ of\ ^{13}CO\ formation\ pre-switch$$

$$Fractional\ Contribution\ of\ Benzene = \frac{Rate\ of\ CO\ formation\ from\ benzene}{Rate\ of\ ^{12}CO\ formation\ pre-switch}$$

Table V-4 summarizes the contributions of benzene oxidation to the rates of CO and CO_2 formation and Figure V-17 and Figure V-18 present the MS signals. Due to the possible contribution of unlabeled and labeled benzene to m/z = 28 and 29 and the large excess of benzene relative to CO formation, the contribution of benzene oxidation to CO formation could not be directly quantified and this analysis was omitted. We hypothesize contributions of benzene oxidation to CO formation rates are similar to benzene's contributions to CO_2 formation rates.

Table V-4. Percent contributions of CH_4 and C_6H_6 to observed rates of formation of CO and CO_2 at 543 and 603 K under tandem oxidation and alkylation reactions. (0.366 g Cu-CHA-2 + 1.097 g H-MFI-3), Flow conditions: 78.3 sccm, P_{CH4} = 17.8 kPa, P_{C6H6} = 0.80 kPa, P_{O2} = 0.09 kPa, P_{H2O} = 3.1 kPa, bal He, atmospheric pressure.

Temperature (K)	Source	CO_2
543	CH_4	81%
	C_6H_6	19%
603	CH_4	58%
	C_6H_6	42%

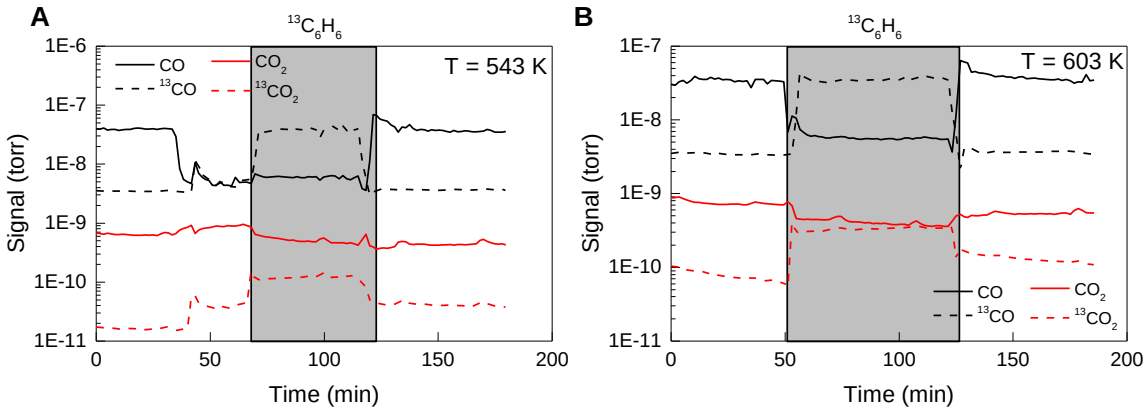

Figure V-17. CO and ^{13}CO and CO_2 and $^{13}CO_2$ signals under tandem oxidation and alkylation conditions and upon the introduction of $^{13}C_6$ benzene (gray box) at **A.** 543 K and **B.** 603 K. (0.366 g Cu-CHA-2 + 1.097 g H-MFI-3), Flow conditions: 78.3 sccm, P_{CH4} = 17.8 kPa, P_{C6H6} = 0.80 kPa, P_{O2} = 0.09 kPa, P_{H2O} = 3.1 kPa, bal He, atmospheric pressure. In Figure A, between ~40-70 min, there was a leak of $^{13}C_6$ benzene and, thus, benzene was not taken into the gas stream during this time.

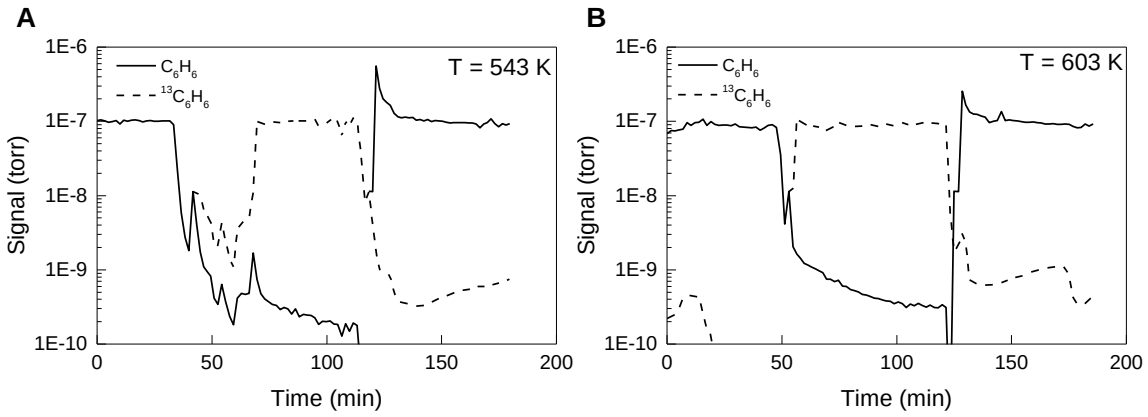

Figure V-18. Benzene and $^{13}C_6H_6$ signals under tandem oxidation and alkylation conditions and upon the introduction of $^{13}C_6$ benzene at **A.** 543 K and **B.** 603 K. (0.366 g Cu-CHA-2 + 1.097 g H-MFI-3), Flow conditions: 78.3 sccm, P_{CH4} = 17.8 kPa, P_{C6H6} = 0.80 kPa, P_{O2} = 0.09 kPa, P_{H2O} = 3.1 kPa, bal He, atmospheric pressure. In Figure A, between ~40-70 min, there was a leak of $^{13}C_6$ benzene and, thus, benzene was not taken into the gas stream during this time.

6.2.2. Estimation of Benzene Oxidation Across Conditions

Based on the observed rate of CO_2 formation stemming from benzene at 543 and 603 K, 1 bar, estimates of the contribution of benzene oxidation to CO_2 formation rates were obtained by using kinetic dependences and an estimate of the apparent activation energy. An estimate of the apparent activation energy for CO_2 formation from benzene was obtained from Figure V-2B. The apparent activation energy for CO_2 formation was 79 kJ/mol. Figure V-4D demonstrates the rate of CO_2 formation was independent of $P_{benzene}$ and Figure V-19 demonstrates the dependence of CO_2 formation from benzene on P_{O2} is 0.4 order. These results allow for estimation of the contribution of benzene oxidation to CO_2 formation rates across temperature and pressure.

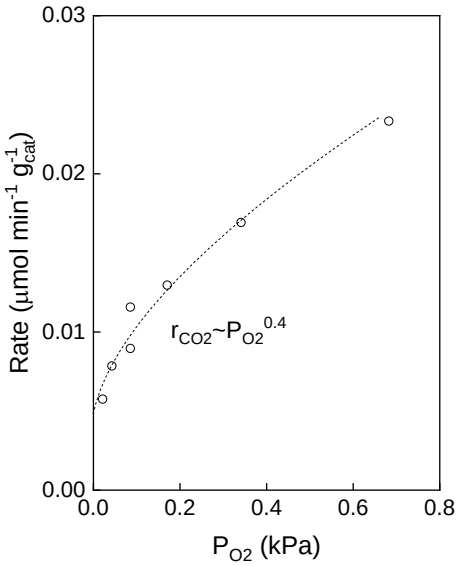

Figure V-19. Product formation rate dependence on P_{O2} for benzene oxidation in the absence of CH_4. CO_2 was the only observed product. (0.2625 g Cu-CHA-1 + 0.7875 g H-MFI-1), 74.5 sccm, 543 K, P_{O2} = 0.1 kPa, $P_{benzene}$ = 0.80 kPa, P_{H2O} = 3.1 kPa, bal He.

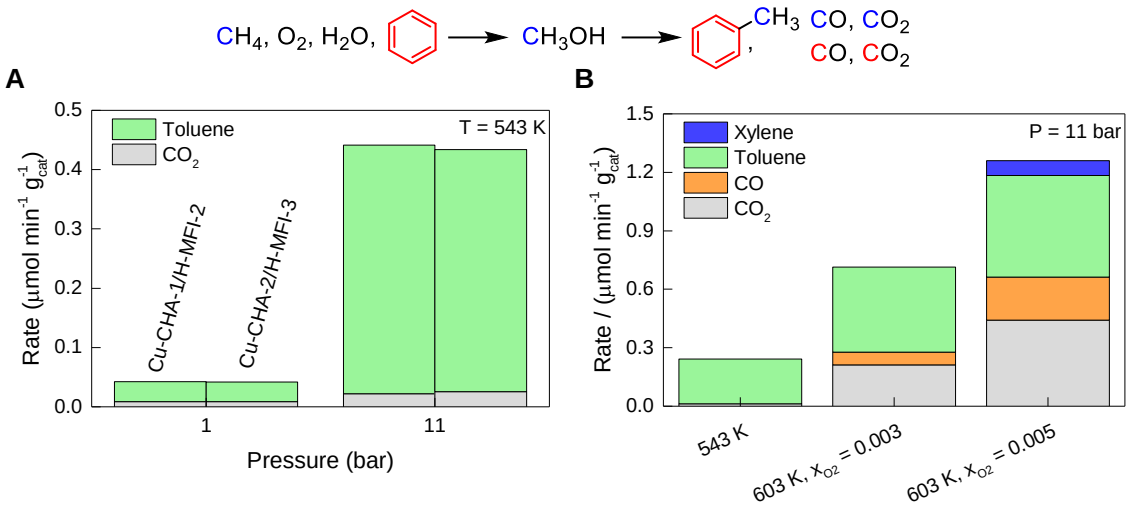

Figure V-20. Rates of product formation over Cu-CHA-2/H-MFI-3 for tandem oxidation and alkylation across conditions. **A.** Comparison of Cu-CHA-1/H-MFI-2 and Cu-CHA-2/H-MFI-3 demonstrating same rates are observed at SV = 329 g_{cat} (mol min^{-1})$^{-1}$ **B.** Product formation rates across multiple conditions over Cu-CHA-2/H-MFI-3. 1372 g_{cat} (mol min^{-1})$^{-1}$. (0.0875 g Cu-CHA-1 + 0.2625 g H-MFI-2), (0.366 g Cu-CHA-2 + 1.097 g H-MFI-3), x_{CH4} = 0.18, x_{C6H6} = 0.008, x_{O2} = 0.001 (unless otherwise noted), P_{H2O} = 3.1 kPa, bal He. When pressurizing, water partial pressure remains unchanged, all other reactants increased proportionally. **Table V-5.** Observed CH_4 conversion, selectivity and product yield for tandem oxidation and alkylation over Cu-CHA/H-MFI[a]

Catalyst	Temperature (K)	Pressure (bar)	Space Velocity (g_{cat} (mol min^{-1})$^{-1}$)	CH_4 Conversion (%)	Toluene + Xylene Selectivity[d] (%)	Product Yield[d] (µmol min^{-1} $g_{Cu\text{-}CHA}^{-1}$)
Cu-CHA-1/ H-MFI-2	543	1	329	0.004	70	0.06
	573	1	329	0.009	100	0.19
	603	1	329	0.023	98	0.48
	633	1	329	0.054	85	0.98
	663	1	329	0.099	77	1.64
	543	11	329	0.039	89	0.68
	543	11	329	0.022	89	1.13
	543	1	329	0.004	77	0.06
	543	1	163	0.003	72	0.08
	543	1	81	0.002	64	0.09
	543	1	41	0.001	51	0.11
Cu-CHA-2/ H-MFI-3	543	1	329	0.003	69	0.06
	543	11	329	0.034	88	0.72
	543	11	1372	0.085	97	0.91
	603[b]	11	1372	0.37	80	1.74
	603[c]	11	1372	0.66	59	2.70

[a]Reactant feed composition: x_{CH4} = 0.18, x_{C6H6} = 0.008, x_{O2} = 0.001, P_{H2O} = 3.1 kPa, bal He

[b]x_{O2} = 0.003

[c]x_{O2} = 0.005

[d]Selectivity and product yield are C-weighted based on number of moles of CH_4 incorporated. (e.g., 1 C/Toluene and 2 C/Xylene); xylene is only observed for the last table entry Selectivities are calculated upon accounting for contribution of benzene oxidation to observed CO and CO_2 rates of formation.

VI. Conclusions and Outlook

1. Conclusions

There is renewed interest in converting natural gas to useful products due to the global abundance of natural gas. Currently, natural gas is often flared as CO_2 instead of transported due to the lack of infrastructure near the newest sources of natural gas. To effectively utilize this abundance of natural gas, a process that can operate economically (e.g., continuously and minimizing compressors and high pressures) with readily available reactants on a small scale is necessary, but no such process yet exists industrially. Cu-exchanged zeolites have the potential to meet these requirements as they selectively activate CH_4 to CH_3OH using only O_2 and H_2O as additional reactants. However, until recently, these catalysts could only operate in a chemical looping process and not catalytically. The first report of eliciting catalytic activity over Cu-exchanged zeolites by Narsimhan et al. presented an opportunity to significantly improve partial CH_4 oxidation capabilities.[91] Thus, the goal of my thesis was to generate fundamental understanding of the catalytic partial oxidation of CH_4 to CH_3OH over Cu-exchanged zeolites to ultimately be applied to designing an improved process for partial CH_4 oxidation. By the end of my work, I increased CH_4 conversion from 0.001% to 0.66% while maintaining >60% partial oxidation selectivity, representing an almost three order of magnitude improvement in CH_4 conversion. These findings provide a pathway forward for improved CH_4 activation while maintaining high selectivity for partial oxidation products over heterogeneous catalysts.

My work began with identifying the reaction pathway for the selective conversion of CH_4 to CH_3OH over Cu-exchanged SSZ-13 zeolites. The reaction pathway proceeds via rate-determining C-H scission of CH_4 in a sequential pathway and the activated methoxy species is desorbed as CH_3OH in the presence of water. In the absence of water, only CO_2 is observed, demonstrating water is kinetically irrelevant but necessary for selective product formation. There is a weak dependence on P_{O2}, indicative of re-oxidation of the active site not being rate-limiting. High selectivity for CH_3OH can be obtained with high P_{CH4} and low P_{O2} at moderate Cu loadings. Furthermore, SSZ-13 zeolites with moderate Cu loadings (Cu/cage < 0.3) and an abundance of Al (Si/Al < 30) are required to promote selective CH_4 oxidation. Higher Cu loadings promote the formation of undesirable Cu_xO_y species that produce only CO_2. Similarly, as Al content decreases, selectivity for CH_3OH decreases, highlighting the additional requirement of an abundance of H^+'s for selective CH_4 oxidation. These findings highlight catalyst and process conditions to promote selective CH_4 oxidation but these catalysts are still subject to a selectivity-conversion limit.

Building on the reaction pathway findings, I then investigated the nature of the active site(s) responsible for selective CH_4 oxidation because understanding of the active site structure and its genesis will enable rational catalyst design targeting a greater density of active sites. NH_3 titration combined with *in situ* x-ray absorption spectroscopy elucidated a $[Cu\text{-}O\text{-}Cu]^{2+}$ motif catalyzes selective CH_4 oxidation. This active site is hypothesized to form by the diffusion of hydrated Cu ions among proximate Al sites. Treatment with NH_3 and re-introduction of methanol synthesis flows reversibly destroyed and reformed the active site. This hypothesis is bolstered by the reduced selectivity for CH_3OH observed when Na^+ or NH_4^+ cations are also present within the zeolite. This hypothesis also explains the necessity of zeolites to contain an abundance of Al to allow for facile diffusion of hydrated Cu ions.

To further investigate the nature of Cu ions for partial CH_4 oxidation and the hypothesis of hydrated Cu ions diffusing within a zeolite, zeolites with low Al content were probed with kinetic experiments. These zeolites contained decreasingly less Al content to disrupt Cu ion diffusion. Kinetic experiments revealed at low Al contents, CH_4 activation proceeds by a parallel pathway where O_2 activation is an important rate-determining step. X-ray absorption spectroscopy suggests isolated Cu ions can be obtained but other species may be present. These species, however, do differ from the $[Cu\text{-}O\text{-}Cu]^{2+}$ dimers that enable high CH_3OH selectivity under identical conditions at isoconversion. In summary, zeolites with low Al content promote Cu sites that are active for partial CH_4 oxidation but result in a majority of CO_2 instead of CH_3OH and are, thus, undesirable for industrial application.

Increasing CH_4 conversion over Cu-SSZ-13 zeolites resulted in decreased CH_3OH selectivity consistent with thermodynamic limitations. Building on the conclusions described, an improved process for partial CH_4 oxidation was designed by chemically scavenging CH_3OH as toluene to circumvent the selectivity-conversion limit for the direct partial oxidation of CH_4 to CH_3OH. The addition of a benzene co-feed and a proton form zeolite enables capturing CH_3OH by its reaction with benzene. 59% selectivity for partial oxidation products was obtained at 0.66% CH_4 conversion, representing a nearly three order of magnitude increase in selective CH_4 conversion from the beginning of this work. The performance limits of this system are unknown but kinetic modeling suggests high selectivity for toluene (>80%) can be obtained even as CH_4 conversion approaches 100% with low P_{O2}.

2. Outlook

Maintaining selectivity for partial CH_4 oxidation as conversion increases is the main barrier to industrial implementation of any system that has shown promising partial oxidation selectivity for one-step CH_4 conversion. Only a few systems have circumvented this barrier and these processes require harsh conditions and/or expensive oxidants, rendering them unattractive industrially. As demonstrated by the interception of methanol with benzene, chemical scavenging presents a way towards industrial direct CH_4 conversion. Aromatic alkylation has the potential to be effective but it will be necessary to know its performance limits by optimizing the catalyst and process.

Because of the potential for tandem partial oxidation and scavenging, along with extensive work to optimizing such a process, technoeconomic analyses will be important to ascertain necessary targets that need to be achieved regarding both the catalyst and process conditions such as activity, selectivity, stability, and pressure. These targets must be kept in mind as work is done to optimize a tandem partial oxidation and scavenging process. Especially attractive with a tandem partial oxidation and scavenging process is the ease of separation of aromatics from water. CH_4-to-CH_3OH processes using Cu-exchanged zeolites currently produce CH_3OH at low rates with water in great abundance. Industrial separation would likely first condense CH_3OH and H_2O prior to the separation of CH_3OH and H_2O. Because of the abundance of H_2O and the miscibility of CH_3OH with H_2O, this poses a costly separation problem. In contrast, aromatics are not miscible with water and separation of aromatics is easily accomplished by distillation upon initial condensation of toluene and excess benzene and H_2O.

2.1. Catalyst Optimization

My work has focused on generating fundamental understanding on Cu-SSZ-13 zeolites in extensive detail. However, it is unclear if improved catalytic activity can be obtained with other zeolites. Narsimhan et al.[91] previously reported higher rates of catalytic methanol formation in small-pore, cage-based zeolites but the specific effects of confinement are not well understood. While SSZ-13 zeolites fit the requirements of a small pore, cage-based zeolite, additional zeolites in this family should be investigated as variations in a zeolite's structure can have noticeable effects on activity. Potential zeolites include those with the LEV, RTH, AFX, and AEI structures. Wulfers et al.[160] reported improved rates of stoichiometric methanol extraction from SSZ-39 (AEI crystal structure) and Mahyuddin et al. has indicated these improved rates are a result of a more constrained Cu-O-Cu bond angle.[101] Thus, a detailed kinetic and characterization study of these zeolites is a worthwhile path to study active site formation in greater detail. The knowledge gained from this study will enable design of Cu-exchanged zeolites with an increased number of more active, active sites.

Besides studying the zeolite responsible for partial CH_4 oxidation, the zeolite active for alkylation must also be optimized. H-ZSM-5 was chosen because it is easily synthesized but other zeolites may be more appropriate that are active for aromatic alkylation and minimally active, or not active at all, for deleterious side reactions. For example, H-ZSM-12[161], NU-87, SSZ-33, and beta[162] have all been studied for aromatic alkylation.

In a similar vein, benzene oxidation is an important contributor to CO and CO_2 formation rates at elevated temperatures and it was hypothesized benzene oxidation on Cu-SSZ-13 occurs on the surface of the zeolite. Catalyst design should be investigated to minimize this undesirable reaction. Because benzene cannot access the pores of SSZ-13, benzene oxidation could perhaps be mitigated by dealumination of surface Al (achieved by dealuminating a zeolite with the organic structure-directing agent still present within the zeolite[163]) to remove the sites responsible for oxidation.

The most ideal system that would result in the shortest diffusion path length is a zeolite that can perform both chemistries. This will be a challenging problem that must be able to partition the Cu active site away from benzene. Trimodal hierarchical SSZ-13 pose an interesting opportunity to attempt to achieve this goal.[164] Importantly, because hydrated Cu ions are hypothesized to be mobile under methanol synthesis conditions, maintaining Cu ions in desirable locations that facilitate sites that are the most active for partial CH_4 oxidation will be of utmost importance. The further Cu ions diffuse away from other nearby Cu ions, the decreased likelihood of forming Cu dimers and the greater the probability of undesirable oxidation. In this vein, it is also possible hydrated Cu ions can move between Cu-SSZ-13 and H-ZSM-5 and this should be ascertained to avoid undesirable catalyst deactivation. If this is the case, then Cu ion diffusion can be limited by inactivating the surfaces of both Cu-SSZ-13 and H-ZSM-5 by dealumination and/or silylation.[165]

2.2. Process Design

While catalyst optimization is important, process optimization will also be just as important. For example, as long as necessary process requirements are met, primarily maintaining selective partial methane oxidation, relevant methanol chemistries can be explored. Kinetic modeling indicated the most viable pathway forward to both high CH_4 conversion and product selectivity is to maintain O_2 partial pressure at a low constant value. This can be studied as a series of CSTRs or with a recycle stream. Furthermore, the temperature and pressure limits are unknown. My data demonstrate high selectivity is maintained at high pressure and temperature and thus these limits are worth exploring as these conditions necessarily come with faster rates of product formation, providing variables to optimize yield and selectivity. Stability must be considered with more extreme conditions as rapid deactivation is undesirable for an effective catalyst. Lastly, benzene concentration was chosen so that there was a large excess of benzene while maintaining a stable flow rate of benzene. Minimizing the flow rate of benzene to its stoichiometric limit will minimize benzene waste and health hazards. As additional kinetic data is obtained, the macrokinetic model can then be refined to better predict performance limits in an iterative process.

It is clear from this outlook much work remains in both catalyst and process design to realize an industrially applicable methanol scavenging system. These thrusts build upon the fundamentals of partial methane oxidation I elucidated over Cu-SSZ-13 zeolites and the demonstration of a tandem CH_4 partial oxidation and scavenging process, setting the stage for future groundbreaking work in CH_4 activation over heterogeneous catalysts.

References

1. Dinh, K. T.; Sullivan, M. M.; Serna, P.; Meyer, R. J.; Dincă, M.; Román-Leshkov, Y. Viewpoint on the Partial Oxidation of Methane to Methanol Using Cu- and Fe-Exchanged Zeolites. *ACS Catal.* 2018, 8, 8306-8313.

2. Annual Energy Outlook 2020 with projections to 2050. Administration, U. S. E. I., Ed. U.S. Department of Energy: Washington, DC, 2020.

3. Natural Gas Information 2019. Association, I. E., Ed. International Energy Association: Paris.

4. Today in Energy: EIA expects 2018 and 2019 natural gas prices to remain relatively flat. Administration, U. S. E. I., Ed. Department of Energy: 2018.

5. *Form EIA-757 Natural Gas Processing Plant Survey Schedule A: Baseline Report*; U.S. Energy Information Administration: Washington, D.C., 2012.

6. Natural gas explained: Natural gas pipelines. https://www.eia.gov/energyexplained/natural-gas/natural-gas-pipelines.php.

7. Hiller, J. Natural gas flaring hits record high in first quarter in U.S. Permian Basin *Reuters* [Online], 2019. https://www.reuters.com/article/us-usa-shale-flaring/natural-gas-flaring-hits-record-high-in-first-quarter-in-us-permian-basin-idUSKCN1T5235.

8. Understanding Global Warming Potentials. https://www.epa.gov/ghgemissions/understanding-global-warming-potentials.

9. Hydrogen Production: Natural Gas Reforming. https://www.energy.gov/eere/fuelcells/hydrogen-production-natural-gas-reforming.

10. Holmen, A. Direct conversion of methane to fuels and chemicals. *Catal. Today* 2009, 142, 2-8.

11. Mohajerani, S.; Kumar, A.; Oni, A. O. A techno-economic assessment of gas-to-liquid and coal-to-liquid plants through the development of scale factors. *Energy* 2018, 150, 681-693.

12. Dong, L.; Wei, S. a.; Tan, S.; Zhang, H. GTL or LNG: which is the best way to monetize “stranded” natural gas? *Petroleum Science* 2008, 5, 388-394.

13. Turaga, U. *Small-scale methanol technologies offer flexibility, cost effectiveness*; 2015.

14. 10.3. Syngas Conversion to Methanol. https://www.netl.doe.gov/research/coal/energy-systems/gasification/gasifipedia/methanol.

15. *Methanol Market Size, Share & Trends Analysis Report By Application (Formaldehyde, Acetic Acid, MTBE, DME, Fuel Blending, MTO, Biodiesel), By Region, And Segment Forecasts, 2019 - 2025*; GVR-4-68038-016-3; Grand View Research: 2019.

16. Global Methanol Market 2020 : Industry Outlook, Top Countries Data, Comprehensive Insights, Growth and Forecast 2026. MarketWatch, 2020.

17. *Chemical Economics Handbook: Methanol*; IHS Markit: 2019.

18. Coal explained: How much coal is left. https://www.eia.gov/energyexplained/coal/how-much-coal-is-left.php.

19. Lunsford, J. H. Catalytic conversion of methane to more useful chemicals and fuels: a challenge for the 21st century. *Catal. Today* 2000, 63, 165-174.

20. Hughes, J. D. A reality check on the shale revolution. *Nature* 2013, 494, 307-308.

21. Tan, S. H.; Barton, P. I. Optimal dynamic allocation of mobile plants to monetize associated or stranded natural gas, part I: Bakken shale play case study. *Energy* 2015, 93, 1581-1594.

22. NIST Chemistry WebBook: NIST Standard Reference Database Number 69. U.S. Department of Commerce National Institute of Standards and Technology: Washington, D.C., 2018.

23. Foster, N. R. Direct catalytic oxidation of methane to methanol — a review. *Applied Catalysis* 1985, 19, 1-11.

24. Gesser, H. D.; Hunter, N. R.; Prakash, C. B. The direct conversion of methane to methanol by controlled oxidation. *Chem. Rev.* 1985, 85, 235-244.

25. Zakaria, Z.; Kamarudin, S. K. Direct conversion technologies of methane to methanol: An overview. *Renewable and Sustainable Energy Reviews* 2016, 65, 250-261.

26. Cortés-Ortiz, W. G.; Guerrero-Fajardo, C. A. OXIDACIÓN CATALÍTICA SELECTIVA PARA LA CONVERSIÓN DE METANO A METANOL: UNA REVISIÓN. *Ciencia e Ingeniería Neogranadina* 2018, 28, 45-71.

27. Ravi, M.; Ranocchiari, M.; Bokhoven, J. A. v. The Direct Catalytic Oxidation of Methane to Methanol—A Critical Assessment. *Angew. Chem. Int. Ed.* 2017, 56, 16464-16483.

28. Park, M. B.; Park, E. D.; Ahn, W.-S. Recent Progress in Direct Conversion of Methane to Methanol Over Copper-Exchanged Zeolites. *Front Chem* 2019, 7, 514-514.

29. Lance, D.; Elworth, E. G. Process for the manufacture of methyl-alcohol from methane. 1906.

30. Boomer, E. H.; Thomas, V. THE OXIDATION OF METHANE AT HIGH PRESSURES: III. EXPERIMENTS USING PURE METHANE AND PRINCIPALLY COPPER AS CATALYST. *Canadian Journal of Research* 1937, 15b, 414-433.

31. Boomer, E. H.; Naldrett, S. N. THE OXIDATION OF METHANE AT HIGH PRESSURES: IV. EXPERIMENTS USING PURE METHANE AND COPPER, SILVER, ZINC, NICKEL, OR MONEL METAL AS CATALYSTS. *Canadian Journal of Research* 1947, 25b, 494-501.

32. Anderson, R. B.; Stein, K. C.; Feenan, J. J.; Hofer, L. J. E. Catalytic Oxidation of Methane. *Industrial & Engineering Chemistry* 1961, 53, 809-812.

33. Dowden, D. A.; Walker, G. T. Oxygenated Hydrocarbons Production. 1244001, 1971.

34. Liu, R. S.; Iwamoto, M.; Lunsford, J. H. Partial oxidation of methane by nitrous oxide over molybdenum oxide supported on silica. *J. Chem. Soc., Chem. Commun.* 1982, 78-79.

35. Faraldos, M.; Bañares, M. A.; Anderson, J. A.; Hu, H.; Wachs, I. E.; Fierro, J. L. s. G. Comparison of Silica-Supported MoO3and V2O5Catalysts in the Selective Partial Oxidation of Methane. *J. Catal.* 1996, 160, 214-221.

36. Spencer, N. D.; Pereira, C. J. V2O5 • SiO2-catalyzed methane partial oxidation with molecular oxygen. *J. Catal.* 1989, 116, 399-406.

37. Chen, S. Y.; Willcox, D. Effect of vanadium oxide loading on the selective oxidation of methane over vanadium oxide (V2O5)/silica. *Ind. Eng. Chem. Res.* 1993, 32, 584-587.

38. Latimer, A. A.; Kakekhani, A.; Kulkarni, A. R.; Nørskov, J. K. Direct Methane to Methanol: The Selectivity–Conversion Limit and Design Strategies. *ACS Catal.* 2018, 8, 6894-6907.

39. Ravi, M.; Sushkevich, V. L.; Knorpp, A. J.; Newton, M. A.; Palagin, D.; Pinar, A. B.; Ranocchiari, M.; van Bokhoven, J. A. Misconceptions and challenges in methane-to-methanol over transition-metal-exchanged zeolites. *Nat. Catal.* 2019, 2, 485-494.

40. Periana, R. A. Platinum Catalysts for the High-Yield Oxidation of Methane to a Methanol Derivative. *Science* 1998, 280, 560-564.

41. Palkovits, R.; Antonietti, M.; Kuhn, P.; Thomas, A.; Schuth, F. Solid catalysts for the selective low-temperature oxidation of methane to methanol. *Angew. Chem. Int. Ed.* 2009, 48, 6909-6912.

42. Holmen, A.; Olsvik, O.; Rokstad, O. A. Pyrolysis of natural gas: chemistry and process concepts. *Fuel Process. Technol.* 1995, 42, 249-267.

43. Razdan, N. K.; Kumar, A.; Bhan, A. Controlling kinetic and diffusive length-scales during absorptive hydrogen removal in methane dehydroaromatization on MoCx/H-ZSM-5 catalysts. *J. Catal.* 2019, 372, 370-381.

44. Dubkov, K. A.; Sobolev, V. I.; Talsi, E. P.; Rodkin, M. A.; Watkins, N. H.; Shteinman, A. A.; Panov, G. I. Kinetic isotope effects and mechanism of biomimetic oxidation of methane and benzene on FeZSM-5 zeolite. *J. Mol. Catal. A: Chem.* 1997, 123, 155-161.

45. Panov, G. I.; Sobolev, V. I.; Dubkov, K. A.; Parmon, V. N.; Ovanesyan, N. S.; Shilov, A. E.; Shteinman, A. A. Iron complexes in zeolites as a new model of methane monooxygenase. *React. Kinet. Catal. Lett.* 1997, 61, 251-258.

46. Smeets, P. J.; Groothaert, M. H.; Schoonheydt, R. A. Cu based zeolites: A UV–vis study of the active site in the selective methane oxidation at low temperatures. *Catal. Today* 2005, 110, 303-309.

47. Groothaert, M. H.; Smeets, P. J.; Sels, B. F.; Jacobs, P. A.; Schoonheydt, R. A. Selective oxidation of methane by the bis(mu-oxo)dicopper core stabilized on ZSM-5 and mordenite zeolites. *J. Am. Chem. Soc.* 2005, 127, 1394-1395.

48. Shan, J.; Li, M.; Allard, L. F.; Lee, S.; Flytzani-Stephanopoulos, M. Mild oxidation of methane to methanol or acetic acid on supported isolated rhodium catalysts. *Nature* 2017, 551, 605-608.

49. Tinberg, C. E.; Lippard, S. J. Dioxygen Activation in Soluble Methane Monooxygenase. *Acc. Chem. Res.* 2011, 44, 280-288.

50. Colby, J.; Stirling, D. I.; Dalton, H. The soluble methane mono-oxygenase of Methylococcus capsulatus (Bath). Its ability to oxygenate n-alkanes, n-alkenes, ethers, and alicyclic, aromatic and heterocyclic compounds. *Biochem. J* 1977, 165, 395-402.

51. Lee, S. J.; McCormick, M. S.; Lippard, S. J.; Cho, U. S. Control of substrate access to the active site in methane monooxygenase. *Nature* 2013, 494, 380-384.

52. Banerjee, R.; Proshlyakov, Y.; Lipscomb, J. D.; Proshlyakov, D. A. Structure of the key species in the enzymatic oxidation of methane to methanol. *Nature* 2015, 518, 431-434.

53. Shu, L. An Fe2IVO2 Diamond Core Structure for the Key Intermediate Q of Methane Monooxygenase. *Science* 1997, 275, 515-518.

54. Dunietz, B. D.; Beachy, M. D.; Cao, Y.; Whittington, D. A.; Lippard, S. J.; Friesner, R. A. Large scale ab initio quantum chemical calculation of the intermediates in the soluble methane monooxygenase catalytic cycle. *J. Am. Chem. Soc.* 2000, 122, 2828-2839.

55. Lee, S. K.; Fox, B. G.; Froland, W. A.; Lipscomb, J. D.; Munck, E. A transient intermediate of the methane monooxygenase catalytic cycle containing an FeIVFeIV cluster. *J. Am. Chem. Soc.* 1993, 115, 6450-6451.

56. Xue, G.; Wang, D.; De Hont, R.; Fiedler, A. T.; Shan, X.; Münck, E.; Que, L. A synthetic precedent for the [FeIV2(μ-O)2] diamond core proposed for methane monooxygenase intermediate Q. *Proc. Natl. Acad. Sci. U. S. A.* 2007, 104, 20713-20718.

57. Liu, K. E.; Wang, D.; Huynh, B. H.; Edmondson, D. E.; Salifoglou, A.; Lippard, S. J. Spectroscopic detection of intermediates in the reaction of dioxygen with the reduced methane monooxygenase/hydroxylase from Methylococcus capsulatus (Bath). *J. Am. Chem. Soc.* 1994, 116, 7465-7466.

58. Liu, K. E.; Valentine, A. M.; Wang, D.; Huynh, B. H.; Edmondson, D. E.; Salifoglou, A.; Lippard, S. J. Kinetic and spectroscopic characterization of intermediates and component interactions in reactions of methane monooxygenase from Methylococcus capsulatus (Bath). *J. Am. Chem. Soc.* 1995, 117, 10174-10185.

59. Lund, J.; Woodland, M. P.; Dalton, H. Electron transfer reactions in the soluble methane monooxygenase of Methylococcus capsulatus (Bath). *The FEBS Journal* 1985, 147, 297-305.

60. Rosenzweig, A. C.; Nordlund, P.; Takahara, P. M.; Frederick, C. A.; Lippard, S. J. Geometry of the soluble methane monooxygenase catalytic diiron center in two oxidation states. *Chem. Biol.* 1995, 2, 409-418.

61. Lee, S.-K.; Lipscomb, J. D. Oxygen activation catalyzed by methane monooxygenase hydroxylase component: Proton delivery during the O− O bond cleavage steps. *Biochemistry* 1999, 38, 4423-4432.

62. Valentine, A. M.; Wilkinson, B.; Liu, K. E.; Komar-Panicucci, S.; Priestley, N. D.; Williams, P. G.; Morimoto, H.; Floss, H. G.; Lippard, S. J. Tritiated chiral alkanes as substrates for soluble methane monooxygenase from Methylococcus capsulatus (Bath): probes for the mechanism of hydroxylation. *J. Am. Chem. Soc.* 1997, 119, 1818-1827.

63. Gherman, B. F.; Dunietz, B. D.; Whittington, D. A.; Lippard, S. J.; Friesner, R. A. Activation of the C− H Bond of Methane by Intermediate Q of Methane Monooxygenase: A Theoretical Study. *J. Am. Chem. Soc.* 2001, 123, 3836-3837.

64. Balasubramanian, R.; Smith, S. M.; Rawat, S.; Yatsunyk, L. A.; Stemmler, T. L.; Rosenzweig, A. C. Oxidation of methane by a biological dicopper centre. *Nature* 2010, 465, 115-119.

65. Yoshizawa, K.; Shiota, Y. Conversion of methane to methanol at the mononuclear and dinuclear copper sites of particulate methane monooxygenase (pMMO): a DFT and QM/MM study. *J. Am. Chem. Soc.* 2006, 128, 9873-9881.

66. Shiota, Y.; Yoshizawa, K. Comparison of the Reactivity of Bis (μ-oxo) CuIICuIII and CuIIICuIII Species to Methane. *Inorg. Chem.* 2008, 48, 838-845.

67. Solomon, E. I.; Heppner, D. E.; Johnston, E. M.; Ginsbach, J. W.; Cirera, J.; Qayyum, M.; Kieber-Emmons, M. T.; Kjaergaard, C. H.; Hadt, R. G.; Tian, L. Copper active sites in biology. *Chemical Reviews* 2014, 114, 3659-3853.

68. Wilkinson, B.; Zhu, M.; Priestley, N. D.; Nguyen, H.-H. T.; Morimoto, H.; Williams, P. G.; Chan, S. I.; Floss, H. G. A concerted mechanism for ethane hydroxylation by the particulate methane monooxygenase from Methylococcus capsulatus (Bath). *J. Am. Chem. Soc.* 1996, 118, 921-922.

69. Sazinsky, M. H.; Lippard, S. J. Methane monooxygenase: functionalizing methane at iron and copper. *Metal Ions in Life Sciences* 2015, 15, 205-256.

70. Ovanesyan, N.; Shteinman, A. A.; Dubkov, K. A.; Sobolev, V.; Panov, G. The State of Iron in the Fe-ZSM-5-N2O System for Selective Oxidation of Methane to Methanol from Data of Mossbauer Spectroscopy. *Kinet. Catal.* 1998, 39, 792-797.

71. Parfenov, M. V.; Starokon, E. V.; Pirutko, L. V.; Panov, G. I. Quasicatalytic and catalytic oxidation of methane to methanol by nitrous oxide over FeZSM-5 zeolite. *J. Catal.* 2014, 318, 14-21.

72. Starokon, E. V.; Parfenov, M. V.; Arzumanov, S. S.; Pirutko, L. V.; Stepanov, A. G.; Panov, G. I. Oxidation of methane to methanol on the surface of FeZSM-5 zeolite. *J. Catal.* 2013, 300, 47-54.

73. Snyder, B. E. R.; Vanelderen, P.; Bols, M. L.; Hallaert, S. D.; Böttger, L. H.; Ungur, L.; Pierloot, K.; Schoonheydt, R. A.; Sels, B. F.; Solomon, E. I. The active site of low-temperature methane hydroxylation in iron-containing zeolites. *Nature* 2016, 536, 317-321.

74. Hammond, C.; Forde, M. M.; Ab Rahim, M. H.; Thetford, A.; He, Q.; Jenkins, R. L.; Dimitratos, N.; Lopez-Sanchez, J. A.; Dummer, N. F.; Murphy, D. M.; Carley, A. F.; Taylor, S. H.; Willock, D. J.; Stangland, E. E.; Kang, J.; Hagen, H.; Kiely, C. J.; Hutchings, G. J. Direct Catalytic Conversion of Methane to Methanol in an Aqueous Medium by using Copper-Promoted Fe-ZSM-5. *Angew. Chem. Int. Ed.* 2012, 51, 5129-5133.

75. Xu, J.; Armstrong, R. D.; Shaw, G.; Dummer, N. F.; Freakley, S. J.; Taylor, S. H.; Hutchings, G. J. Continuous selective oxidation of methane to methanol over Cu-and Fe-modified ZSM-5 catalysts in a flow reactor. *Catal. Today* 2016, 270, 93-100.

76. Hammond, C.; Jenkins, R. L.; Dimitratos, N.; Lopez-Sanchez, J. A.; ab Rahim, M. H.; Forde, M. M.; Thetford, A.; Murphy, D. M.; Hagen, H.; Stangland, E. E.; Moulijn, J. M.; Taylor, S. H.; Willock, D. J.; Hutchings, G. J. Catalytic and Mechanistic Insights of the Low-Temperature Selective Oxidation of Methane over Cu-Promoted Fe-ZSM-5. *Chemistry – A European Journal* 2012, 18, 15735-15745.

77. Hammond, C.; Dimitratos, N.; Jenkins, R. L.; Lopez-Sanchez, J. A.; Kondrat, S. A.; Hasbi ab Rahim, M.; Forde, M. M.; Thetford, A.; Taylor, S. H.; Hagen, H.; Stangland, E. E.; Kang, J. H.; Moulijn, J. M.; Willock, D. J.; Hutchings, G. J. Elucidation and Evolution of the Active Component within Cu/Fe/ZSM-5 for Catalytic Methane Oxidation: From Synthesis to Catalysis. *ACS Catal.* 2013, 3, 689-699.

78. Hammond, C.; Hermans, I.; Dimitratos, N. Biomimetic Oxidation with Fe-ZSM-5 and H2O2? Identification of an Active, Extra-Framework Binuclear Core and an FeIII-OOH Intermediate with Resonance-Enhanced Raman Spectroscopy. *ChemCatChem* 2015, 7, 434-440.

79. Hutchings, G. J. Methane Activation by Selective Oxidation. *Top. Catal.* 2016, 59, 658-662.

80. Elwell, C. E.; Gagnon, N. L.; Neisen, B. D.; Dhar, D.; Spaeth, A. D.; Yee, G. M.; Tolman, W. B. Copper–oxygen complexes revisited: structures, spectroscopy, and reactivity. *Chem. Rev.* 2017, 117, 2059-2107.

81. Choudhary, T.; Banerjee, S.; Choudhary, V. Catalysts for combustion of methane and lower alkanes. *Appl. Catal., A* 2002, 234, 1-23.

82. Kalamaras, C.; Palomas, D.; Bos, R.; Horton, A.; Crimmin, M.; Hellgardt, K. Selective Oxidation of Methane to Methanol Over Cu- and Fe-Exchanged Zeolites: The Effect of Si/Al Molar Ratio. *Catalysis Letters* 2016, 146, 483-492.

83. Kulkarni, A. R.; Zhao, Z.-J.; Siahrostami, S.; Nørskov, J. K.; Studt, F. Monocopper Active Site for Partial Methane Oxidation in Cu-Exchanged 8MR Zeolites. *ACS Catal.* 2016, 6, 6531-6536.

84. Grundner, S.; Markovits, M. A.; Li, G.; Tromp, M.; Pidko, E. A.; Hensen, E. J.; Jentys, A.; Sanchez-Sanchez, M.; Lercher, J. A. Single-site trinuclear copper oxygen clusters in mordenite for selective conversion of methane to methanol. *Nat. Commun.* 2015, 6, 7546-7555.

85. Vogiatzis, K. D.; Li, G.; Hensen, E. J.; Gagliardi, L.; Pidko, E. A. Electronic Structure of the [Cu3 (μ-O) 3] 2+ Cluster in Mordenite Zeolite and Its Effects on the Methane to Methanol Oxidation. *J. Phys. Chem. C* 2017, 121, 22295-22302.

86. Mahyuddin, M. H.; Tanaka, T.; Shiota, Y.; Staykov, A.; Yoshizawa, K. Methane Partial Oxidation over [Cu2 (μ-O)] 2+ and [Cu3 (μ-O) 3] 2+ Active Species in Large-Pore Zeolites. *ACS Catal.* 2018, 8, 1500-1509.

87. Pappas, D. K.; Borfecchia, E.; Dyballa, M.; Pankin, I. A.; Lomachenko, K. A.; Martini, A.; Signorile, M.; Teketel, S.; Arstad, B.; Berlier, G.; Lamberti, C.; Bordiga, S.; Olsbye, U.; Lillerud, K. P.; Svelle, S.; Beato, P. Methane to Methanol: Structure–Activity Relationships for Cu-CHA. *J. Am. Chem. Soc.* 2017, 139, 14961-14975.

88. Ipek, B.; Wulfers, M. J.; Kim, H.; Göltl, F.; Hermans, I.; Smith, J. P.; Booksh, K. S.; Brown, C. M.; Lobo, R. F. Formation of [Cu2O2]2+ and [Cu2O]2+ toward C–H Bond Activation in Cu-SSZ-13 and Cu-SSZ-39. *ACS Catal.* 2017, 7, 4291-4303.

89. Tomkins, P.; Mansouri, A.; Bozbag, S. E.; Krumeich, F.; Park, M. B.; Alayon, E. M.; Ranocchiari, M.; van Bokhoven, J. A. Isothermal Cyclic Conversion of Methane into Methanol over Copper-Exchanged Zeolite at Low Temperature. *Angew. Chem. Int. Ed.* 2016, 55, 5467-5471.

90. Knorpp, A. J.; Newton, M. A.; Pinar, A. B.; van Bokhoven, J. A. Conversion of methane to methanol on copper mordenite: redox mechanism of isothermal and high temperature activation procedures. *Ind. Eng. Chem. Res.* 2018.

91. Narsimhan, K.; Iyoki, K.; Dinh, K.; Roman-Leshkov, Y. Catalytic Oxidation of Methane into Methanol over Copper-Exchanged Zeolites with Oxygen at Low Temperature. *ACS Central Science* 2016, 2, 424-429.

92. Sushkevich, V. L.; Palagin, D.; Ranocchiari, M.; van Bokhoven, J. A. Selective anaerobic oxidation of methane enables direct synthesis of methanol. *Science* 2017, 356, 523-527.

93. Periana, R. A. Comment on “Selective anaerobic oxidation of methane enables direct synthesis of methanol”. *Science* 2017, 358.

94. Comito, R. J.; Fritzsching, K. J.; Sundell, B. J.; Schmidt-Rohr, K.; Dincă, M. Single-site heterogeneous catalysts for olefin polymerization enabled by cation exchange in a metal-organic framework. *J. Am. Chem. Soc.* 2016, 138, 10232-10237.

95. Dubey, R. J.-C.; Comito, R. J.; Wu, Z.; Zhang, G.; Rieth, A. J.; Hendon, C. H.; Miller, J. T.; Dinca, M. Highly Stereoselective Heterogeneous Diene Polymerization by Co-MFU-4 l: A Single-Site Catalyst Prepared by Cation Exchange. *J. Am. Chem. Soc.* 2017, 139, 12664-12669.

96. Park, H. D.; Dincă, M.; Román-Leshkov, Y. Heterogeneous Epoxide Carbonylation by Cooperative Ion-Pair Catalysis in Co (CO) 4−-Incorporated Cr-MIL-101. *ACS Central Science* 2017, 3, 444-448.

97. Stubbs, A. W.; Braglia, L.; Borfecchia, E.; Meyer, R. J.; Román-Leshkov, Y.; Lamberti, C.; Dincă, M. Selective Catalytic Olefin Epoxidation with MnII-Exchanged MOF-5. *ACS Catal.* 2017, 8, 596-601.

98. Ikuno, T.; Zheng, J.; Vjunov, A.; Sanchez-Sanchez, M.; Ortuño, M. A.; Pahls, D. R.; Fulton, J. L.; Camaioni, D. M.; Li, Z.; Ray, D.; Mehdi, B. L.; Browning, N. D.; Farha, O. K.; Hupp, J. T.; Cramer, C. J.; Gagliardi, L.; Lercher, J. A. Methane Oxidation to Methanol Catalyzed by Cu-Oxo Clusters Stabilized in NU-1000 Metal‑Organic Framework. *J. Am. Chem. Soc.* 2017, 139, 10294-10301.

99. Osadchii, D.; Olivos Suarez, A. I.; Szécsényi, Á.; Li, G.; Nasalevich, M. A.; Dugulan, A. I.; Serra-Crespo, P.; Hensen, E. J. M.; Veber, S. L.; Fedin, M. V.; Sankar, G.; Pidko, E. A.; Gascon, J. Isolated Fe sites in Metal Organic Framework catalyze the direct conversion of methane to methanol. *ACS Catal.* 2018.

100. Zhao, Z.-J.; Kulkarni, A.; Vilella, L.; Nørskov, J. K.; Studt, F. Theoretical Insights into the Selective Oxidation of Methane to Methanol in Copper-Exchanged Mordenite. *ACS Catal.* 2016, 6, 3760-3766.

101. Mahyuddin, M. H.; Staykov, A.; Shiota, Y.; Miyanishi, M.; Yoshizawa, K. Roles of Zeolite Confinement and Cu–O–Cu Angle on the Direct Conversion of Methane to Methanol by [Cu2 (μ-O)] 2+-Exchanged AEI, CHA, AFX, and MFI Zeolites. *ACS Catal.* 2017, 7, 3741-3751.

102. Wang, W.; Liang, A. D.; Lippard, S. J. Coupling oxygen consumption with hydrocarbon oxidation in bacterial multicomponent monooxygenases. *Acc. Chem. Res.* 2015, 48, 2632-2639.

103. Ross, M. O.; Rosenzweig, A. C. A tale of two methane monooxygenases. *JBIC Journal of Biological Inorganic Chemistry* 2017, 22, 307-319.

104. Shilov, A. E.; Shul'pin, G. B. Activation of C−H Bonds by Metal Complexes. *Chem. Rev.* 1997, 97, 2879-2932.

105. Periana, R. A.; Taube, D. J.; Evitt, E. R.; Löffler, D. G.; Wentrcek, P. R.; Voss, G.; Masuda, T. A Mercury-Catalyzed, High-Yield System for the Oxidation of Methane to Methanol. *Science* 1993, 259, 340-343.

106. O'Reilly, M. E.; Kim, R. S.; Oh, S.; Surendranath, Y. Catalytic Methane Monofunctionalization by an Electrogenerated High-Valent Pd Intermediate. *ACS Central Science* 2017, 3, 1174-1179.

107. Richards, A. K. Anhydrous processing of methane into methane-sulfonic acid, methanol, and other compounds. U.S. Patent 7,282,603, Oct 16, 2007.

108. Mukhopadhyay, S.; Bell, A. T. Direct Liquid-Phase Sulfonation of Methane to Methanesulfonic Acid by SO3 in the Presence of a Metal Peroxide. *Angew. Chem. Int. Ed.* 2003, 42, 1019-1021.

109. Narsimhan, K.; Michaelis, V. K.; Mathies, G.; Gunther, W. R.; Griffin, R. G.; Roman-Leshkov, Y. Methane to acetic acid over Cu-exchanged zeolites: mechanistic insights from a site-specific carbonylation reaction. *J. Am. Chem. Soc.* 2015, 137, 1825-1832.

110. Dinh, K. T.; Sullivan, M. M.; Narsimhan, K.; Serna, P.; Meyer, R. J.; Dincă, M.; Román-Leshkov, Y. Continuous Partial Oxidation of Methane to Methanol Catalyzed by Diffusion-Paired Copper Dimers in Copper-Exchanged Zeolites. *J. Am. Chem. Soc.* 2019, 141, 11641-11650.

111. Borfecchia, E.; Beato, P.; Svelle, S.; Olsbye, U.; Lamberti, C.; Bordiga, S. Cu-CHA – a model system for applied selective redox catalysis. *Chem. Soc. Rev.* 2018, 47, 8097-8133.

112. Paolucci, C.; Parekh, A. A.; Khurana, I.; Di Iorio, J. R.; Li, H.; Albarracin Caballero, J. D.; Shih, A. J.; Anggara, T.; Delgass, W. N.; Miller, J. T.; Ribeiro, F. H.; Gounder, R.; Schneider, W. F. Catalysis in a Cage: Condition-Dependent Speciation and Dynamics of Exchanged Cu Cations in SSZ-13 Zeolites. *J. Am. Chem. Soc.* 2016, 138, 6028-6048.

113. Di Iorio, J. R.; Gounder, R. Controlling the Isolation and Pairing of Aluminum in Chabazite Zeolites Using Mixtures of Organic and Inorganic Structure-Directing Agents. *Chem. Mater.* 2016, 28, 2236-2247.

114. Doan, H. A.; Li, Z.; Farha, O. K.; Hupp, J. T.; Snurr, R. Q. Theoretical insights into direct methane to methanol conversion over supported dicopper oxo nanoclusters. *Catal. Today* 2018, 312, 2-9.

115. Alayon, E. M. C.; Nachtegaal, M.; Bodi, A.; van Bokhoven, J. A. Reaction Conditions of Methane-to-Methanol Conversion Affect the Structure of Active Copper Sites. *ACS Catal.* 2014, 4, 16-22.

116. Alswat, A. A.; Ahmad, M. B.; Hussein, M. Z.; Ibrahim, N. A.; Saleh, T. A. Copper oxide nanoparticles-loaded zeolite and its characteristics and antibacterial activities. *Journal of Materials Science & Technology* 2017, 33, 889-896.

117. Tandon, S. P.; Gupta, J. P. Diffuse Reflectance Spectrum of Cupric Oxide. *Spectrosc. Lett.* 1969, 2, 357-360.

118. Tandon, S. P.; Gupta, J. P. Diffuse Reflectance Spectrum of Cuprous Oxide. *physica status solidi (b)* 1970, 37, 43-45.

119. Martínez-Franco, R.; Moliner, M.; Thogersen, J. R.; Corma, A. Efficient One-Pot Preparation of Cu-SSZ-13 Materials using Cooperative OSDAs for their Catalytic Application in the SCR of NOx. *ChemCatChem* 2013, 5, 3316-3323.

120. Ren, L.; Zhu, L.; Yang, C.; Chen, Y.; Sun, Q.; Zhang, H.; Li, C.; Nawaz, F.; Meng, X.; Xiao, F.-S. Designed copper–amine complex as an efficient template for one-pot synthesis of Cu-SSZ-13 zeolite with excellent activity for selective catalytic reduction of NOx by NH3. *Chem. Commun.* 2011, 47, 9789-9791.

121. Eilertsen, E. A.; Arstad, B.; Svelle, S.; Lillerud, K. P. Single parameter synthesis of high silica CHA zeolites from fluoride media. *Microporous Mesoporous Mater.* 2012, 153, 94-99.

122. Díaz-Cabañas, M.-J.; A. Barrett, P. Synthesis and structure of pure SiO2 chabazite: the SiO2 polymorph with the lowest framework density. *Chem. Commun.* 1998, 1881-1882.

123. Baerlocher, C.; McCusker, L. B. Database of Zeolite Structures. 1996.

124. Center, P. C.; Company, D. C. *GraidentCheck for Heterogeneous Catalysis*, 0.95; West Lafayette, Indiana, 2016.

125. Gao, F.; Mei, D.; Wang, Y.; Szanyi, J.; Peden, C. H. Selective Catalytic Reduction over Cu/SSZ-13: Linking Homo- and Heterogeneous Catalysis. *J. Am. Chem. Soc.* 2017, 139, 4935-4942.

126. Borfecchia, E.; Lomachenko, K. A.; Giordanino, F.; Falsig, H.; Beato, P.; Soldatov, A. V.; Bordiga, S.; Lamberti, C. Revisiting the nature of Cu sites in the activated Cu-SSZ-13 catalyst for SCR reaction. *Chem. Sci.* 2015, 6, 548-563.

127. Gao, F.; Kwak, J. H.; Szanyi, J.; Peden, C. H. F. Current Understanding of Cu-Exchanged Chabazite Molecular Sieves for Use as Commercial Diesel Engine DeNOx Catalysts. *Top. Catal.* 2013, 56, 1441-1459.

128. Paolucci, C.; Khurana, I.; Parekh, A. A.; Li, S.; Shih, A. J.; Li, H.; Di Iorio, J. R.; Albarracin-Caballero, J. D.; Yezerets, A.; Miller, J. T.; Delgass, W. N.; Ribeiro, F. H.; Schneider, W. F.; Gounder, R. Dynamic multinuclear sites formed by mobilized copper ions in NO x selective catalytic reduction. *Science* 2017, 357, 898-903.

129. Paolucci, C.; Verma, A. A.; Bates, S. A.; Kispersky, V. F.; Miller, J. T.; Gounder, R.; Delgass, W. N.; Ribeiro, F. H.; Schneider, W. F. Isolation of the copper redox steps in the standard selective catalytic reduction on Cu-SSZ-13. *Angew. Chem. Int. Ed.* 2014, 53, 11828-11833.

130. Di Iorio, J. R.; Bates, S. A.; Verma, A. A.; Delgass, W. N.; Ribeiro, F. H.; Miller, J. T.; Gounder, R. The Dynamic Nature of Brønsted Acid Sites in Cu–Zeolites During NOx Selective Catalytic Reduction: Quantification by Gas-Phase Ammonia Titration. *Top. Catal.* 2015, 58, 424-434.

131. Moreno-González, M.; Hueso, B.; Boronat, M.; Blasco, T.; Corma, A. Ammonia-containing species formed in Cu-chabazite as per in situ EPR, solid-state NMR, and DFT calculations. *J. Phys. Chem. Lett.* 2015, 6, 1011-1017.

132. Szanyi, J.; Kwak, J. H.; Zhu, H.; Peden, C. H. Characterization of Cu-SSZ-13 NH3 SCR catalysts: an in situ FTIR study. *PCCP* 2013, 15, 2368-2380.

133. Ma, L.; Cheng, Y.; Cavataio, G.; McCabe, R. W.; Fu, L.; Li, J. In situ DRIFTS and temperature-programmed technology study on NH3-SCR of NOx over Cu-SSZ-13 and Cu-SAPO-34 catalysts. *Appl. Catal., B* 2014, 156-157, 428-437.

134. Lezcano-Gonzalez, I.; Deka, U.; Arstad, B.; Van Yperen-De Deyne, A.; Hemelsoet, K.; Waroquier, M.; Van Speybroeck, V.; Weckhuysen, B. M.; Beale, A. M. Determining the storage, availability and reactivity of NH3 within Cu-Chabazite-based Ammonia Selective Catalytic Reduction systems. *PCCP* 2014, 16, 1639-1650.

135. Zhu, H.; Kwak, J. H.; Peden, C. H.; Szanyi, J. In situ DRIFTS-MS studies on the oxidation of adsorbed NH3 by NOx over a Cu-SSZ-13 zeolite. *Catal. Today* 2013, 205, 16-23.

136. Giordanino, F.; Vennestrom, P. N.; Lundegaard, L. F.; Stappen, F. N.; Mossin, S.; Beato, P.; Bordiga, S.; Lamberti, C. Characterization of Cu-exchanged SSZ-13: a comparative FTIR, UV-Vis, and EPR study with Cu-ZSM-5 and Cu-beta with similar Si/Al and Cu/Al ratios. *Dalton Trans.* 2013, 42, 12741-12761.

137. Bordiga, S.; Groppo, E.; Agostini, G.; van Bokhoven, J. A.; Lamberti, C. Reactivity of Surface Species in Heterogeneous Catalysts Probed by In Situ X-ray Absorption Techniques. *Chem. Rev.* 2013, 113, 1736-1850.

138. Li, H.; Paolucci, C.; Khurana, I.; Wilcox, L. N.; Goltl, F.; Albarracin-Caballero, J. D.; Shih, A. J.; Ribeiro, F. H.; Gounder, R.; Schneider, W. F. Consequences of exchange-site heterogeneity and dynamics on the UV-visible spectrum of Cu-exchanged SSZ-13. *Chem Sci* 2019, 10, 2373-2384.

139. Woertink, J. S.; Smeets, P. J.; Groothaert, M. H.; Vance, M. A.; Sels, B. F.; Schoonheydt, R. A.; Solomon, E. I. A [Cu2O]2+ core in Cu-ZSM-5, the active site in the oxidation of methane to methanol. *Proc. Natl. Acad. Sci. U. S. A.* 2009, 106, 18908-18913.

140. Li, H.; Paolucci, C.; Khurana, I.; Wilcox, Laura N.; Göltl, F.; Albarracin-Caballero, J. D.; Shih, A. J.; Ribeiro, F. H.; Gounder, R.; Schneider, W. F. Consequences of exchange-site heterogeneity and dynamics on the UV-visible spectrum of Cu-exchanged SSZ-13. *Chem. Sci.* 2019, 10, 2373-2384.

141. Psofogiannakis, G. M.; McCleerey, J. F.; Jaramillo, E.; van Duin, A. C. T. ReaxFF Reactive Molecular Dynamics Simulation of the Hydration of Cu-SSZ-13 Zeolite and the Formation of Cu Dimers. *J. Phys. Chem. C* 2015, 119, 6678-6686.

142. Göltl, F.; Love, A. M.; Hermans, I. Developing a Thermodynamic Model for the Interactions between Water and Cu in the Zeolite SSZ-13. *J. Phys. Chem. C* 2017, 121, 6160-6169.

143. Perea, D. E.; Arslan, I.; Liu, J.; Ristanović, Z.; Kovarik, L.; Arey, B. W.; Lercher, J. A.; Bare, S. R.; Weckhuysen, B. M. Determining the location and nearest neighbours of aluminium in zeolites with atom probe tomography. *Nat. Commun.* 2015, 6, 7589-7597.

144. Han, O. H.; Kim, C.-S.; Hong, S. B. Direct Evidence for the Nonrandom Nature of Al Substitution in Zeolite ZSM-5: An Investigation by 27Al MAS and MQ MAS NMR. *Angew. Chem. Int. Ed.* 2002, 41, 469-472.

145. Brezicki, G.; Kammert, J. D.; Gunnoe, T. B.; Paolucci, C.; Davis, R. J. Insights into the Speciation of Cu in the Cu-H-Mordenite Catalyst for the Oxidation of Methane to Methanol. *ACS Catal.* 2019, 9, 5308-5319.

146. Li, G.; Vassilev, P.; Sanchez-Sanchez, M.; Lercher, J. A.; Hensen, E. J. M.; Pidko, E. A. Stability and reactivity of copper oxo-clusters in ZSM-5 zeolite for selective methane oxidation to methanol. *J. Catal.* 2016, 338, 305-312.

147. van Bokhoven, J. A.; Lamberti, C. XAS Techniques to Determine Catalytically Active Sites in Zeolites: The Case of Cu-Zeolites. 2017, 299-316.

148. Pappas, D. K.; Martini, A.; Dyballa, M.; Kvande, K.; Teketel, S.; Lomachenko, K. A.; Baran, R.; Glatzel, P.; Arstad, B.; Berlier, G.; Lamberti, C.; Bordiga, S.; Olsbye, U.; Svelle, S.; Beato, P.; Borfecchia, E. The Nuclearity of the Active Site for Methane to Methanol Conversion in Cu-Mordenite: A Quantitative Assessment. *J. Am. Chem. Soc.* 2018, 140, 15270-15278.

149. Clausen Cell Reactor. https://you.stonybrook.edu/scc2/clausen-cell-reactor/.

150. Baerlocher, C.; McCusker, L. B. Database of Zeolite Structures. 2016 ed.; International Zeolite Association.

151. Kondratenko, E. V.; Peppel, T.; Seeburg, D.; Kondratenko, V. A.; Kalevaru, N.; Martin, A.; Wohlrab, S. Methane conversion into different hydrocarbons or oxygenates: current status and future perspectives in catalyst development and reactor operation. *Catal. Sci. Technol.* 2017, 7, 366-381.

152. Ahlquist, M.; Nielsen, R. J.; Periana, R. A.; Goddard Iii, W. A. Product Protection, the Key to Developing High Performance Methane Selective Oxidation Catalysts. *J. Am. Chem. Soc.* 2009, 131, 17110-17115.

153. Yashima, T.; Ahmad, H.; Yamazaki, K.; Katsuta, M.; Hara, N. Alkylation on synthetic zeolites: I. Alkylation of toluene with methanol. *J. Catal.* 1970, 16, 273-280.

154. Svelle, S.; Visur, M.; Olsbye, U.; Saepurahman; Bjørgen, M. Mechanistic Aspects of the Zeolite Catalyzed Methylation of Alkenes and Aromatics with Methanol: A Review. *Top. Catal.* 2011, 54, 897.

155. Baertsch, C. D.; Funke, H. H.; Falconer, J. L.; Noble, R. D. Permeation of Aromatic Hydrocarbon Vapors through Silicalite−Zeolite Membranes. *The Journal of Physical Chemistry* 1996, 100, 7676-7679.

156. Kaeding, W. W.; Chu, C.; Young, L. B.; Weinstein, B.; Butter, S. A. Selective alkylation of toluene with methanol to produce para-Xylene. *J. Catal.* 1981, 67, 159-174.

157. Kennedy, E. M.; Lonyi, F.; Ballinger, T. H.; Rosynek, M. P.; Lunsford, J. H. Conversion of benzene to substituted aromatic products over zeolite catalysts at elevated pressures. *Energy & Fuels* 1994, 8, 846-850.

158. Adebajo, M. O.; Howe, R. F.; Long, M. A. Methylation of Toluene with Methane over ZSM-5 Catalysts. *Energy & Fuels* 2001, 15, 671-674.

159. Sushkevich, V. L.; van Bokhoven, J. A. Methane-to-Methanol: Activity Descriptors in Copper-Exchanged Zeolites for the Rational Design of Materials. *ACS Catal.* 2019, 9, 6293-6304.

160. Wulfers, M. J.; Teketel, S.; Ipek, B.; Lobo, R. F. Conversion of methane to methanol on copper-containing small-pore zeolites and zeotypes. *Chem. Commun.* 2015, 51, 4447-4450.

161. Hou, Y.; Wang, N.; Zhang, J.; Qian, W. Highly selective synthesis of large aromatic molecules with nano-zeolite: beyond the shape selectivity effect. *RSC Advances* 2017, 7, 14309-14313.

162. Llopis, F. J.; Sastre, G.; Corma, A. Xylene isomerization and aromatic alkylation in zeolites NU-87, SSZ-33, β, and ZSM-5: molecular dynamics and catalytic studies. *J. Catal.* 2004, 227, 227-241.

163. Carpenter, J. R.; Yeh, S.; Zones, S. I.; Davis, M. E. Further investigations on Constraint Index testing of zeolites that contain cages. *J. Catal.* 2010, 269, 64-70.

164. Zhu, X.; Hofmann, J. P.; Mezari, B.; Kosinov, N.; Wu, L.; Qian, Q.; Weckhuysen, B. M.; Asahina, S.; Ruiz-Martínez, J.; Hensen, E. J. M. Trimodal Porous Hierarchical SSZ-13 Zeolite with Improved Catalytic Performance in the Methanol-to-Olefins Reaction. *ACS Catal.* 2016, 6, 2163-2177.

165. Jin, Z.; Wang, L.; Zuidema, E.; Mondal, K.; Zhang, M.; Zhang, J.; Wang, C.; Meng, X.; Yang, H.; Mesters, C.; Xiao, F.-S. Hydrophobic zeolite modification for in situ peroxide formation in methane oxidation to methanol. *Science* 2020, 367, 193.